U.S. Department of
Transportation

**Federal Railroad
Administration**

Fatigue Crack Growth Behavior of Railroad Tank Car Steel TC-128B Subjected to Various Environments Volume I

Office of Research
and Development
Washington, DC 20590

DOT/FRA/ORD-06/04.I

Final Report
December 2006

REPORT DOCUMENTATION PAGE

Form Approved
OMB No. 0704-0188

1. AGENCY USE ONLY (Leave blank)	2. REPORT DATE	3. REPORT TYPE AND DATES COVERED
	December 2006	Final Report December 2006

4. TITLE AND SUBTITLE
Fatigue Crack Growth Behavior of Railroad Tank Car Steel TC-128B Subjected to Various Environments
Volume I

5. FUNDING NUMBERS
DB034/RR28

6. AUTHOR(S)
Peter C. McKeighan, James H. Feiger

7. PERFORMING ORGANIZATION NAME(S) AND ADDRESS(ES)
Southwest Research Institute*
6220 Culebra Road
P.O. Drawer 28510
San Antonio, TX 78228-0510

8. PERFORMING ORGANIZATION REPORT NUMBER
DOT-VNTSC-FRA-02-03

9. SPONSORING/MONITORING AGENCY NAME(S) AND ADDRESS(ES)
U.S. Department of Transportation
Federal Railroad Administration
Office of Research and Development
1120 Vermont Avenue, NW-Mail Stop 20
Washington, DC 20590

10. SPONSORING/MONITORING AGENCY REPORT NUMBER
DOT/FRA/ORD-06/04.I

11. SUPPLEMENTARY NOTES
*Under contract to:

U.S. Department of Transportation
Research and Innovative Technology Administration
John A. Volpe National Transportation Systems Center
55 Broadway
Cambridge, MA 02142-1093

12a. DISTRIBUTION/AVAILABILITY STATEMENT
This document is available to the public through the National Technical Information Service, Springfield, Virginia 22161. This document (both volumes) is also available on the FRA Web site at www.fra.dot.gov. Note: The appendices are in a separate volume. Contact FRA for a copy.

12b. DISTRIBUTION CODE

13. ABSTRACT (Maximum 200 words)

As part of an effort to apply damage tolerance concepts to railroad tank cars, the fatigue crack growth (FCG) behavior of two lots of TC-128B steel was investigated. In addition to the material lot difference, variables assessed include: load ratio, orientation, environment, and crack growth test technique. The two material lots yielded essentially identical FCG properties for low and high stress ratios. The influence of stress ratio was slight, except in the near-threshold regime. The in-plane orientation (L-T) exhibits a growth rate approximately two times faster than the out-of-plane orientation (L-S). The influence of varying the test environment from −60 °F to +140 °F, with moisture content ranging from high to low humidity, was slight.

14. SUBJECT TERMS
Fatigue crack growth, damage tolerance, tank cars, baseline material behavior, environmental effects, steel alloy, TC-128B steel

15. NUMBER OF PAGES
92

16. PRICE CODE

17. SECURITY CLASSIFICATION OF REPORT	18. SECURITY CLASSIFICATION OF THIS PAGE	19. SECURITY CLASSIFICATION OF ABSTRACT	20. LIMITATION OF ABSTRACT
Unclassified	Unclassified	Unclassified	Unlimited

METRIC/ENGLISH CONVERSION FACTORS

ENGLISH TO METRIC	METRIC TO ENGLISH
LENGTH (APPROXIMATE)	**LENGTH (APPROXIMATE)**
1 inch (in) = 2.5 centimeters (cm)	1 millimeter (mm) = 0.04 inch (in)
1 foot (ft) = 30 centimeters (cm)	1 centimeter (cm) = 0.4 inch (in)
1 yard (yd) = 0.9 meter (m)	1 meter (m) = 3.3 feet (ft)
1 mile (mi) = 1.6 kilometers (km)	1 meter (m) = 1.1 yards (yd)
	1 kilometer (km) = 0.6 mile (mi)
AREA (APPROXIMATE)	**AREA (APPROXIMATE)**
1 square inch (sq in, in^2) = 6.5 square centimeters (cm^2)	1 square centimeter (cm^2) = 0.16 square inch (sq in, in^2)
1 square foot (sq ft, ft^2) = 0.09 square meter (m^2)	1 square meter (m^2) = 1.2 square yards (sq yd, yd^2)
1 square yard (sq yd, yd^2) = 0.8 square meter (m^2)	1 square kilometer (km^2) = 0.4 square mile (sq mi, mi^2)
1 square mile (sq mi, mi^2) = 2.6 square kilometers (km^2)	10,000 square meters (m^2) = 1 hectare (ha) = 2.5 acres
1 acre = 0.4 hectare (he) = 4,000 square meters (m^2)	
MASS - WEIGHT (APPROXIMATE)	**MASS - WEIGHT (APPROXIMATE)**
1 ounce (oz) = 28 grams (gm)	1 gram (gm) = 0.036 ounce (oz)
1 pound (lb) = 0.45 kilogram (kg)	1 kilogram (kg) = 2.2 pounds (lb)
1 short ton = 2,000 pounds (lb) = 0.9 tonne (t)	1 tonne (t) = 1,000 kilograms (kg)
	= 1.1 short tons
VOLUME (APPROXIMATE)	**VOLUME (APPROXIMATE)**
1 teaspoon (tsp) = 5 milliliters (ml)	1 milliliter (ml) = 0.03 fluid ounce (fl oz)
1 tablespoon (tbsp) = 15 milliliters (ml)	1 liter (l) = 2.1 pints (pt)
1 fluid ounce (fl oz) = 30 milliliters (ml)	1 liter (l) = 1.06 quarts (qt)
1 cup (c) = 0.24 liter (l)	1 liter (l) = 0.26 gallon (gal)
1 pint (pt) = 0.47 liter (l)	
1 quart (qt) = 0.96 liter (l)	
1 gallon (gal) = 3.8 liters (l)	
1 cubic foot (cu ft, ft^3) = 0.03 cubic meter (m^3)	1 cubic meter (m^3) = 36 cubic feet (cu ft, ft^3)
1 cubic yard (cu yd, yd^3) = 0.76 cubic meter (m^3)	1 cubic meter (m^3) = 1.3 cubic yards (cu yd, yd^3)
TEMPERATURE (EXACT)	**TEMPERATURE (EXACT)**
[(x-32)(5/9)] °F = y °C	[(9/5) y + 32] °C = x °F

QUICK INCH - CENTIMETER LENGTH CONVERSION

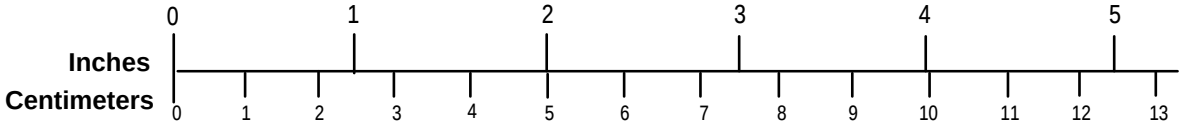

QUICK FAHRENHEIT - CELSIUS TEMPERATURE CONVERSION

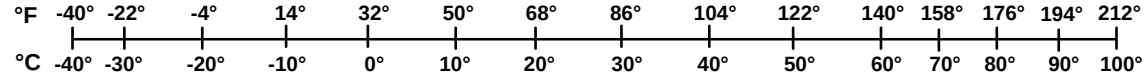

For more exact and or other conversion factors, see NIST Miscellaneous Publication 286, Units of Weights and Measures. Price $2.50 SD Catalog No. C13 10286

Updated 6/17/98

Table of Contents

1 Introduction 3
2 Materials 5
2.1 Material Procurement 5
2.2 Thermal Processing of Materials 5
3 Experimental Methods 11
3.1 Specimen Geometries and Extraction 11
3.2 Phase A Test Methods 11
3.3 Phase B Test Methods 13
4 Results 29
4.1 Material Characterization 29
4.2 Phase A FCG Curves 29
4.3 Other Phase A Data 30
4.4 Phase B Environmental Assessments 31
5 Discussion 59
5.1 Phase A FCG Characterization 59
5.1.1 K-Gradient and Material Lot Effects 59
5.1.2 Orientation and R-Ratio Effects 59
5.1.3 Comparison of FCG Data with Other Sources 60
5.2 Phase B Environmental FCG Data 61
5.2.1 Role of Environmental Variables 61
5.2.2 Comparison to Literature Data 62
5.2.3 FCG Rate Transients with Environmental Variation 62
5.3 Fatigue Crack Closure 63
6 Conclusions 77
7 References 79
8 Abbreviations and Acronyms 81

List of Tables

Table 1. Pedigree of Originally Supplied TC-128B Material 6
Table 2. Description of the Normalization and Stress Relieving Required on the Supplied Material 7
Table 3. Summary of All FCG Tests Performed During Phase A of Testing 15
Table 4. AAR TC-128B Specification, Mill-Certified Chemistries and Measured Chemistries for the Two Different Materials Supplied by the Two Tank Car Manufacturers (Quantities Are Shown in Weight Percent) 32
Table 5. Tensile Test Results for TC-128B (Trinity and Union Material) 33
Table 6. Summary of Grain Size Measurements Performed on Both Materials 34
Table 7. Summary of MC-Burst Closure Data (CMOD and BFS) 35

List of Figures

Figure 1. Two Pallets of Material in the As-Received Condition Prior to Any Processing at SwRI 8
Figure 2. Description of the Original A Material Supplied 8
Figure 3. Description of the Original B Material Supplied 9
Figure 4. Specimen Drawing for the C(T) Specimens Utilized During This Program..... 16
Figure 5. Specimen Drawing for the SE(B) Specimens Utilized During This Program 17
Figure 6. Drawing for the M(T) Specimens Utilized During This Program 18
Figure 7. FCG Specimens Used in Test Program 19
Figure 8. Description of the Layout of the Specimens Excised from Material A 19
Figure 9. Description of the Layout of the Specimens Excised from Material B..... 20
Figure 10. Plate Material Prior to Shipping to the Machine Shop for Fabrication of Specimens 21
Figure 11. FCG Testing Setup for the C(T) Specimen Geometry Used in Phase A..... 22
Figure 12. FCG Testing Setup for the SE(B) Specimen Geometry Used in Phase A 22
Figure 13. FCG Testing Setup for the M(T) Specimen Geometry Used in Phase A..... 23
Figure 14. Front Panel Display of the MC-Burst Program Used for Continuous Data Recording..... 24
Figure 15. Environmental Chamber Used in Phase B Testing 25
Figure 16. Schematic of the Plastic Enclosure Used with the Pin-Loaded C(T) Specimen 26
Figure 17. High-Humidity Setup Used in Phase B Testing..... 27
Figure 18. Grain Structure for the Three Planes of Material A (Material B Was Virtually Identical)..... 36
Figure 19. Test TC-A-1B: K-Decreasing and K-Increasing FCG Results at R = 0.1 (Union) 37
Figure 20. Test TC-A-1A: K-Decreasing and K-Increasing FCG Results at R = 0.1 (Union) 38
Figure 21. Test TC-B-1A: K-Decreasing and K-Increasing FCG Results for R = 0.1 (Trinity) 39
Figure 22. Test TC-B-1B: K-Decreasing and K-Increasing FCG Results for R = 0.1 (Trinity) 40
Figure 23. Test TC-A-2A: K-Increasing and K-Decreasing FCG Results for R = 0.6 (Union) 41
Figure 24. Test TC-B-2A: K-Decreasing and K-Increasing FCG Results for R = 0.6 (Trinity) 42
Figure 25. Test TC-A-2B: Constant K_{max} Results for L-T Orientation (Union) 43
Figure 26. Test TC-A-7: R = -1 Results for L-T Orientation 44
Figure 27. Tests TC-A-9, 10, and 12: FCG Results at R = 0.1 for L-S Orientation (K-Decreasing and K-Increasing Tests)..... 45
Figure 28. Test TC-A-11: Constant K_{max} FCG Behavior for L-S Orientation (Portion of Data Smoothed) 46
Figure 29. Test TC-A-11 (Smoothed): Constant K_{max} FCG Behavior for L-S Orientation 47

List of Figures (continued)

Figure 30. Raw Load-Displacement/Strain Data Overfiltered (50 Hz Top) and Filtered Appropriately (200 Hz Bottom) Showing (a) Clip Gage and (b) Strain Gage Data 48
Figure 31. Comparison between Unfiltered and Filtered Data for the Clip Gage with Regard to Crack Closure Measurement (Data is from Specimen TC-B-1A at Approximately 9.5M Cycles) 49
Figure 32. Typical Load-Compliance Offset Plot for Test TC-A-1A at Approximately 10M Cycles 50
Figure 33. Closure Program Printout Corresponding to Data Shown in Previous Figure 51
Figure 34. Typical Flat Fracture Surfaces Observed in Bend and C(T) Specimens 52
Figure 35. SEM Micrograph of the Fracture Surface of an R = 0.1 Specimen at (a) 8 ksi√in and (b) 20 ksi√in (Crack Growth Direction Is from Bottom to Top) 53
Figure 36. SEM Micrograph of the Fracture Surface of an R = 0.6 Specimen at (a) 8 ksi√in and (b) 20 ksi√in (Crack Growth Direction Is from Bottom to Top) 54
Figure 37. Phase B Environmental Crack Growth for High Constant ΔK, Low R-Ratio Conditions 55
Figure 38. Phase B Environmental Crack Growth for High Constant ΔK, High R-Ratio Conditions 56
Figure 39. Phase B Environmental Crack Growth for Low Constant ΔK, Low R-Ratio Conditions 56
Figure 40. Phase B Environmental Crack Growth for Low Constant ΔK, High R-Ratio Conditions 58
Figure 41. FCG Data Scatter for A36 Steel[3] 64
Figure 42. Effect of K-Gradient on FCG Behavior 65
Figure 43. Effect of Material Lot on FCG Behavior at Low and High R-Ratio 66
Figure 44. Influence of Orientation on FCG Behavior 67
Figure 45. Comparison between Fixed R-Ratio and Constant K_{max} FCG Data for the L-T and L-S Orientations 68
Figure 46. FCG Data for All R-Ratios (L-T) 69
Figure 47. Comparison to HBC Relation[4] 70
Figure 48. Comparison to Literature Data[7] 71
Figure 49. Phase B Environmental FCG Rates for High Constant ΔK, Low R-Ratio Conditions 72
Figure 50. Phase B Environmental FCG Rates for High Constant ΔK, High R-Ratio Conditions 73
Figure 51. Phase B Environmental FCG Rates for Low Constant ΔK, Low R-Ratio Conditions 74
Figure 52. Phase B Environmental FCG Rates for Low Constant ΔK, High R-Ratio Conditions 75
Figure 53. Applied ΔK and Crack Closure Derived ΔK_{eff} for the Constant ΔK Tests with Different Environmental Segments Applied 76

ACKNOWLEDGMENTS

A number of individuals and organizations made significant contributions to this program. The generous material donations of Trinity Industries (Tom Dalrymple and Woodie Land) and Union Tank Car Company (Phil Daum, Frank Reiner, and Al Henzi) made this program possible. Metal Samples Inc. (Ben Lackey) and Lindberg Houston Heat Treatment provided excellent service in processing the material. Southwest Research Institute's (SwRI) metallurgical laboratory staff (Harold Saldaña, Isaac Rodriguez, and Jim Spencer) was always available at an instant's notice to provide some type of service. Special thanks are also extended to Dale Haines and Darryl Wagar in the SwRI Solids Lab for keeping this program running in an excellent manner. Forrest Campbell and Rick Fess provided invaluable program support at the initiation of this project. Gratitude is further extended to Loretta Mesa for having the patience to guide and allow this report to evolve to its current state. Finally, appreciation is extended to Volpe Center program managers Will Riddell and David Jeong for their comments and direction throughout this program.

EXECUTIVE SUMMARY

As part of an effort to apply damage tolerance concepts to railroad tank cars, the fatigue crack growth (FCG) behavior of two lots of TC-128B steel (similar to A612 Grade B steel) was investigated. Advanced test control strategies were used to optimize testing, resulting in 21 FCG datasets using 13 specimens in the program's initial characterization phase. In addition, 27 FCG datasets assessing the influence of environment (different humidities for –60 ^{o}F and 140 ^{o}F air) on crack growth behavior were also generated in a subsequent phase of the program. In addition to the material lot difference, variables assessed include load ratio (R = 0.1, 0.6, and –1.0), orientation (L-T and L-S), and, indirectly, crack growth test technique (K-decreasing, -increasing, constant-K_{max} with increasing K_{min}).

The two material lots yielded virtually identical FCG properties at both low and high r-ratios. The influence of r-ratio was slight, on the order of a 50 percent increase in growth rate at the high r-ratio when compared to low r-ratio conditions (R = 0.6 versus 0.1). The in-plane orientation (L-T) exhibited a growth rate approximately two times (2x) faster than the through-thickness orientation (L-S). Furthermore, constant K_{max} test results suggest that the FCG threshold is approximately 2-3 ksi√in and 3-4 ksi√in for the L-T and L-S orientations, respectively.

In general, the effect of crack closure on FCG rate during the lab air testing phase was fairly small with the exception of behavior at near-threshold conditions where closure had more of an effect. In the case of the environmental testing, closure conditions were remarkably stable during testing. Moreover, the impact of the environmental perturbations included in this report on the FCG rate behavior was fairly slight, on the order of 1.5x. Finally, the data generated for TC-128B in the two orientations tested (a) agree well with A617-Grade B data extracted from the literature and (b) exhibited slightly slower growth rates when compared to a generalized FCG response derived for common structural and low-alloy steels. Nevertheless, the data generated in this report on TC-128B show less environmental influence than noted in the single reference available in the literature.

1 Introduction

The Federal Railroad Administration (FRA) and the Association of American Railroads (AAR) agree that periodic inspections for cracks are required for safe operation of tank cars carrying hazardous materials. It is important that an inspection schedule entails the relevant combination of inspection technique accuracy and inspection interval (e.g., the period of time between inspections) in order to prevent fatigue failures. To develop this inspection strategy, a firm understanding of FCG behavior is needed to demonstrate that a given inspection strategy provides adequate reliability.

The aerospace industry has performed the vast majority of FCG tests on light alloys, most notably aluminum, titanium, and high-strength steels. Although the nuclear and offshore oil and gas industries have performed some crack growth characterization, the materials utilized tend to differ significantly from the materials used in tank car construction. The scant data available that are relevant for tank car construction materials do not adequately address near-threshold regime behavior, the effect of stress ratio, or the deleterious impact of environment on FCG rates.

Clearly, all these factors can have a significant effect on predicted crack growth life. Without understanding the role of these factors on the baseline FCG behavior of tank car steels, it is difficult to make an accurate prediction of crack growth life of a tank car structure. Consequently, it is essential that the impact of near-threshold, stress ratio, and environmental effects be understood for the railroad tank car damage tolerance analysis.

The objective of this test program was to develop a database of FCG rate information for TC-128 Grade B steel used in the construction of tank cars. In order to achieve this, a two-part program was undertaken, with the first portion focusing on determining baseline material behavior and the second portion directed toward understanding environmental effects.

2 Materials

2.1 Material Procurement

In order to ensure the best applicability of the results obtained from this work, the tank car industry was solicited for suitable material. Union Tank Car Company (Phil Daum and Frank Reiner) in East Chicago, IN, and Trinity Industries (Tom Dalrymple) in Dallas, TX, offered materials suitable for excising test specimens. The pedigree of these materials, however, differed as shown in Table 1. Figure 1 shows a photograph of the as-received material from both manufacturers.

In the case of the Union Tank Car material, designated material A, the nominal material thickness was 25/32 in. Three pieces of this material were supplied with the geometry shown in Figure 2. As can be observed, the shape of the pieces is somewhat nonstandard since they represent scrap cutoff generated during tank car manufacture. In particular, the three pieces were torch-cut from scrap of head plates that were to be used for liquid propane gas (LPG) tank car heads. These cars are constructed in accordance with specification DOT105J400W. The material supplied was normalized at 1650 °F, and three pieces were supplied from a single heat. Union Tank Car created these scrap pieces from tank car production in May 2000.

Trinity Industries supplied the material, designated material B, from Plant 56 at Navasota, TX. This material represented stock that was used in April 2000. The geometry of the pieces, shown in Figure 3, was similar to the Union material, except that in several cases the pieces were split in half. The material supplied was in the as-rolled condition, and the 13/16 in thickness was slightly greater than the thickness of material A. SwRI purchased the steel, which was used for fabricating tank heads for tank cars transporting liquefied chlorine gas. These cars are constructed in accordance with specification DOT105J500W. The material is from the scrap portion of the rectangular plate from which circular blanks are cut using an oxy-fuel torch.

2.2 Thermal Processing of Materials

It was a paramount concern to ensure that the condition of the tested material was consistent with the material in the fleet and represented some of the possible range of TC-128B in service. Fleet consistency was believed to be especially important with regard to thermal processing since heat treatment can sometimes alter FCG properties. For instance, it was believed to be important to stress relieve the material since this is an integral step in tank car production for all manufacturers. Stress relieving, however, is primarily used to ensure that residual stresses associated with welding are relieved, and all testing was performed on base plate material with no welds.

Furthermore, some fundamental differences could exist between the manufacturing processes that different tank car builders apply that could impact material properties. In the case of the Trinity material, the tank head is hot formed, which leads to double normalization of the head and single normalization of the shell. Although the difference between single and double normalization should be minimal with regard to FCG rate, it was decided to treat the two

materials slightly differently. Material A underwent single normalization (prior to delivery) whereas material B underwent double normalization.

The research team used industry specifications to determine the relevant heat treatment schedule applied to the two materials. The research team performed heat treating at Texas Heat Treat (Round Rock, TX). Table 2 shows the full heat treatment specification utilized; only a portion of the original material supplied was actually heat treated and stress relieved to the conditions required.

Table 1. Pedigree of Originally Supplied TC-128B Material

Material Identifier	Material Supplier	Material Manufacturer	Heat No.	Dimensions	Mill Certs	Comments
A	Union Tank Car	Bethlehem Steel Corp.	811L06730	25/32 in (0.781 in)	σ_{TS} = 85 ksi σ_{YS} = 60 ksi ϵ = 21%	Supplied in normalized but not stress-relieved condition.
B	Trinity Industries	U.S. Steel Corp.	D01057	13/16 in (0.848 in measured)	σ_{TS} = 86 ksi σ_{YS} = 62 ksi ϵ = 24%	Supplied in as-rolled condition, requiring double normalization and stress relieving.

Table 2. Description of the Normalization and Stress Relieving Required on the Supplied Material

PCM
5/18/00

Thermal Treatment of TC128 Steel Plate Material

MATERIAL A

Plate Shape: Trapezoidal (87" x 47" footprint)
Number: One plate
Thickness: 0.781"
Weight: 575 lbs

Thermal Cycle:

Stress Relieve - Requires controlled heating and cooling. Furnace shall not exceed 600°F when plate(s) are placed inside. During heating, the rate of heating should be no greater than 400°F per hour. Heat material to 1125°F ± 25°F and hold for 60 minutes. Cool to 600°F at a rate of cooling no greater than 500°F per hour. Complete cooling to ambient air condition in still air.

MATERIAL B

Plate Shape: Trapezoidal (40" x 40" footprint)
Number: Two plates
Thickness: 0.813"
Weight: 225 lbs

Thermal Cycle:

Please insure that the two plates are treated as one lot for both processes

Double Normalization - Heat to 1655°F ± 25°F and hold for 30 minutes. Cool to ambient temperature in still air. Reheat to 1600°F ± 25°F and hold for 30 minutes. Cool to ambient temperature in still air.

Stress Relieve - Requires controlled heating and cooling. Furnace shall not exceed 600°F when plate(s) are placed inside. During heating, the rate of heating should be no greater than 400°F per hour. Heat material to 1125°F ± 25°F and hold for 60 minutes. Cool to 600°F at a rate of cooling no greater than 500°F per hour. Complete cooling to ambient air condition in still air.

Figure 1. Two Pallets of Material in the As-Received Condition Prior to Any Processing at SwRI

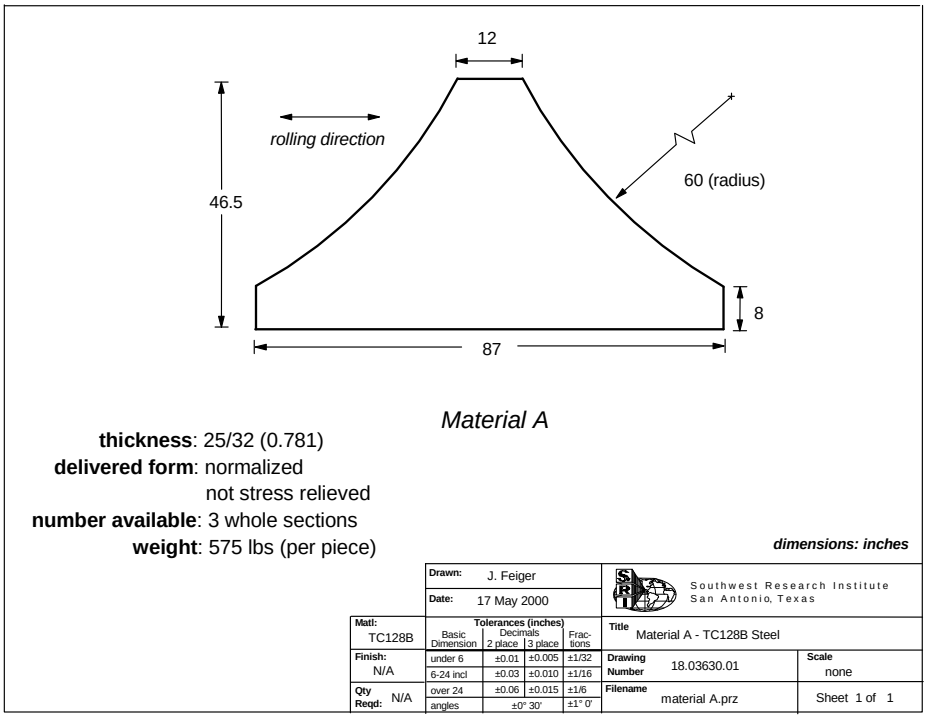

Figure 2. Description of the Original A Material Supplied

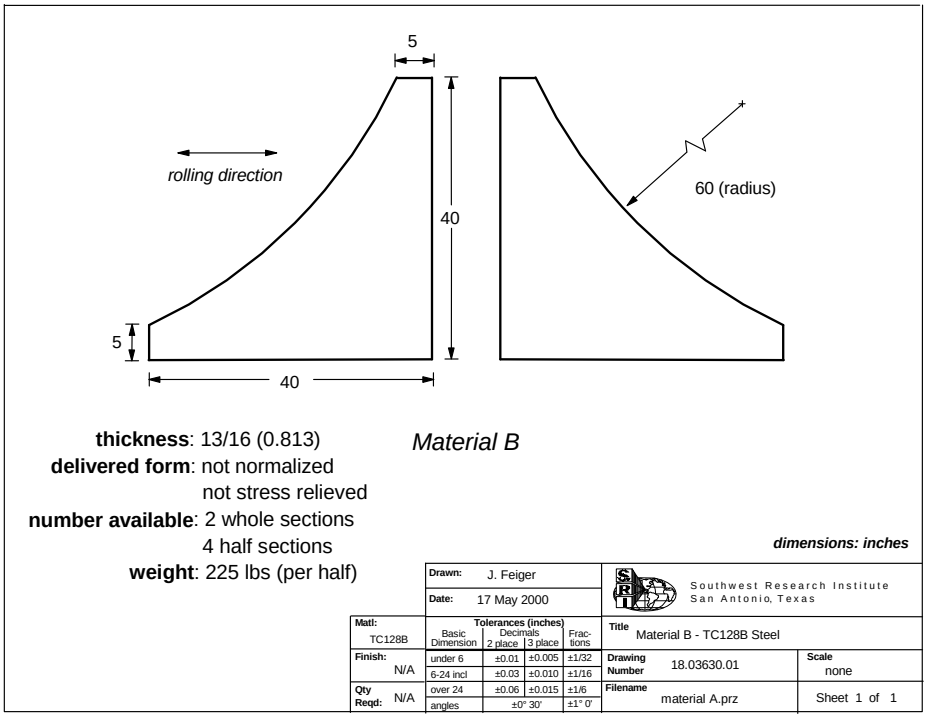

Figure 3. Description of the Original B Material Supplied

3 Experimental Methods

SwRI divided the testing into two phases, A and B. Phase A was geared toward baseline material characterization. SwRI performed K-controlled FCG tests to generate the full FCG curves. This approach differs markedly from that employed in Phase B, where constant ΔK tests were used to determine the impact on FCG behavior. This section will describe the procedures used in Phases A and B more fully.

3.1 Specimen Geometries and Extraction

SwRI performed FCG testing of the TC-128B tank car steel in accordance with ASTM E647, the FCG testing standard described in Reference 1. SwRI used special K-control techniques to perform ΔK-decreasing, ΔK-increasing, and constant K_{max}-increasing K_{min} testing. Three FCG specimen geometries were tested during Phase A, including the following FCG specimens:

- Compact tension C(T), W = 3 in), as shown in Figure 4
- Single-edge bend SE(B), W = 0.75 in), depicted in Figure 5
- Middle-crack tension M(T), W = 4 in), as shown in Figure 6

Figure 7 shows a relative comparison of the size differences between the three specimen geometries. The small bend specimens were specifically used to evaluate properties through the thickness of the plate whereas the larger specimens were used for the in-plane orientations in the original supplied plates.

With respect to the C(T) specimens, a ΔK-decreasing and a ΔK-increasing segment could both be achieved given the relatively large ligament length. Given the relatively short ligament length of the SE(B) specimens, however, only one segment (ΔK-decreasing or -increasing) was possible. SwRI used the C(T) and M(T) specimens to test the L-T orientation while the SE(B) geometry was used to characterize the L-S orientation.

At the start of this program, the importance of the different material variables was unknown. Consequently, a larger than normal number of replicate specimens were fabricated in order to preserve some flexibility in material choice later during testing. Figures 8 and 9 show the layout of the specimens in materials A and B. Integral to the central region of each of the specimen's identification is the material type, either A or B. Figure 10 shows a photograph of the plates before shipping them to the machine shop. The most outer 2 in of material for each of the plates was not used to ensure that the flame-cut region of the plate was omitted from testing.

3.2 Phase A Test Methods

A key objective in the Phase A testing was an r-ratio investigation, and, three stress ratios were tested: 0.1, 0.6, and –1. The K-gradient for the ΔK-decreasing tests was C = -2 in^{-1}. For the ΔK-increasing testing, two K-gradients were used: +2 and +6 in^{-1}. In addition to the constant r-ratio tests, SwRI performed constant K_{max} – increasing K_{min} tests. SwRI performed this

procedure on the C(T) and SE(B) coupons with the initial r-ratio at 0.1 and an ending ratio of near 0.9. The K-gradient used for the constant K_{max} testing was $C = -15$ in^{-1}.

SwRI used Fracture Technology Associates (FTA) software, integrated with a 10-kip closed-loop servohydraulic test frame, to perform the various FCG tests. The software allows execution of the specialized test strategies mentioned previously. SwRI performed all Phase A testing at lab temperature (70-78 °F) and at lab humidity (40-75 percent).

SwRI used standard clevis grips for testing of the C(T) specimens, with 0.75-in nominal pin holes (Figure 11). Testing of the SE(B) utilized a four-point bending configuration with a inner span of 3 in and an outer span of 5 in (Figure 12). Additionally, the loading point radii were 0.5W. Mechanical clamping grips (with alignment holes in each end of the specimen) were used for the M(T) coupons, providing the required uniform stress distribution during fatigue loading (Figure 13). Test frequencies ranged from 5 to 10 Hz and depended on mainly specimen geometry.

SwRI made visual and compliance crack length measurements during testing of the C(T) and SE(B) specimens. The visual crack length measurements were made to post-test correct the data to account for any error in the compliance crack length measurements. Compliance data, used in the determination of closure levels, were gathered with a front-face mounted clip gage as well as a back-face strain gage for the C(T) and SE(B) specimens. SwRI made KRAK gage and visual crack length (both sides, left and right crack tips) measurements during the testing of the M(T) specimens. When testing the M(T) specimens, a strain gage was placed at a 2a/W of 0.7 to measure potential closure levels.

Closure data, including both clip gage and strain gage, were gathered with an SwRI custom-developed LabVIEW software program called Multiple Channel Burst Recording (MC-Burst). This program simply records data periodically as the test progresses for analysis offline at some future date. In order to successfully analyze closure data, the data must be high resolution. The benefit of the MC-Burst program is that it captures short bursts of high-resolution data at specified cycle counts (or immediately at a keystroke if so desired). The bursts typically lasted over three to four cycles and nominally contained 4,000 data points. Figure 14 shows an example of a screen for the MC-Burst program.

The FTA software also analyzed closure data in which a reduced offset plot was established and ultimately a crack closure level determined. The nominal reported closure level utilized in this work was the 2 percent-offset method, as described in the relevant annex to ASTM E647.

Table 3 shows the overall matrix of test conditions, which clearly illustrates the range of variables involved in the testing. Specimen geometry (e.g., orientation) and material type were varied along with type of test, K-gradient rate, and r-ratio.

3.3 Phase B Test Methods

The main objective of Phase B testing is to characterize the environmental effects on the FCG behavior of the TC-128B tank car steel. While full FCG curves can be developed at fixed environmental conditions, a more efficient technique uses K-control strategies that more efficiently utilize FCG coupons. The approach used in the Phase B testing involved constant ΔK-control testing while varying the environmental parameters that mainly included temperature and humidity. Constant ΔK tests nominally yield a constant FCG rate. By varying environmental conditions during this type of test, the impact of the environmental variable can be definitively assessed by comparing sequential segments.

Similar to the Phase A testing, SwRI investigated the stress ratios of 0.1 and 0.6. The two stress intensity ranges chosen for constant ΔK testing were 8 and 20 ksi√in. These levels were based on the corresponding FCG curves determined in Phase A testing. The two levels were chosen to yield nominal crack growth rates that differed by an order of magnitude. Overall, four loading conditions were evaluated in Phase B testing:

- R = 0.1, ΔK = 8 ksi√in
- R = 0.6, ΔK = 20 ksi√in
- R = 0.1, ΔK = 8 ksi√in
- R = 0.6, ΔK = 20 ksi√in

SwRI collected closure data by MC-Burst back-face strain (BFS) and crack mouth opening displacement (CMOD), using the FTA software to control the test. Due to the work's environmental aspect, a 1-Hz test frequency was used throughout. Measurements were made of compliance crack length (used in the control strategy) and visual crack length during the testing of each specimen. Few visual crack length measurements were made to minimize interruption of the test.

As mentioned previously, the environmental parameters mainly included temperature and humidity. Testing included varying combinations of these parameters, as well as baseline lab air/lab temperature conditions. Specimens were precracked (lab air/lab temperature) per ASTM E647 and subsequently subjected to the following varying environmental conditions:

- Segment 1: 74 °F, lab air humidity
- Segment 2: -60 °F, low humidity (5-10 percent relative humidity [RH])
- Segment 3: 74 °F, low humidity
- Segment 4: 140 °F, low humidity
- Segment 5: repeat segment 1
- Segment 6: 74 °F, high-humidity (95-99 percent RH)
- Segment 7: 140 °F, high-humidity
- Segment 8: repeat segment 1

SwRI did not conduct a low temperature (-60 °F) combined with high-humidity (95-99 percent RH) segment. This is due to the fact that under cold conditions, the air can support very small

moisture concentrations. Furthermore, SwRI performed lab air condition segments as a baseline measure not only to compare to the environmental segments but also to investigate any residual stress effects (e.g., growth rate variations as the crack length extended). Segments were nominally 0.125 to 0.25 in. in crack length and ultimately depended on the presence of any transient crack growth behavior.

The varying humidity and temperature conditions were achieved by using environment chambers, as shown in Figure 15. The chambers themselves were used to monitor and control the temperature, while subchambers were used to control the humidity directly adjacent to the specimen. SwRI achieved heating through forced convection and cooling using liquid nitrogen managed by a proportional-integral-derivative (PID) controller in concert with a solenoid valve. SwRI controlled humidity through the use of a plastic subchamber enclosure surrounding the specimen. Figure 16 shows a schematic of this sealing system. For dry conditions (5-10 percent RH), SwRI staff used desiccant and placed it in the bottom of the plastic bag. SwRI achieved wet conditions by using a wet sponge placed in the enclosure, as shown in Figure 17. For all cases, SwRI staff monitored the humidity *in situ* with a hygrometer whose probe is also shown in Figure 17.

Table 3. Summary of All FCG Tests Performed During Phase A of Testing

Specimen ID	Type of Specimen			Material		Seg. ID	Type of Test				C in^{-1}	r-ratio	Comments
	C(T)	M(T)	SE(B)	Trinity	Union		$\Delta K\downarrow$	$\Delta K\uparrow$	$\rightarrow K_{max}$	$\rightarrow \Delta K$			
TC-A-1A	✓				✓	A	✓				-2	0.1	
						B		✓			+2	0.1	
TC-B-1A	✓			✓		A	✓				-2	0.1	
						B		✓			+6	0.1	
TC-A-1B	✓				✓	A	✓				-2	0.1	
						B		✓			+6	0.1	
TC-B-1B	✓			✓		A	✓				-2	0.1	
						B		✓			+2	0.1	
TC-A-2A	✓				✓	A	✓				-2	0.6	
						B		✓			+2	0.6	
TC-B-2A	✓			✓		A	✓				-2	0.6	
						B		✓			+6	0.6	
TC-A-2B	✓				✓	A			✓		-10	0.1-0.9	
TC-A-6		✓			✓	A	✓				-2	-1	crk tip probs
TC-A-7		✓			✓	A	✓				-2	-1	crk tip probs
						B		✓			+6	-1	
TC-A-8			✓		✓	A		✓			+6	0.1	load point probs
TC-A-9			✓		✓	A	✓				-2	0.1	
TC-A-10			✓		✓	A		✓			+6	0.1	
						B				✓	--	0.1	
TC-A-11			✓		✓	A			✓		-10	0.1-0.9	
TC-A-12			✓		✓	A		✓			+6	0.1	

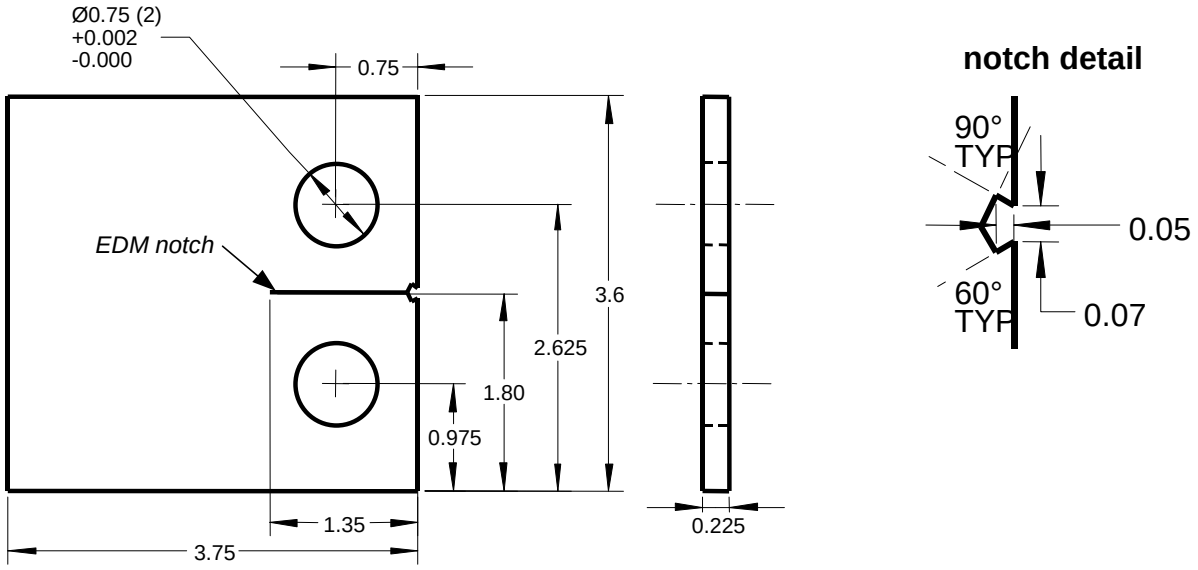

C(T) specimen geometry

- *TC128B steel (mild steel)*
- *W= 3 in*
- *wire EDM notch (0.005 in)*
- *knife edge gage length: 0.075 in*

dimensions: ***inches***

	Drawn: J. Feiger			Southwest Research San Antonio, Texas	
	Date: 08 June 2000				
Matl: TC128B	**Tolerances (inches)** Basic Dimension	Decimals 2 place	3 place	fract.	**Title: C(T) specimen W=3**
Finish: 32 RMS	under 6	±0.005	±0.005	±1/32	
	6-24 incl	±0.010	±0.005	±1/16	**Drawing Number** 18.03630.01 — **Scale** none
Qty Reqd: 10	over 24	±0.025	±0.015	±1/6	**Filename** C(T) W=3.ppt — Sheet of
	angles	±0°30'		±1°0'	

Figure 4. Specimen Drawing for the C(T) Specimens Utilized During This Program

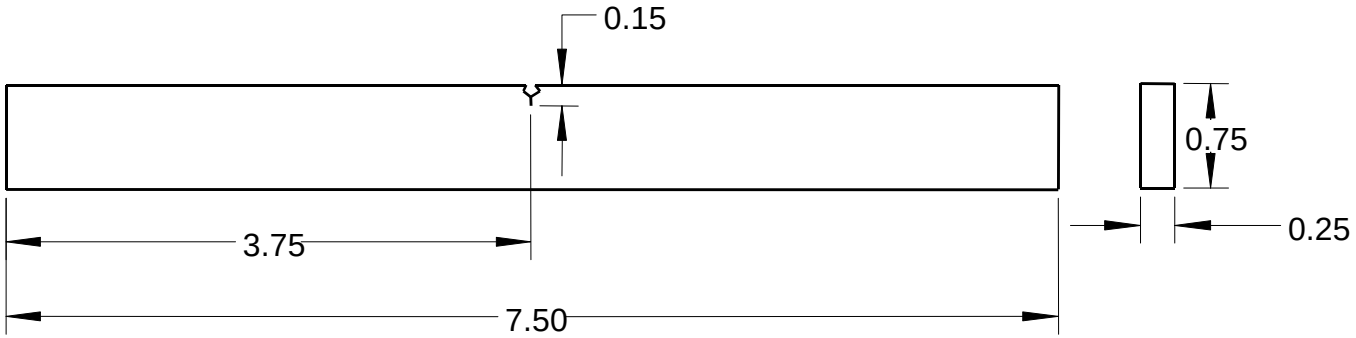

notch detail

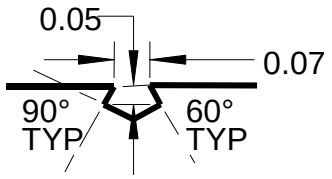

SE(B) specimen geometry

- *TC128B steel (mild steel)*
- *W= 0.75 in*
- *wire EDM notch (0.005 in)*
- *knife edge gage length: 0.075 in*

dimensions: ***inches***

	Drawn: J. Feiger			Southwest Research San Antonio, Texas	
	Date: 08 June 2000				
Matl: TC128B	**Tolerances (inches)** Basic Dimension	Decimals 2 place	3 place	fract.	**Title: SE(B) specimen**
Finish: 32 RMS	under 6	±0.005	±0.005	±1/32	
	6-24 incl	±0.010	±0.005	±1/16	**Drawing Number** 18.03630.01 — **Scale** none
Qty Reqd: 16	over 24	±0.025	±0.015	±1/6	**Filename** SE(B).ppt — Sheet of
	angles	±0°30’		±1°0’	

Figure 5. Specimen Drawing for the SE(B) Specimens Utilized During This Program

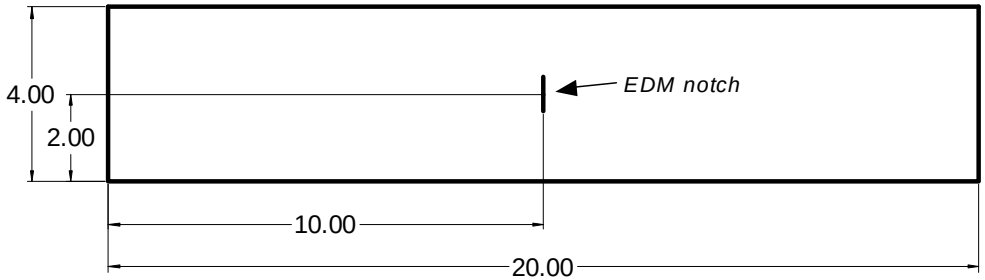

EDM notch detail

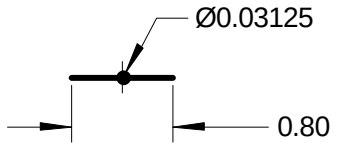

M(T) specimen geometry

- *TC128B steel (mild steel)*
- *W= 4 in*
- *wire EDM notch (0.005 in)*
- *1/32" diameter starter hole for EDM notch*

dimensions: ***inches***

	Drawn: J. Feiger				Southwest Research Institute San Antonio, Texas	
	Date: 08 June 2000					
Matl: TC128B	**Tolerances (inches)** Basic Dimension	Decimals 2 place	3 place	fract.	**Title: M(T)) specimen W=4**	
Finish: 32 RMS	under 6	±0.005	±0.005	±1/32	**Drawing Number** 18.03630.01	**Scale** none
	6-24 incl	±0.010	±0.005	±1/16		
Qty Reqd: 4	over 24	±0.025	±0.015	±1/6	**Filename** M(T) W=4.ppt	Sheet of
	angles	±0°30'		±1°0'		

Figure 6. Drawing for the M(T) Specimens Utilized During This Program

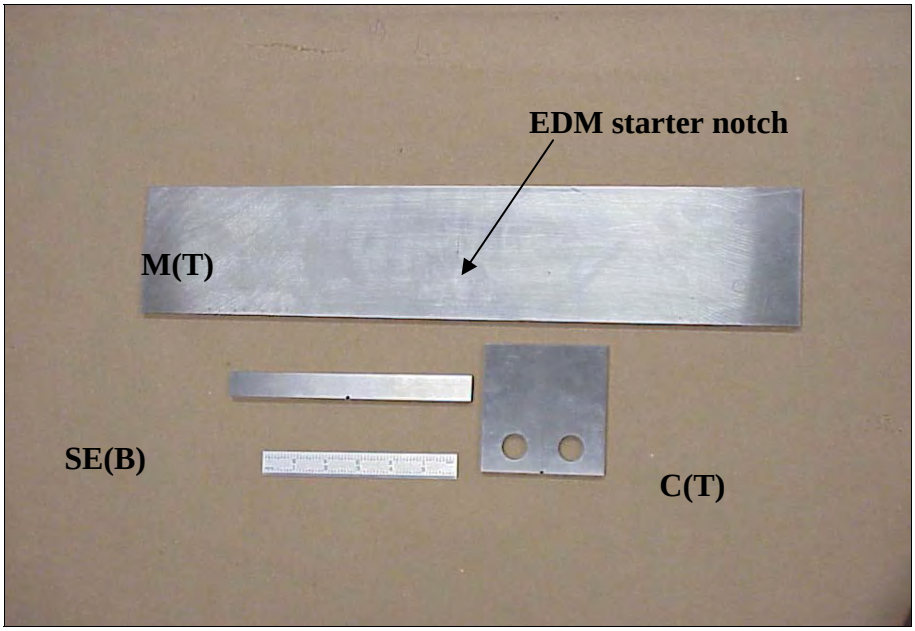

Figure 7. FCG Specimens Used in Test Program

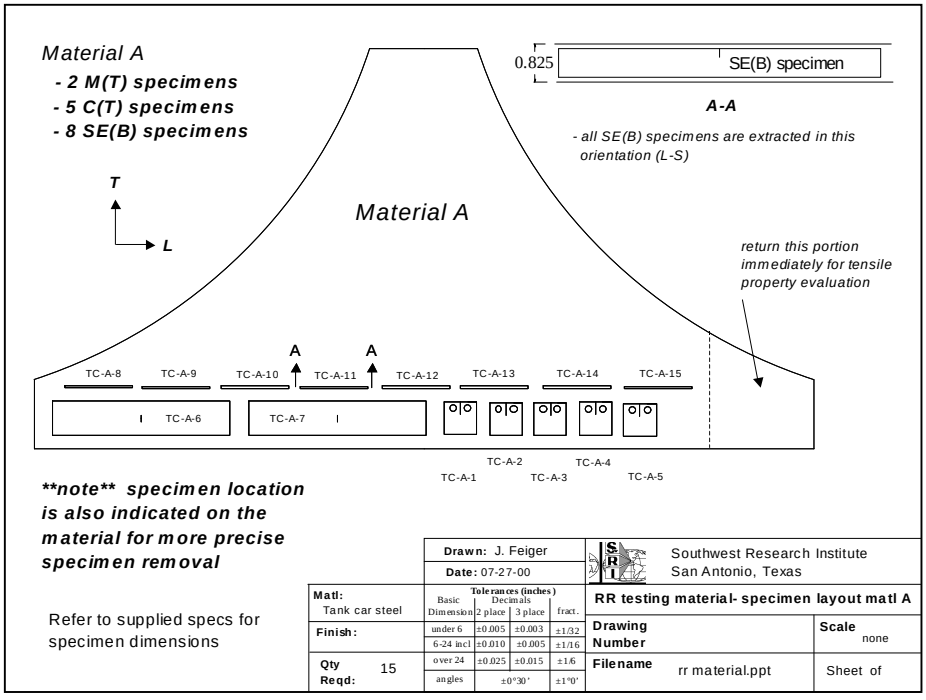

Figure 8. Description of the Layout of the Specimens Excised from Material A

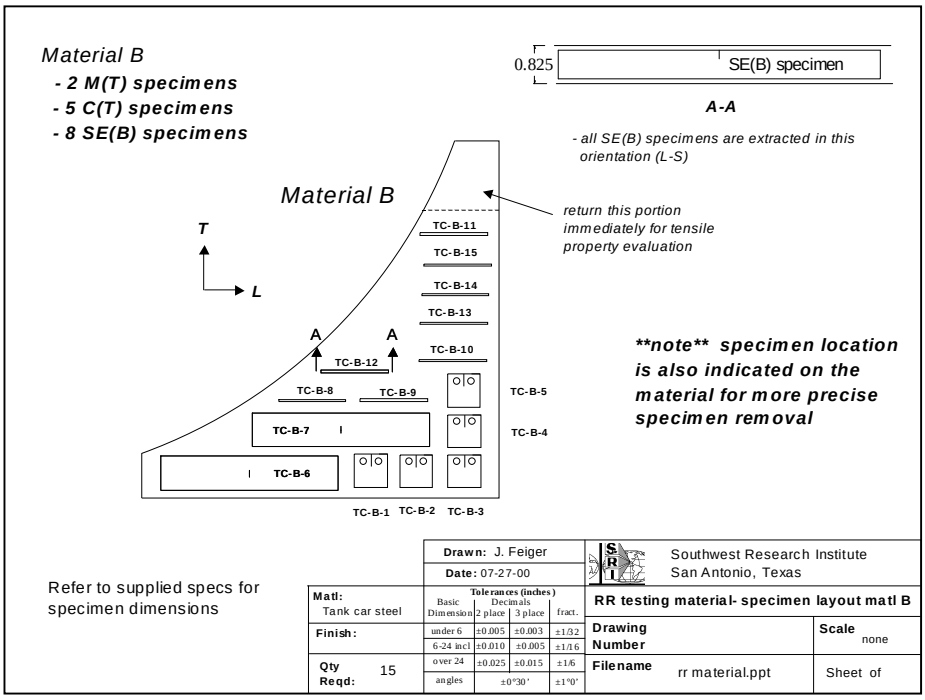

Figure 9. Description of the Layout of the Specimens Excised from Material B

Figure 10. Plate Material Prior to Shipping to the Machine Shop for Fabrication of Specimens

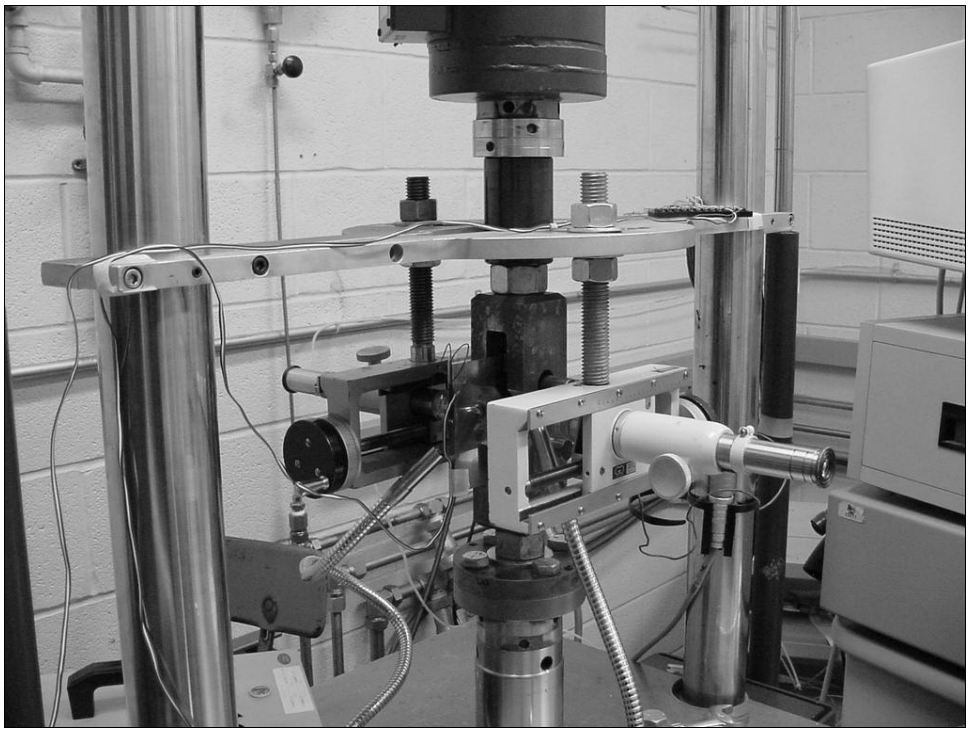

Figure 11. FCG Testing Setup for the C(T) Specimen Geometry Used in Phase A

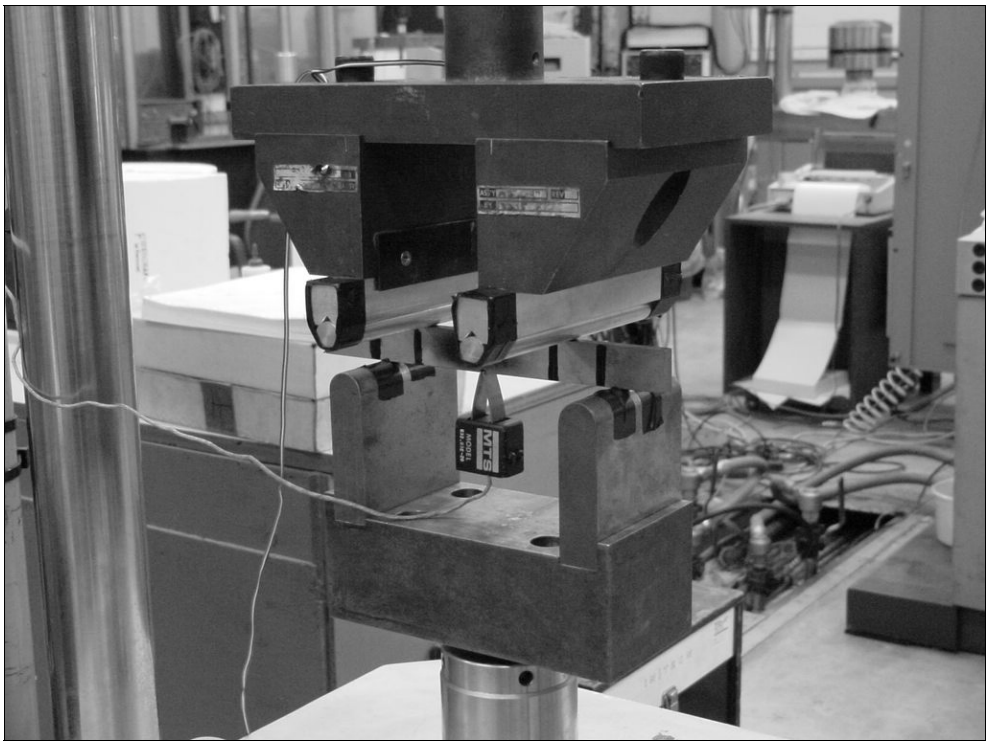

Figure 12. FCG Testing Setup for the SE(B) Specimen Geometry Used in Phase A

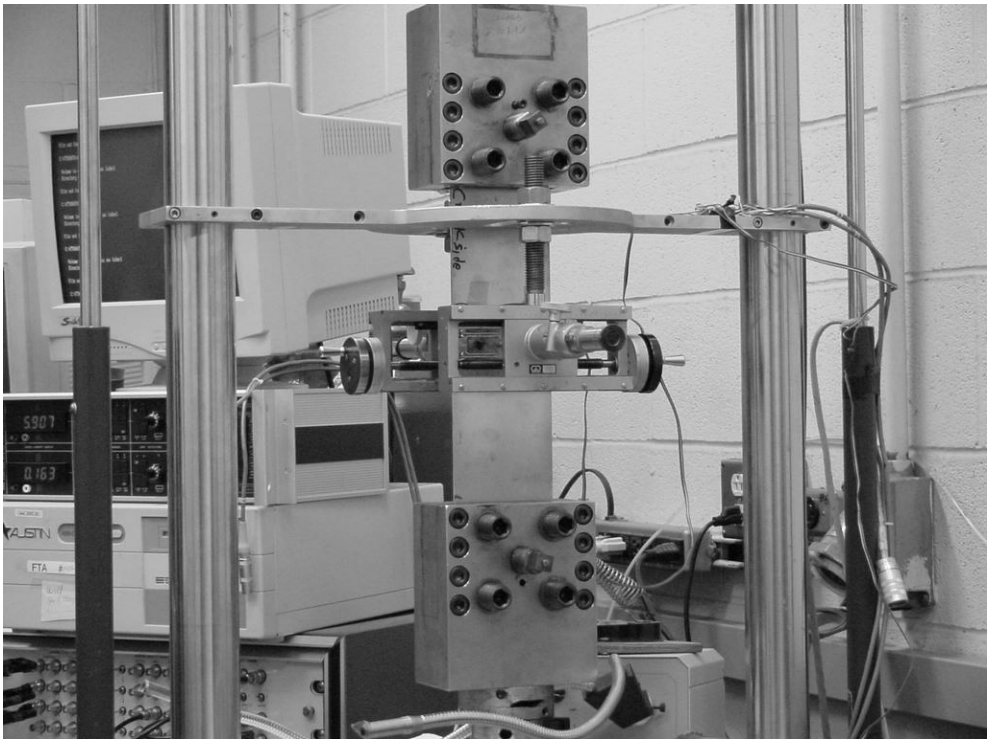

Figure 13. FCG Testing Setup for the M(T) Specimen Geometry Used in Phase A

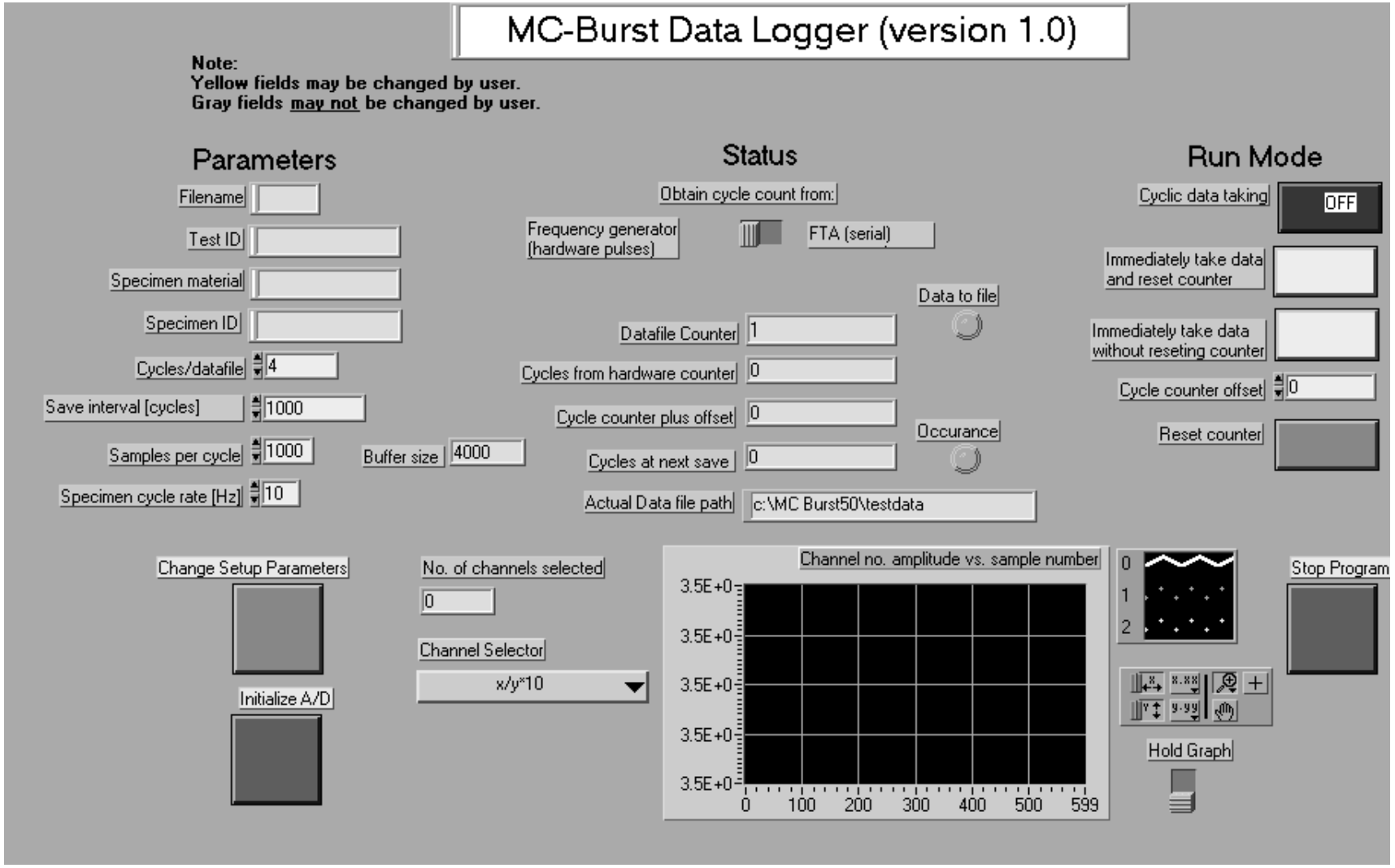

Figure 14. Front Panel Display of the MC-Burst Program Used for Continuous Data Recording

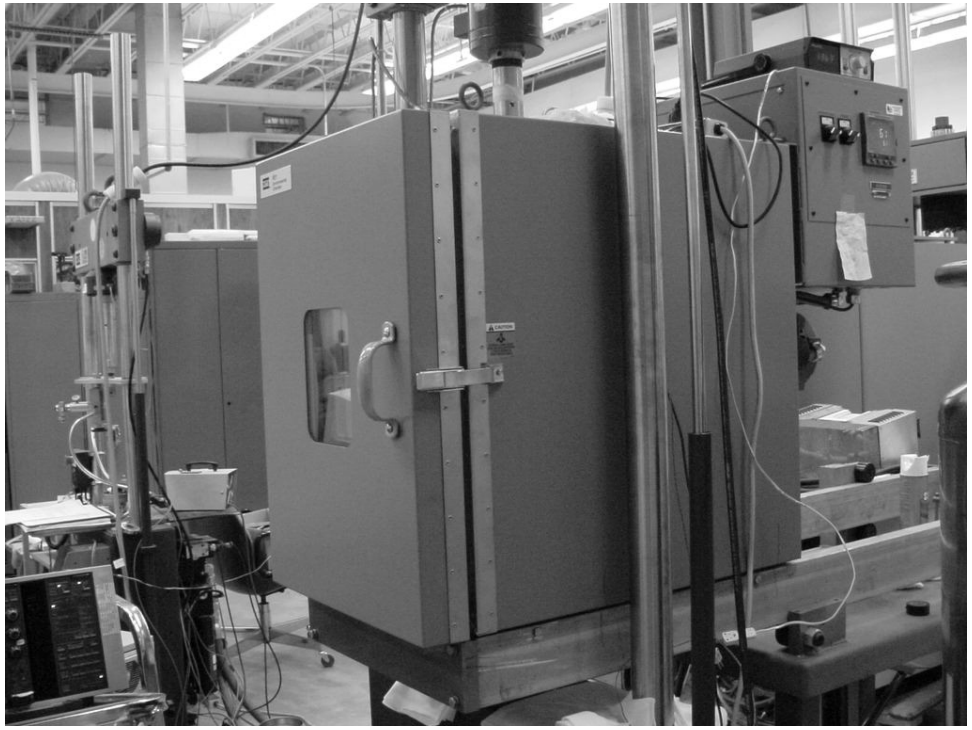

Figure 15. Environmental Chamber Used in Phase B Testing

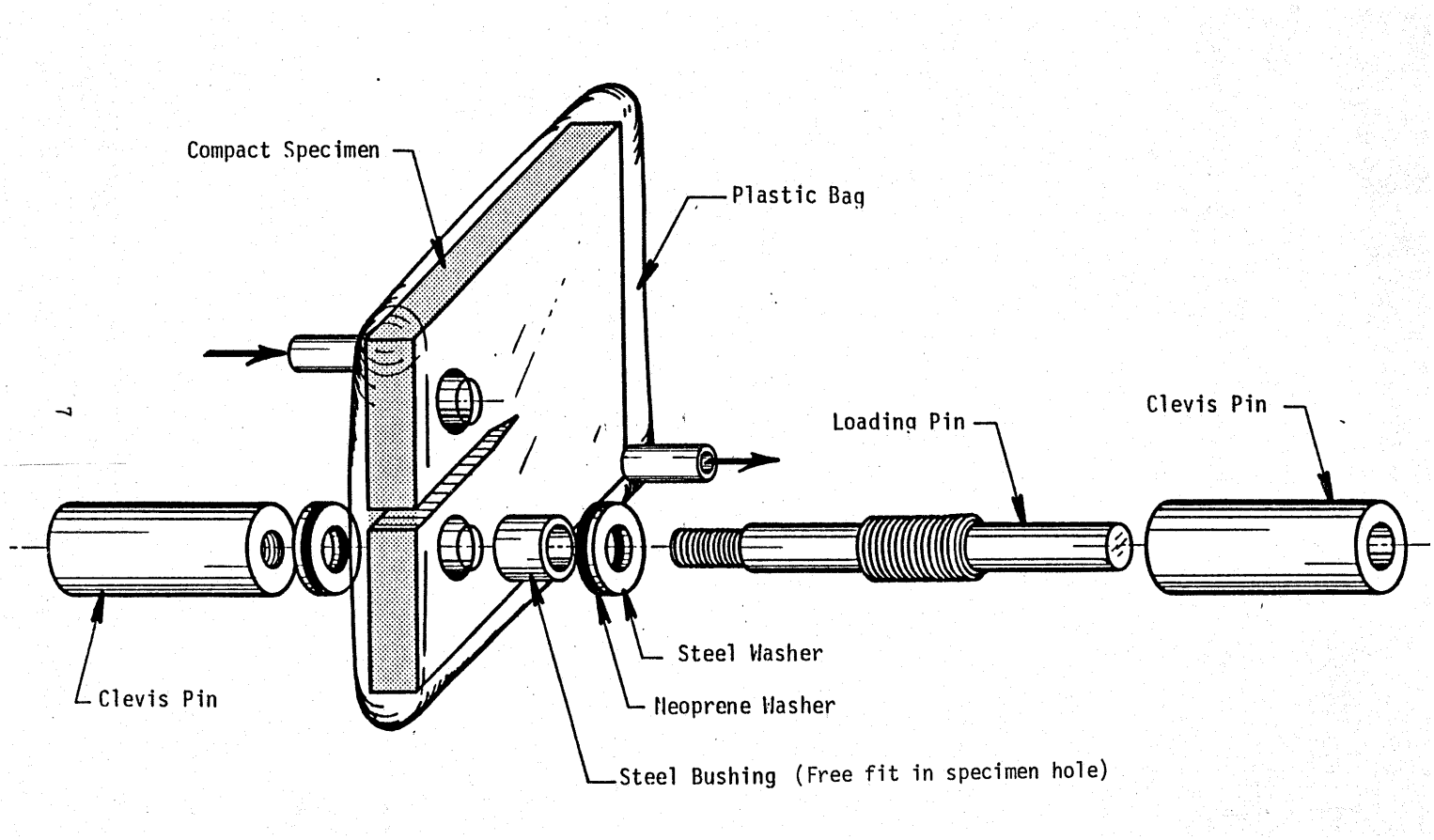

Figure 16. Schematic of the Plastic Enclosure Used with the Pin-Loaded C(T) Specimen

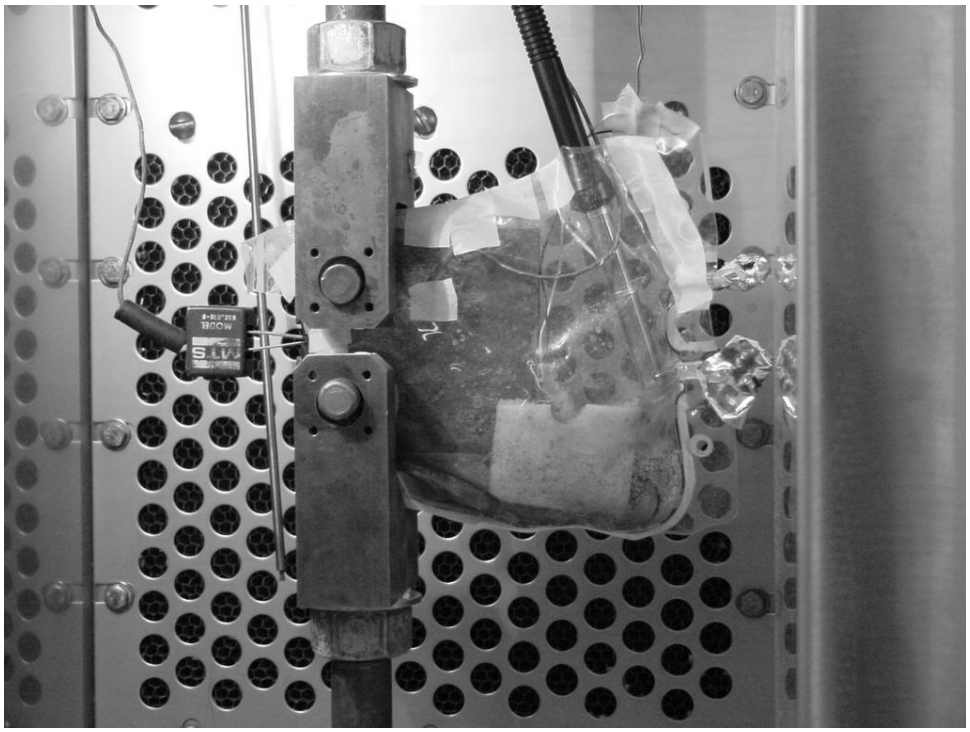

Figure 17. High-Humidity Setup Used in Phase B Testing

4 Results

This section includes the fundamental results generated during this program. It presents the raw data only, with a fuller interpretation provided in a later portion of this report. Volume 2 of this report includes the laboratory printouts documenting the FCG results.

4.1 Material Characterization

SwRI performed basic material characterization on three different levels: chemistries, tensile properties, and grain structure. Table 4 shows the measured chemistries for materials A and B. The mill test results, supplied with the material certifications for each material, are also documented. The two materials clearly meet the AAR specifications [2] for TC-128 Grade B steel. Furthermore, the chemistries are very comparable between materials A and B. The only noticeable difference appears to be in silicon content, with the Union material (A) having 50 percent more by weight percent than the Trinity material (B).

Table 5 shows tensile test results for materials in the L-T orientation. Due to the thickness of the material, it was not possible to measure properties in the short transverse (thickness) direction. Nevertheless, in the two orientations indicated, little measurable anisotropy occurs. Typically, less than 1 ksi exists for either yield or tensile strength. Furthermore, there appears to be little noticeable or statistically significant difference in strength properties between the Union and Trinity materials.

The grain structures between the two materials are also very similar. Table 6 shows the grain size measurements for both materials. Little influence of orientation occurred since the grains were generally equiaxed. The grain size typically ranges from 0.7 to 1.0 x 10^{-3} in. This equiaxed nature is further evident in Figure 18. The in-plane orientations (e.g., T and L planes sectioned through the thickness) tend to exhibit texture or preferential alignment of the darker pearlite. The lighter grain structure shown in Figure 18 is ferrite.

The foregoing assessments clearly indicated that (a) both materials meet AAR specifications for TC-128B and (b) there appears to be little measurable difference between the two lots of material supplied by different tank car builders.

4.2 Phase A FCG Curves

Figures 19 to 29 show the FCG results for all the Phase A testing. Data are included from each of the tests referenced in Table 3. The data have been plotted to illustrate each of the different segments of the test. Although the global trends observed will be discussed in more detail later, it is worthwhile to briefly summarize the series of plots.

Figures 19 to 22 show low r-ratio data for both materials at different K-gradient rates. Each test initially includes a K-decreasing segment where FCG rates decrease followed by generation of the complete crack growth curve under K-increasing conditions. Figures 23 and 24 show high r-

ratio FCG data for both materials. Figure 25 shows results from a variable r-ratio, constant K_{max} test (low R at high rates and high R at low rates). Figure 26 shows FCG data from the last of the in-plane tests, including negative r-ratio results for material A.

Whereas the previous data focused on the L-T orientation, FCG results for the L-S orientation are included in Figure 27. Since these bend specimens were so small, only one segment (K-increasing or -decreasing) was possible per test. Furthermore, the small specimen size made signal-to-noise ratios slightly higher, which resulted in greater FCG variability. Whereas the previous data were at low r-ratio, high and low r-ratio results are shown in Figure 28. At growth rates below 10^{-7} in/cycle, considerable scatter occurs in the FCG results shown. This is again a consequence of issues associated with the 0.75-in-wide, thin bend specimen. Using a multiple-point averaging technique, these data are smoothed as shown in Figure 29.

4.3 Other Phase A Data

Enormous amounts of load-strain and load-displacement data were continuously recorded during this program. SwRI simply recorded the vast majority of data and did not process it. The intent was to gather data only with a view toward possibly analyzing it later to better interpret the results. Table 7 provides a list of the files recorded during each of the FCG tests. As can be seen, almost 4,000 files of load-displacement and load-strain data were recorded.

Figure 30 shows some typical load-displacement and load-strain data. One of the issues that was initially investigated concerned the filtering requirements for the data. The upper plot insets in Figure 30 are filtered using one strategy (an 8-pole, low-pass Butterworth filter) whereas the lower insets are filtered using another strategy (200-Hz low-pass commercial filters). Extreme care must be taken to ensure that the characteristics desired in the signal are not filtered out of the response. As it turned out, during this program the higher cutoff frequency option was the optimum to ensure measurement of conventional crack closure behavior. Figure 31 shows the difference between unfiltered and filtered data for some reduced load-displacement data. Clearly, the signal-to-noise ratio is high in the unfiltered data shown by the plot on the left side. The filtered data on the right of Figure 31 is clearly more suitable for measuring crack closure behavior.

SwRI performed crack closure measurements using the built-in techniques incorporated in the FTA test control computer. Nevertheless, the load-strain and load-displacement data measured also can be used to analyze net crack closure results. Figures 32 and 33 show some typical data and analysis using load-displacement data. The majority of the data included in Appendix A (except for some of the initial tests) include ΔK_{eff} columns in the tabular data where the crack closure analysis has already been performed.

The fracture surfaces generated during this program were generally quite smooth and somewhat featureless. Figure 34 shows two typical examples for a small bend specimen and one of the larger compact tension specimens. For each fracture surface, the Electrical Discharge Machining (EDM) notch can be observed on the right side, the fatigue region in the middle, and plane-stress plastic wings on the left side where fast fracture occurred. Global crack morphology issues, such

as planarity, deflection, and bifurcation, often observed during FCG and fracture investigations, were not an issue with TC-128B.

Figures 35 and 36 show photomicrographs of some typical fracture surfaces taken in the scanning electron microscope. In the case of the low r-ratio specimen (Figure 35), clear differences can be observed between low and high ΔK. The fracture surface features at higher ΔK clearly have a larger size than at lower ΔK. Furthermore, the fracture surface at higher ΔK tends to exhibit more texture and apparent roughness (e.g., more stringy lateral features) than at lower ΔK. These observations are contrasted with little observable difference between low and high ΔK for the high r-ratio fracture surface shown in Figure 36. Any other differences between the four images shown in Figures 35 and 36 are sufficiently subtle to require the careful analysis of a trained metallurgist.

4.4 Phase B Environmental Assessments

During Phase B, the tests were nominally constant ΔK tests that, in the absence of any change in environment, would have yielded a constant FCG rate. In terms of a crack growth curve, a constant crack growth rate test yields a linear crack length versus cycle count curve. Figures 37 to 40 plotted the data from each of the four constant ΔK tests in terms of the crack length versus applied cycle response. Each of the environmental segments is clearly identified in the legend associated with each set of data points.

In the case of test TC-A-3B shown in Figure 39, the test was stopped after only the third segment. Crack arrest was a continual problem in this test, and the growth rate was exceedingly small, especially after approximately 1.25 million cycles. The remainder of the tests behaved well and yielded data consistent with expectation.

Table 4. AAR TC-128B Specification, Mill-Certified Chemistries and Measured Chemistries for the Two Different Materials Supplied by the Two Tank Car Manufacturers (Quantities Are Shown in Weight Percent)

Element	AAR Spec (Tbl M128.04)	*Material A (Union)*		*Material B (Trinity)*	
		Mill Test	Measured	Mill Test	Measured
C	< 0.29	0.23	0.23	0.23	0.23
Mn	0.92 - 1.62	1.40	1.32	1.38	1.33
P	< 0.035	0.013	0.023	0.013	0.021
S	< 0.040	0.007	0.008	0.007	0.006
Si	0.13 - 0.45	0.440	0.37	0.21	0.22
Cu	< 0.35	0.012	0.03	0.04	0.05
Ni	< 0.25	0.01	0.01	0.02	0.02
Cr	< 0.25	0.02	0.02	0.17	0.17
Mo	< 0.08	0.059	0.07	0.05	0.07
V	< 0.08	0.060	0.05	0.040	0.07
Al	-	0.040	0.03	0.027	0.03
Nb	-	*n/r*	< 0.01	0.001	< 0.01
Ti	-	*n/r*	< 0.01	*n/r*	< 0.01
B	-	*n/r*	< 0.0005	*n/r*	< 0.0005
N	-	*n/r*	0.0092	*n/r*	0.0066
Sn	-	*n/r*	< 0.01	*n/r*	0.01

n/r-not reported (not necessarily required by AAR specification)

Table 5. Tensile Test Results for TC-128B (Trinity and Union Material)

Material	Orientation	Specimen ID	σ_{ts} (ksi)	σ_{ys} (ksi)	Elong. (%)	RA (%)
0.813-in plate (Trinity)	L	BL-1	*83.9*	*57.0*	*30.0*	*64.3*
	L	BL-2	*84.4*	*57.7*	*28.5*	*65.1*
	L	BL-3	*84.2*	*57.2*	*28.5*	*63.5*
	L_{avg}		**84.2**	**57.3**	**29**	**64.3**
	T	BT-1	*84.5*	*57.8*	*31*	*68.9*
	T	BT-2	*84.5*	*57.7*	*31.5*	*69.7*
	T	BT-3	*84.5*	*58.1*	*31*	*69.1*
	T_{avg}		**84.5**	**57.9**	**31.2**	**69.2**
0.781-in plate (Union)	L	AL-1	*85.3*	*59.0*	*29*	*61.9*
	L	AL-2	*85.6*	*58.8*	*28*	*62.2*
	L	AL-3	*85.3*	*58.6*	*29*	*63.7*
	L_{avg}		**85.4**	**58.8**	**28.7**	**62.6**
	T	AT-1	*86.2*	*59.6*	*30*	*68.1*
	T	AT-2	*87.9*	*59.5*	*29*	*66.4*
	T	AT-3	*86.7*	*59.9*	*30*	*68.1*
	T_{avg}		**86.9**	**59.7**	**29.7**	**67.5**
AAR Appendix M		**–**	**81-102**	**50 (min)**	**22 (min)**	

Table 6. Summary of Grain Size Measurements Performed on Both Materials

Material ID	Plane Normal	Measurement Position	ASTM Grain Size No.	Equiv. Grain Diam. 10^{-4} in
A	L	mid-thickness	8	9.74
	L	quarter point	8.5	8.19
	L	near-surface	9	6.89
	S	near-surface	8.5	8.19
	S	mid-thickness	9	6.89
	T	mid-thickness	8.5	8.19
	T	quarter point	9	6.89
	T	near-surface	9	6.89
B	L	mid-thickness	8.5	8.19
	L	quarter point	8.5	8.19
	L	near-surface	8.5	8.19
	S	near-surface	8	9.74
	S	mid-thickness	8.5	8.19
	T	mid-thickness	8	9.74
	T	quarter point	8.5	8.19
	T	near-surface	9	6.89

Table 7. Summary of MC-Burst Closure Data (CMOD and BFS)

Phase	Specimen ID	Test Condition	R-Ratio	File Prefix	File No.	Comments
A	TC-A-1A	K↓	0.1	a1aa	5-197	filter issues
		K↑	0.1	a1ab	7-627	
	TC-B-1A	K↓	0.1	vb1a	1-356	filter issues
		K↑	0.1	b1ab	1-56	
	TC-A-1B	K↓	0.1	a1ba	1-117	
		K↑		a1bb	1-49	
	TC-B-1B	K↓	0.1	b1ba	1-163	changed filtering hardware
		K↑	0.1	b1byb	1-158	
	TC-A-2A	K↓	0.6	a2ap	1-120	
		K↑	0.6	a2ab	1-206	
	TC-B-2A	K↓	0.6	b2ba	10-253	
		K↑	0.6	b2bb	1-71	
	TC-A-2B	Const ΔK	0.1-0.9	a2ab	1-373	
	TC-A-9	K↓	0.1	ba9a	1-33	
	TC-A-10	K↑	0.1	a10a	1-117	
	TC-A-11	Const ΔK	0.1-0.9	a11a	10-428	
	TC-A-12	K↑	0.1	a12a	1-219	
B	TC-B-3B	Const ΔK = 20 ksi√in	0.1	3bla	1-87	continuous data
	TC-B-2B	Const ΔK = 20 ksi√in	0.6	b2bf	1-126	
	TC-A-3B	Const ΔK = 8 ksi√in	0.1	a3bc	1-145	
	TC-A-3A	Const ΔK = 8 ksi√in	0.6	3ad6	1-699	

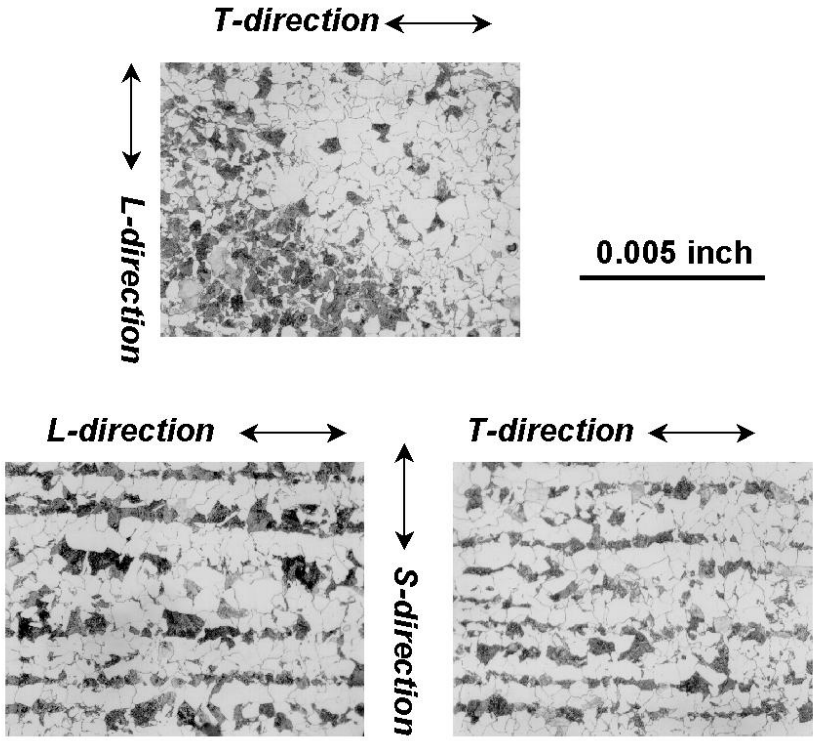

Figure 18. Grain Structure for the Three Planes of Material A (Material B Was Virtually Identical)

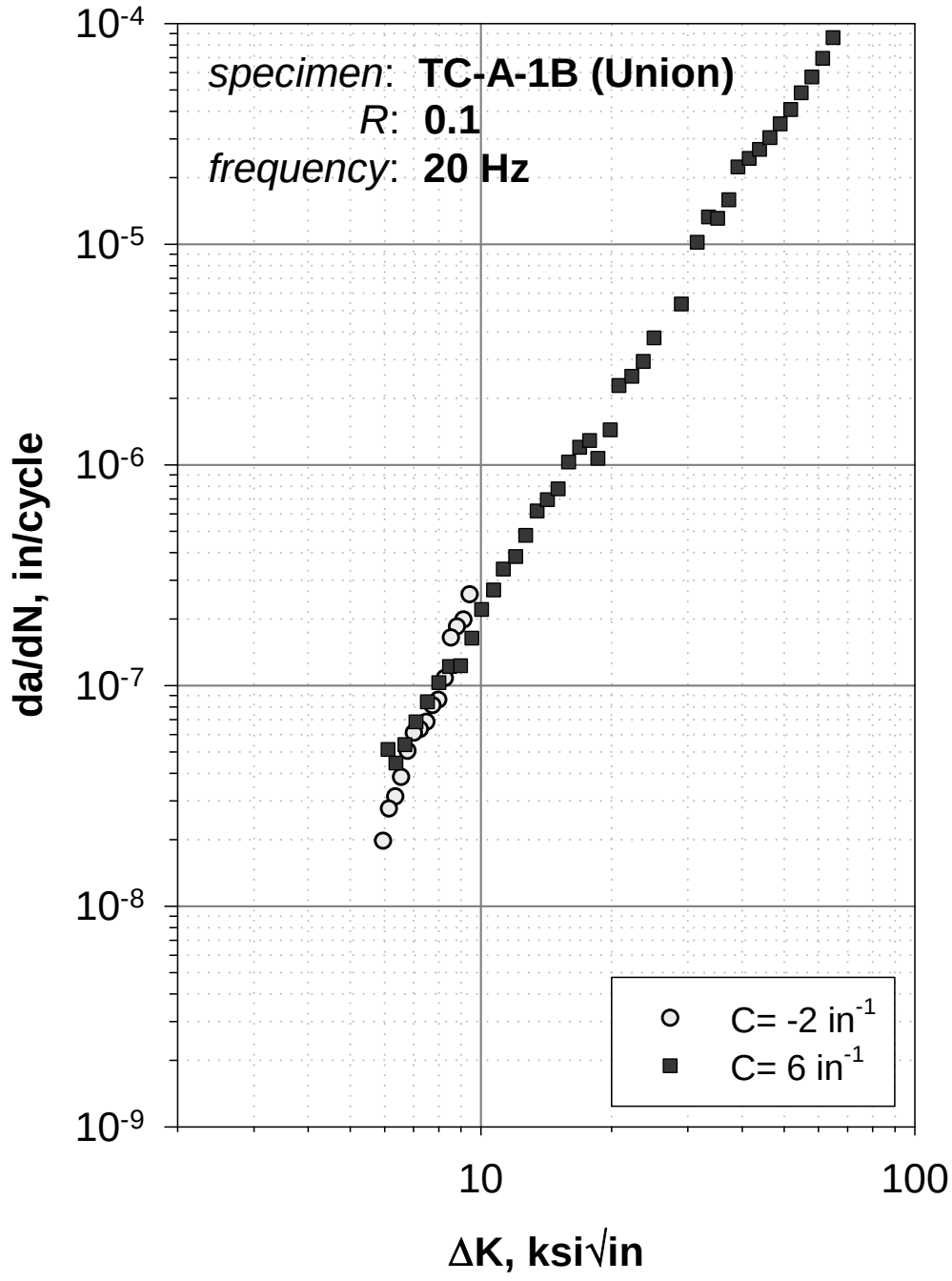

Figure 19. Test TC-A-1B: K-Decreasing and K-Increasing FCG Results at R = 0.1 (Union)

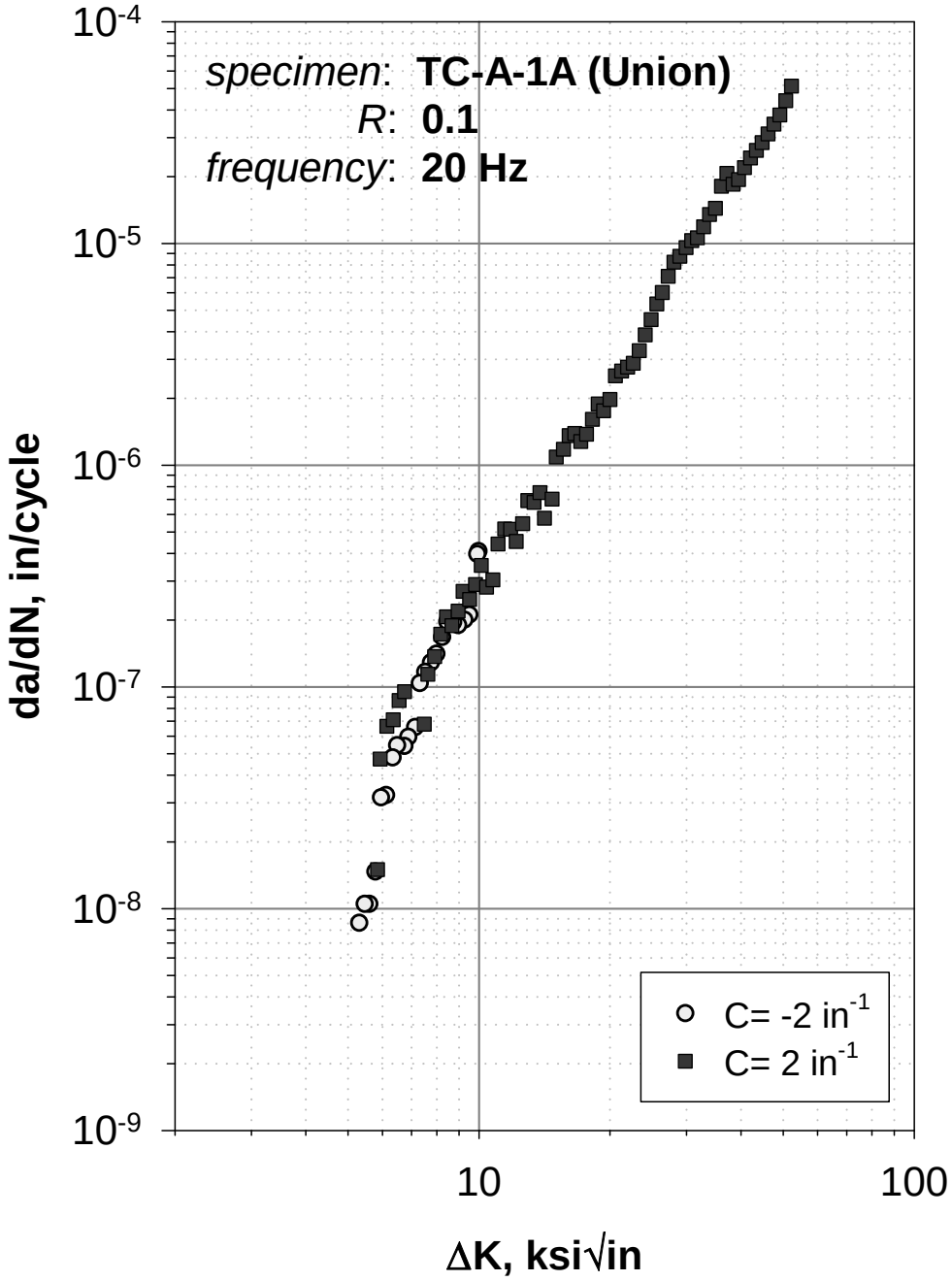

Figure 20. Test TC-A-1A: K-Decreasing and K-Increasing FCG Results at R = 0.1 (Union)

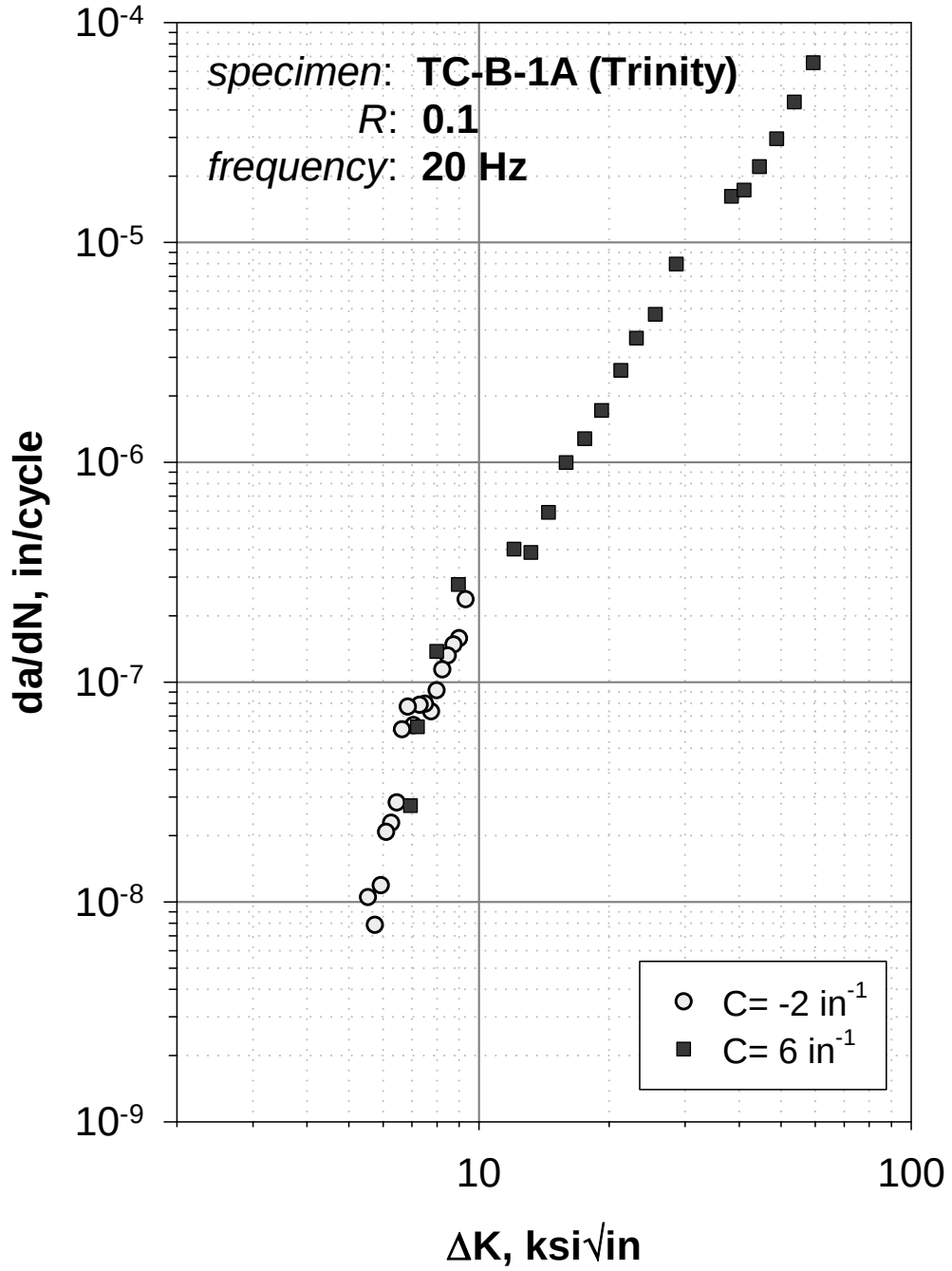

Figure 21. Test TC-B-1A: K-Decreasing and K-Increasing FCG Results for R = 0.1 (Trinity)

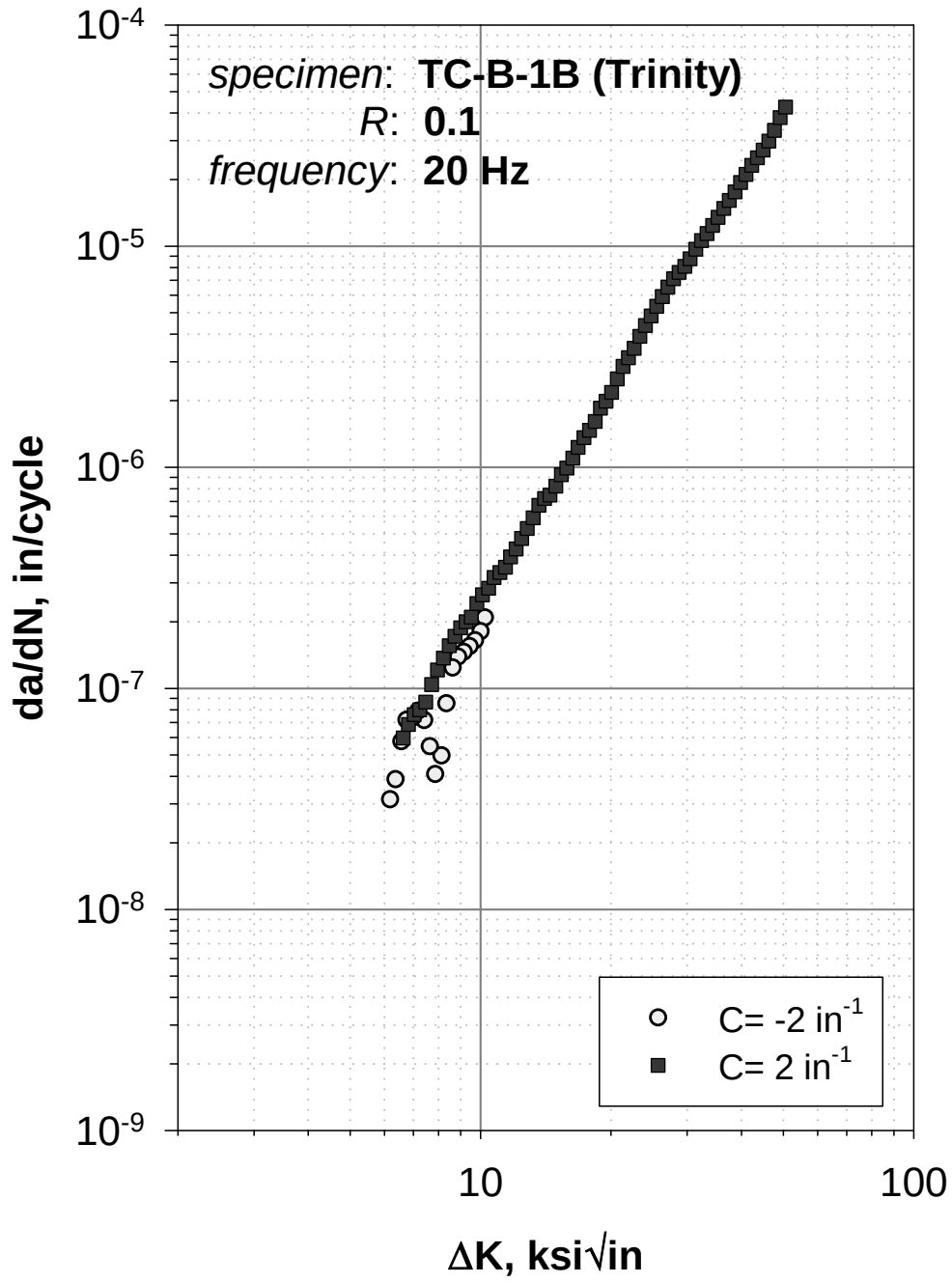

Figure 22. Test TC-B-1B: K-Decreasing and K-Increasing FCG Results for R = 0.1 (Trinity)

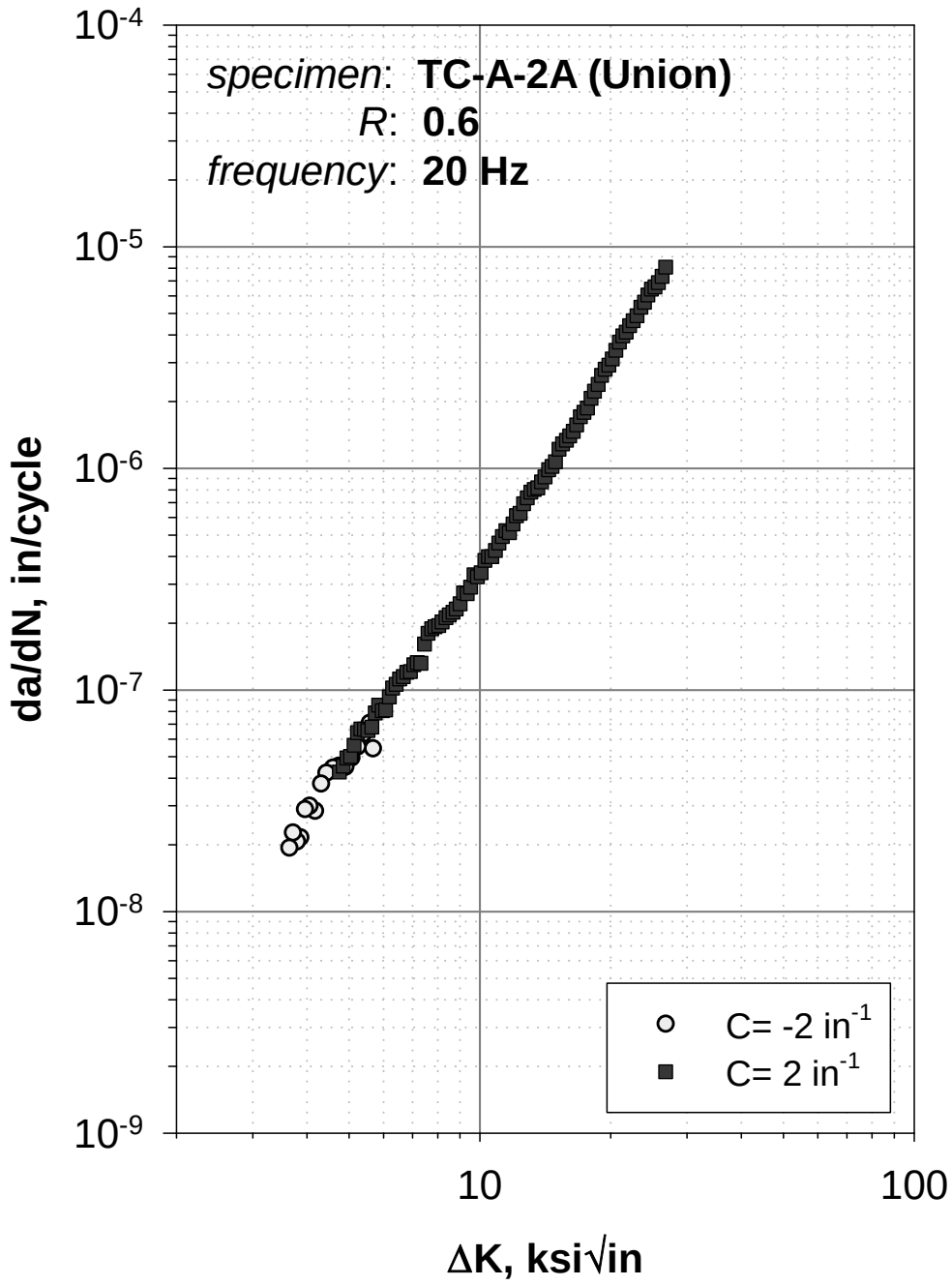

Figure 23. Test TC-A-2A: K-Increasing and K-Decreasing FCG Results for R = 0.6 (Union)

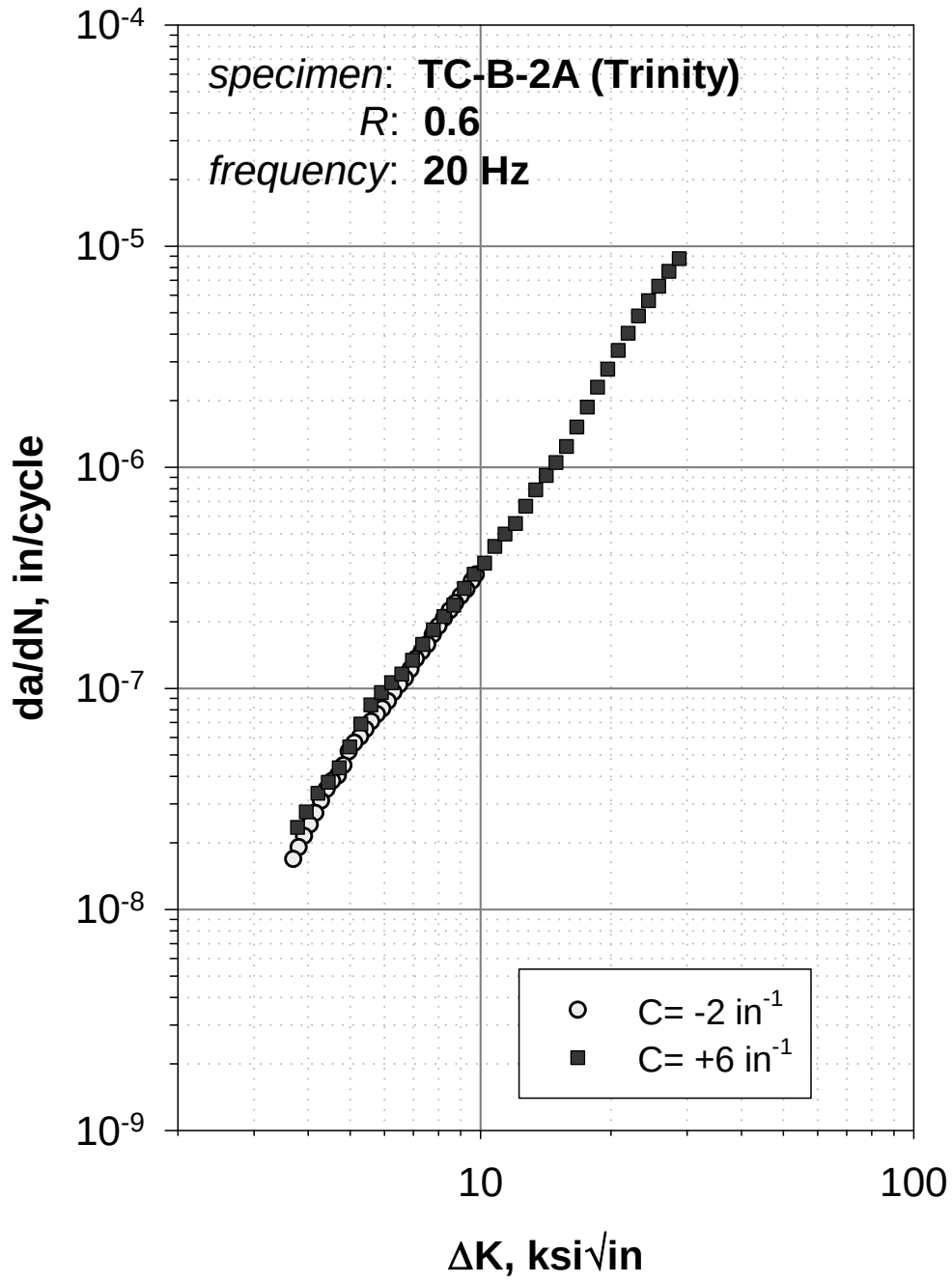

Figure 24. Test TC-B-2A: K-Decreasing and K-Increasing FCG Results for R = 0.6 (Trinity)

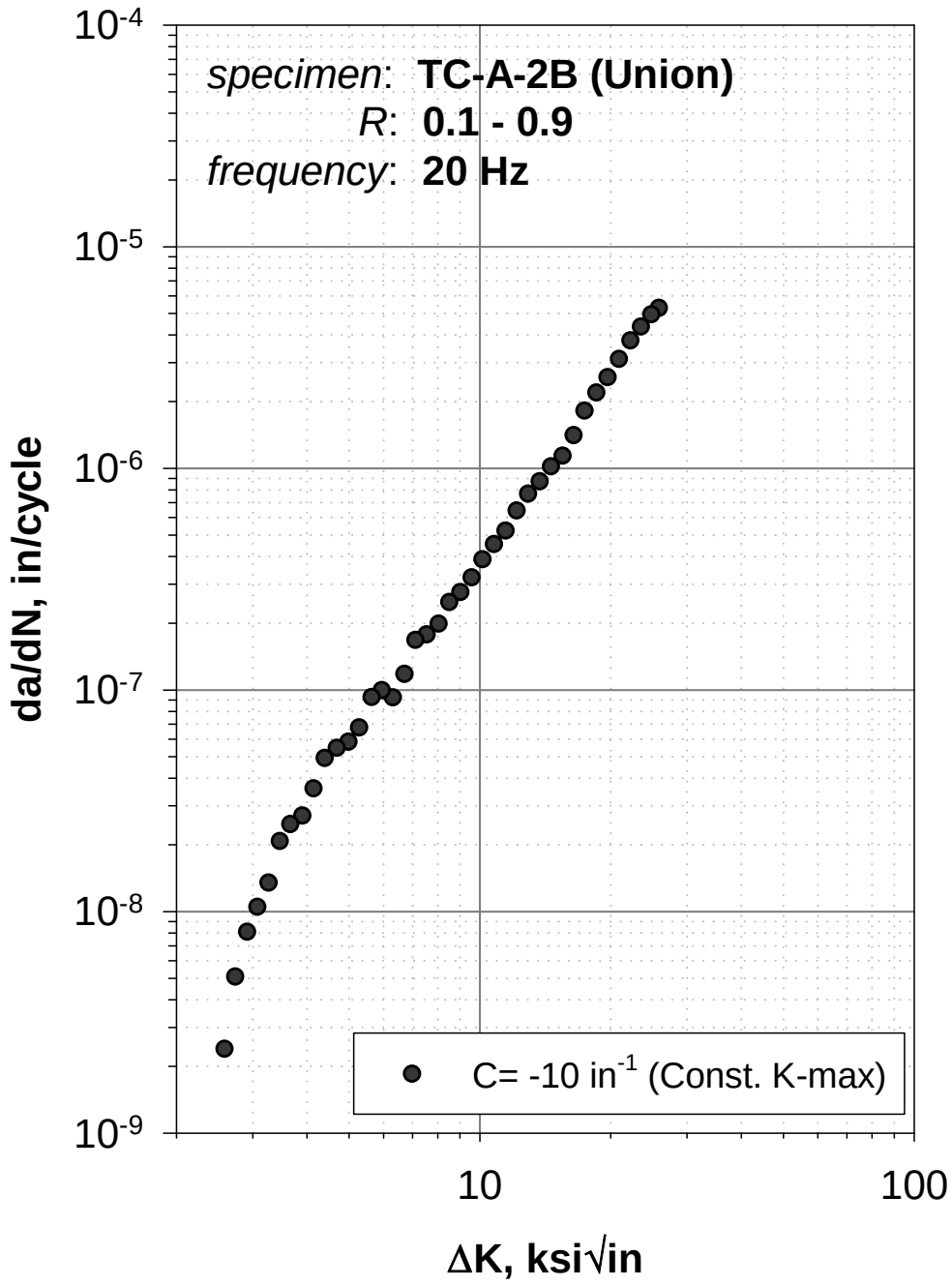

Figure 25. Test TC-A-2B: Constant K_{max} Results for L-T Orientation (Union)

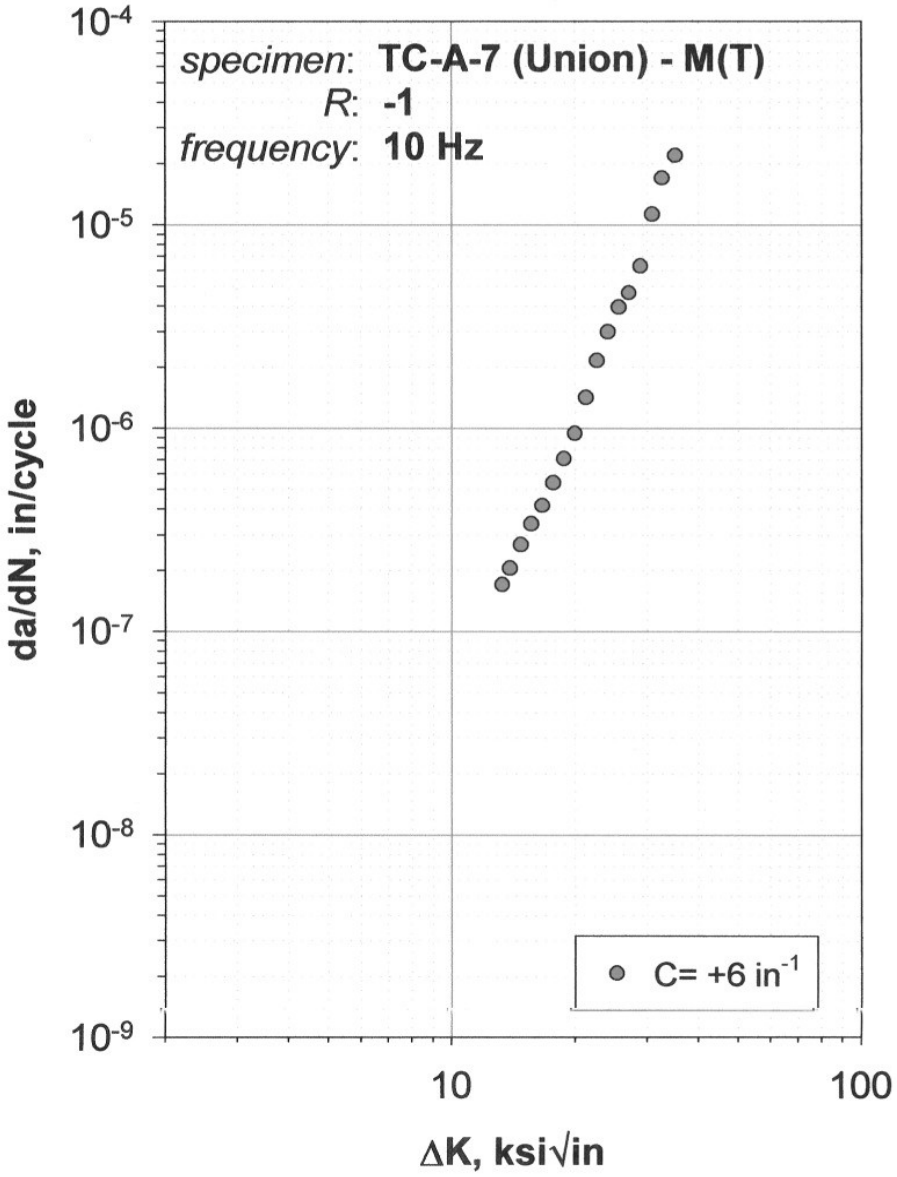

Figure 26. Test TC-A-7: R = -1 Results for L-T Orientation

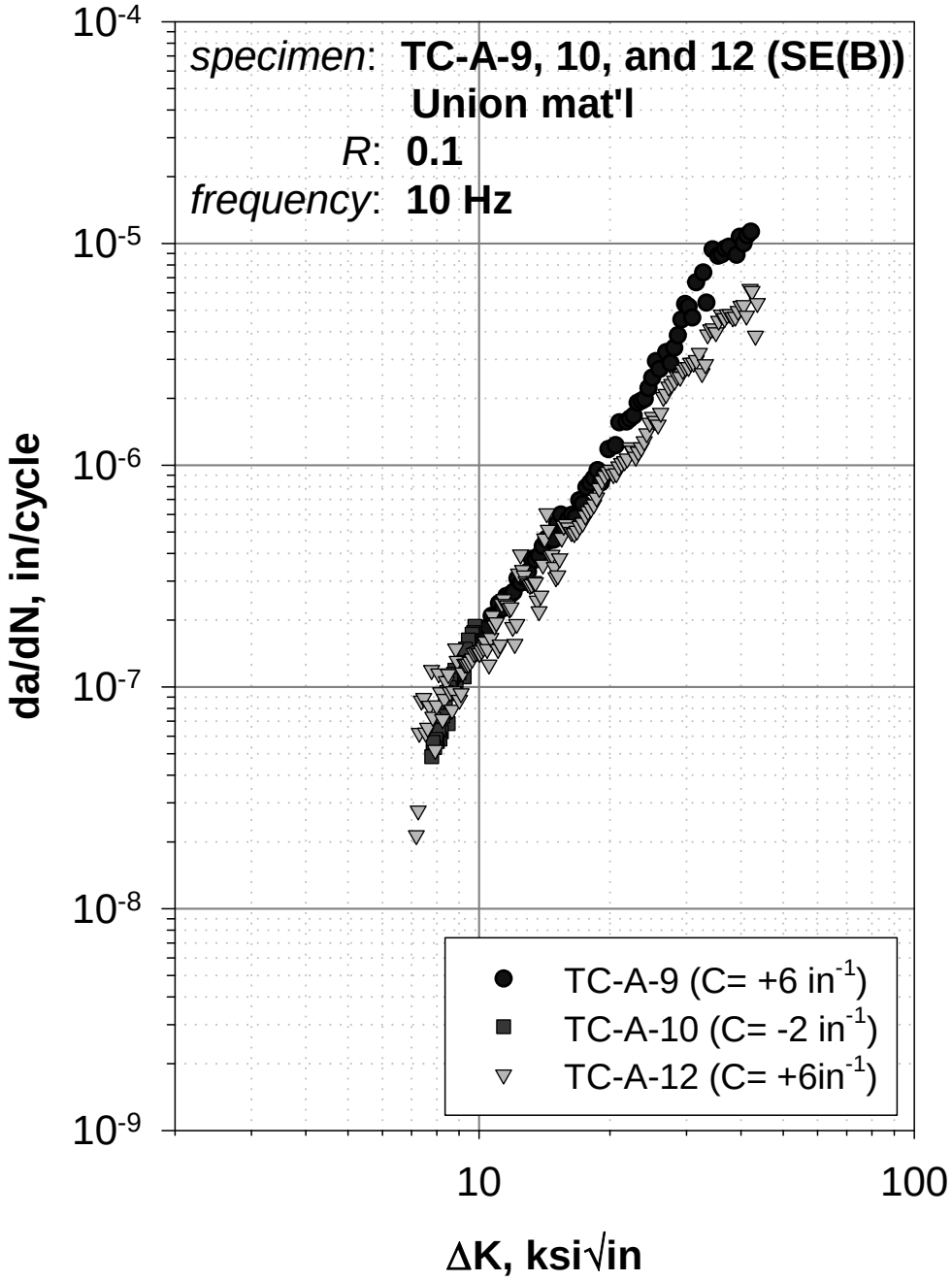

Figure 27. Tests TC-A-9, 10, and 12: FCG Results at R = 0.1 for L-S Orientation (K-Decreasing and K-Increasing Tests)

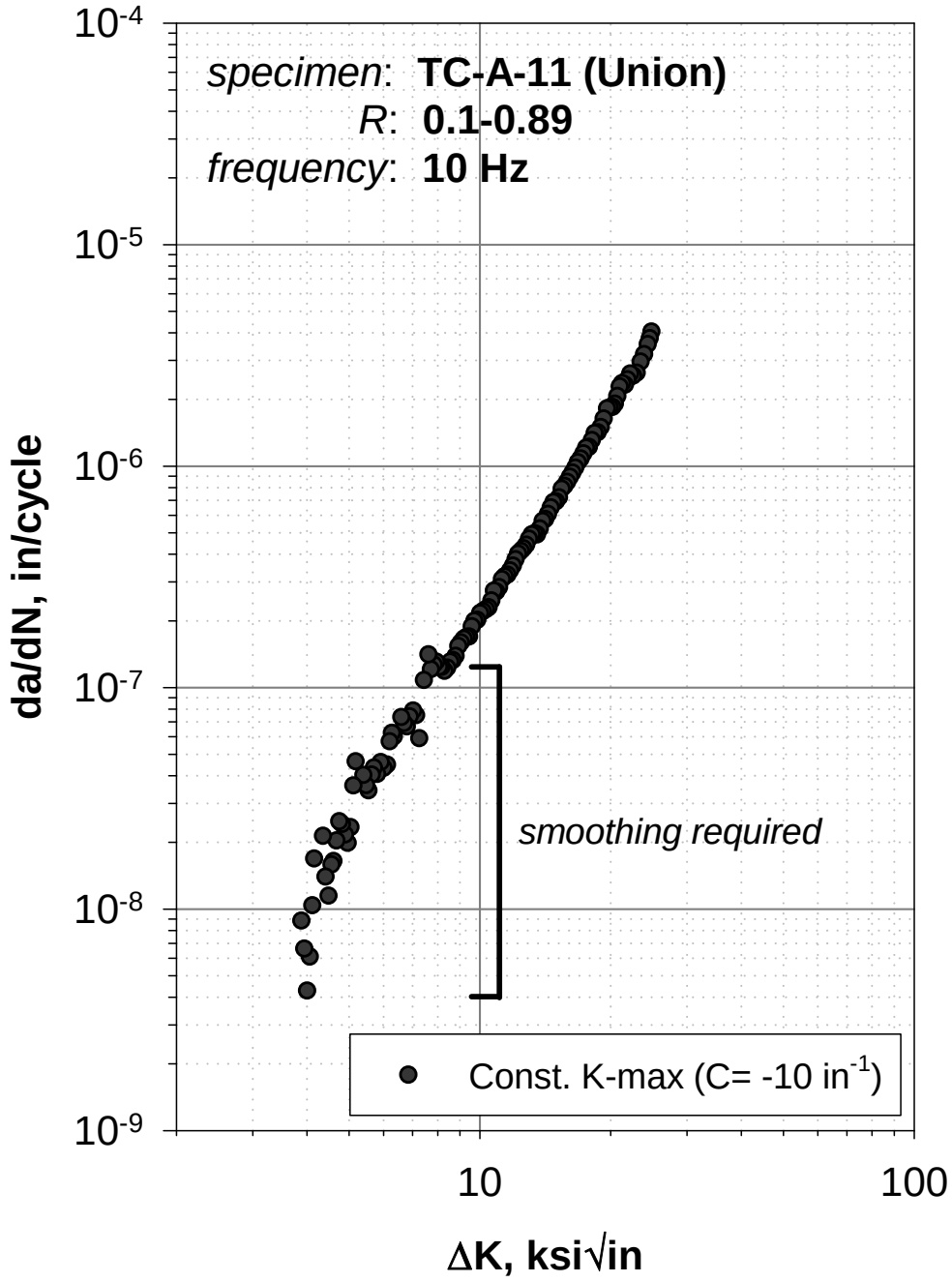

Figure 28. Test TC-A-11: Constant K_{max} FCG Behavior for L-S Orientation (Portion of Data Smoothed)

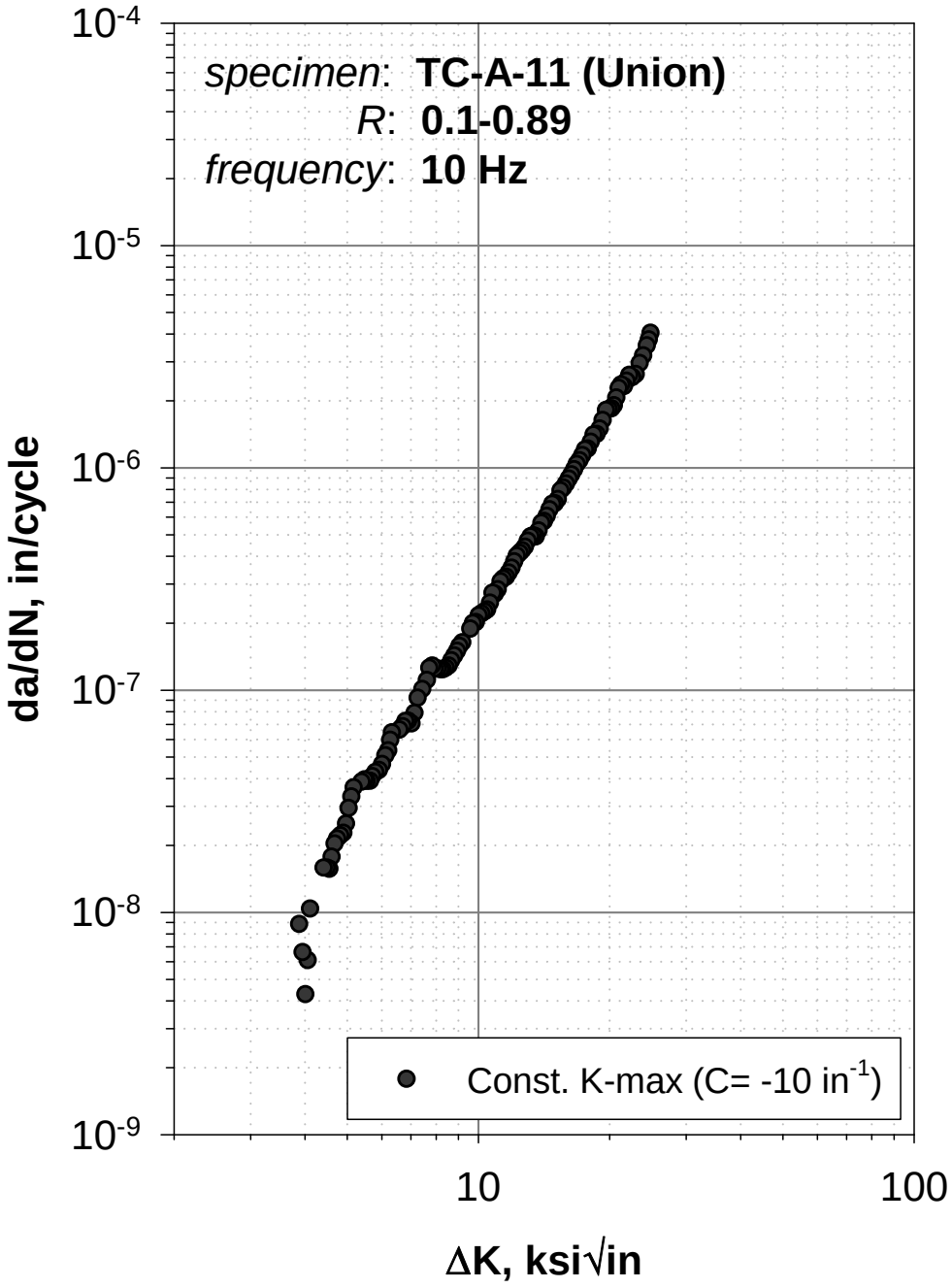

Figure 29. Test TC-A-11 (Smoothed): Constant K_{max} FCG Behavior for L-S Orientation

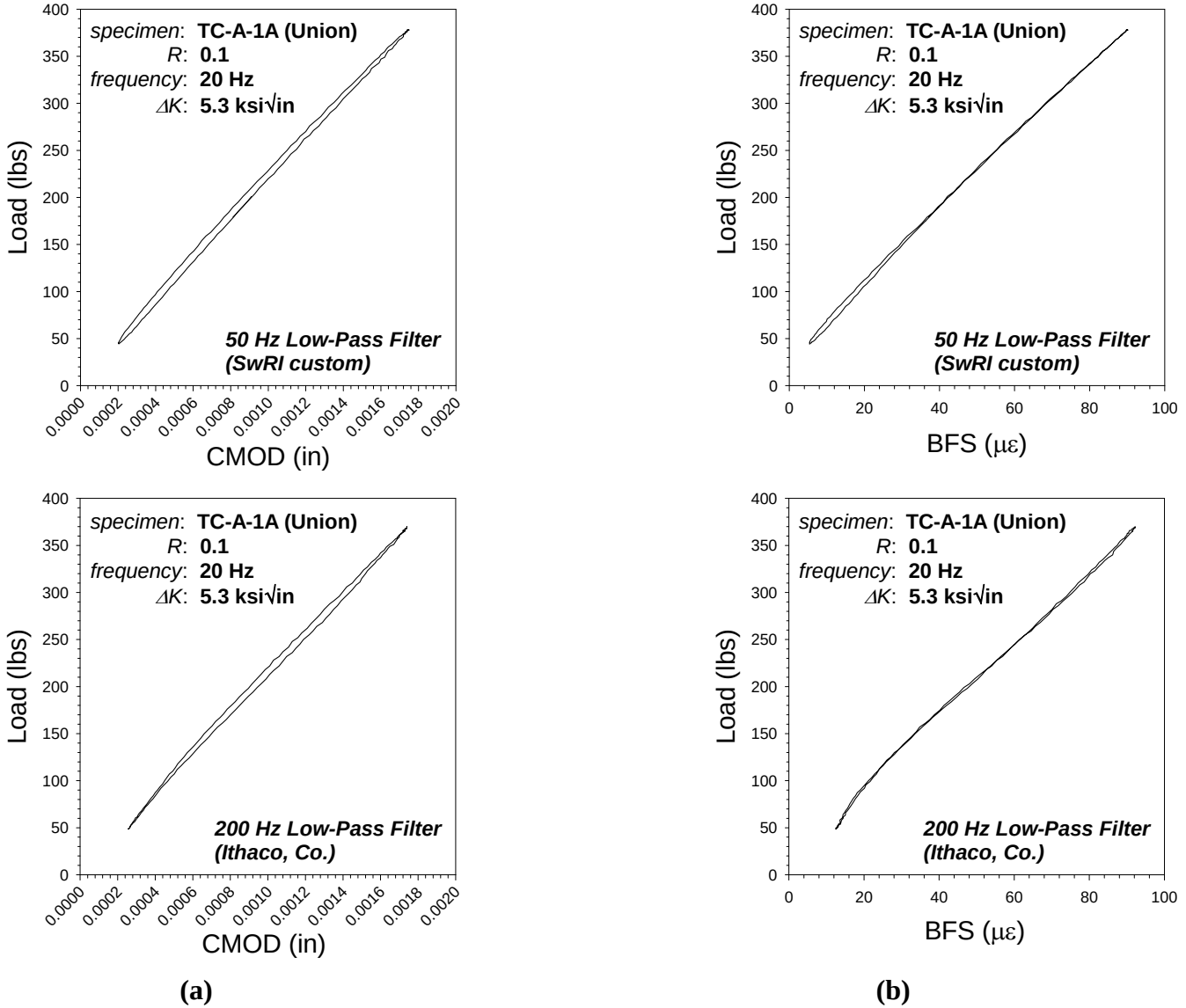

Figure 30. Raw Load-Displacement/Strain Data Overfiltered (50 Hz Top) and Filtered Appropriately (200 Hz Bottom) Showing (a) Clip Gage and (b) Strain Gage Data

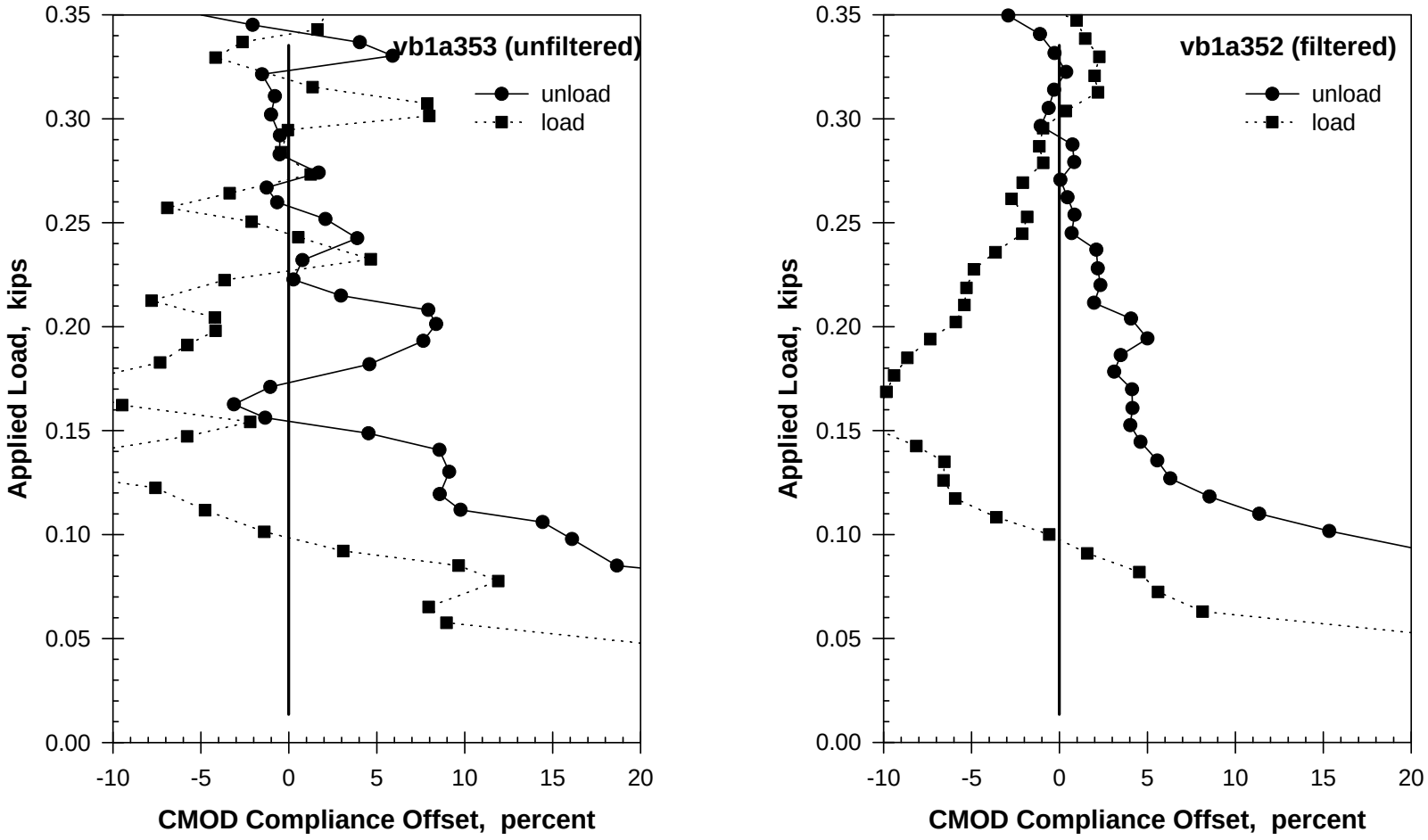

Figure 31. Comparison between Unfiltered and Filtered Data for the Clip Gage with Regard to Crack Closure Measurement (Data is from Specimen TC-B-1A at Approximately 9.5M Cycles)

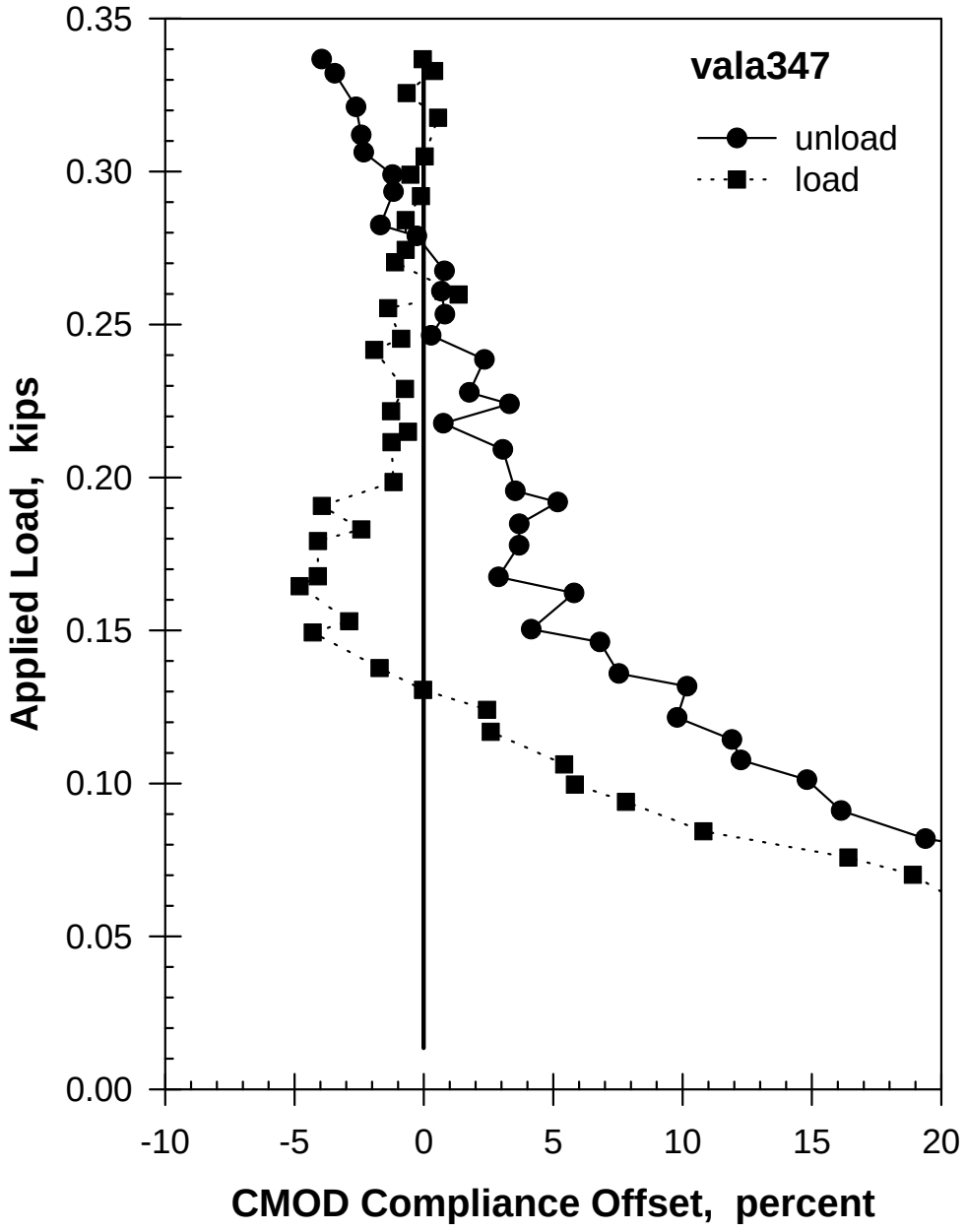

Figure 32. Typical Load-Compliance Offset Plot for Test TC-A-1A at Approximately 10M Cycles

```
                    * * * CLOSURE LOAD ANALYZER * * *

INPUT VALUES:
          Input file = va1a347.dat
         Consists of = 13 junklines and  4 chans
           Key Chans = No.  2 (load  1.0 kip/volt)
                       No.  3 (disp, polarity =  1.0)
     Anal start/stop = 1781,2748 (cycle No. 2)
       Big Intervals = 10 or 10.000 %
     Small Intervals =  4 or  2.500 %

LOAD TRIGGERS (kip):
     Max Load =  0.318 (90%)      Max Unload =  0.318 (90%)
     Min Load =  0.229 (65%)      Min Unload =  0.229 (65%)

DATASET EXTREMES (kip, volt):
     Max Load =  0.353      Max Strain =  0.334
     Min Load =  0.047      Min Strain =  0.049

DATASET COMPLIANCE:
     Unloading - C =    0.996   Int =  -0.019   Var =  0.0005   for 116 pts
       Loading - C =    0.956   Int =  -0.003   Var =  0.0006   for 115 pts

SEGMENTAL ANALYSIS:

       |       Unload Segments                    |       Loading Segments
  Seg  | #PTS  Pmin  Pmean    Var    CompOff      | #PTS  Pmin  Pmean    Var    CompOff
   1   |  84  0.322  0.337  0.0004    -3.95       |  89  0.320  0.337  0.0005    -0.04
   2   |  69  0.315  0.332  0.0004    -3.44       |  97  0.313  0.333  0.0005     0.39
   3   |  51  0.309  0.321  0.0003    -2.62       |  65  0.306  0.326  0.0004    -0.67
   4   |  50  0.300  0.312  0.0004    -2.42       |  62  0.298  0.318  0.0005     0.55
   5   |  39  0.293  0.306  0.0004    -2.32       |  48  0.291  0.305  0.0006     0.03
   6   |  49  0.285  0.299  0.0004    -1.21       |  38  0.281  0.299  0.0006    -0.52
   7   |  38  0.277  0.293  0.0005    -1.17       |  49  0.274  0.292  0.0007    -0.11
   8   |  37  0.270  0.283  0.0005    -1.68       |  39  0.267  0.284  0.0007    -0.70
   9   |  37  0.262  0.279  0.0005    -0.27       |  37  0.259  0.274  0.0006    -0.70
  10   |  36  0.254  0.268  0.0004     0.80       |  38  0.251  0.270  0.0005    -1.11
  11   |  45  0.247  0.261  0.0004     0.68       |  35  0.244  0.260  0.0004     1.34
  12   |  36  0.238  0.253  0.0004     0.82       |  35  0.237  0.255  0.0005    -1.38
  13   |  43  0.231  0.246  0.0005     0.28       |  34  0.229  0.245  0.0005    -0.88
  14   |  34  0.226  0.239  0.0005     2.34       |  32  0.222  0.242  0.0004    -1.92
  15   |  36  0.216  0.228  0.0005     1.76       |  35  0.213  0.229  0.0004    -0.73
  16   |  34  0.210  0.224  0.0005     3.31       |  42  0.206  0.222  0.0003    -1.27
  17   |  27  0.200  0.218  0.0005     0.75       |  34  0.199  0.215  0.0003    -0.61
  18   |  34  0.193  0.209  0.0005     3.05       |  35  0.191  0.212  0.0003    -1.25
  19   |  33  0.185  0.196  0.0005     3.53       |  33  0.182  0.199  0.0005    -1.17
  20   |  35  0.178  0.192  0.0005     5.17       |  24  0.176  0.191  0.0005    -3.94
  21   |  43  0.170  0.185  0.0006     3.69       |  35  0.167  0.183  0.0005    -2.42
  22   |  35  0.163  0.178  0.0006     3.69       |  35  0.160  0.179  0.0005    -4.09
  23   |  32  0.154  0.167  0.0005     2.89       |  35  0.152  0.168  0.0005    -4.10
  24   |  33  0.147  0.162  0.0005     5.81       |  36  0.146  0.164  0.0004    -4.80
  25   |  33  0.139  0.150  0.0004     4.15       |  34  0.139  0.153  0.0005    -2.89
  26   |  34  0.133  0.146  0.0004     6.80       |  34  0.131  0.149  0.0004    -4.30
  27   |  39  0.125  0.136  0.0005     7.54       |  35  0.123  0.138  0.0004    -1.71
  28   |  36  0.117  0.132  0.0005    10.18       |  45  0.114  0.131  0.0005    -0.03
  29   |  39  0.109  0.122  0.0006     9.79       |  36  0.108  0.124  0.0005     2.44
  30   |  48  0.102  0.114  0.0007    11.91       |  47  0.100  0.117  0.0005     2.59
  31   |  37  0.095  0.108  0.0006    12.26       |  48  0.092  0.106  0.0006     5.42
  32   |  49  0.087  0.101  0.0007    14.81       |  38  0.084  0.100  0.0006     5.83
  33   |  50  0.079  0.091  0.0007    16.13       |  50  0.077  0.094  0.0006     7.81
  34   |  53  0.071  0.082  0.0009    19.39       |  52  0.069  0.084  0.0006    10.81
  35   |  65  0.063  0.077  0.0009    23.29       |  52  0.062  0.076  0.0006    16.41
  36   |  83  0.056  0.066  0.0009    25.89       |  67  0.055  0.070  0.0007    18.90
  37   |  90  0.047  0.059  0.0008    25.75       | 105  0.047  0.059  0.0007    21.10

SEGMENTAL SUMMARY (compl. off.):
    Linear          Unload           Loading
              Min:  -3.95             -1.38
          Mean(-):  -2.12  ( 9)       -0.66  ( 8)
          Mean(+):   0.64  ( 4)        0.58  ( 4)
              Max:   0.82              1.34
    Global
              Max:  25.89             21.10

 CLOSURE LOADS:
                          Loads (kip)         Load Ratio          Status
     Absolute Criteria    Unload  Load       Unload  Load      Unload  Load
                    1% :  0.217  0.128       0.614  0.362       NO      ok
                    2% :  0.213  0.125       0.604  0.355       NO      ok
                    5% :  0.149  0.108       0.422  0.306       NO      ok

       Biased Criteria
            Mean(+)+1% :  0.214  0.126       0.608  0.358       NO      ok
            Mean(+)+2% :  0.211  0.117       0.597  0.333       NO      ok
            Mean(+)+5% :  0.148  0.104       0.420  0.294       NO      ok

             Max(+)+1% :  0.214  0.124       0.606  0.352       NO      ok
             Max(+)+2% :  0.210  0.114       0.595  0.323       NO      ok
             Max(+)+5% :  0.148  0.098       0.419  0.278       NO      ok
```

Figure 33. Closure Program Printout Corresponding to Data Shown in Previous Figure

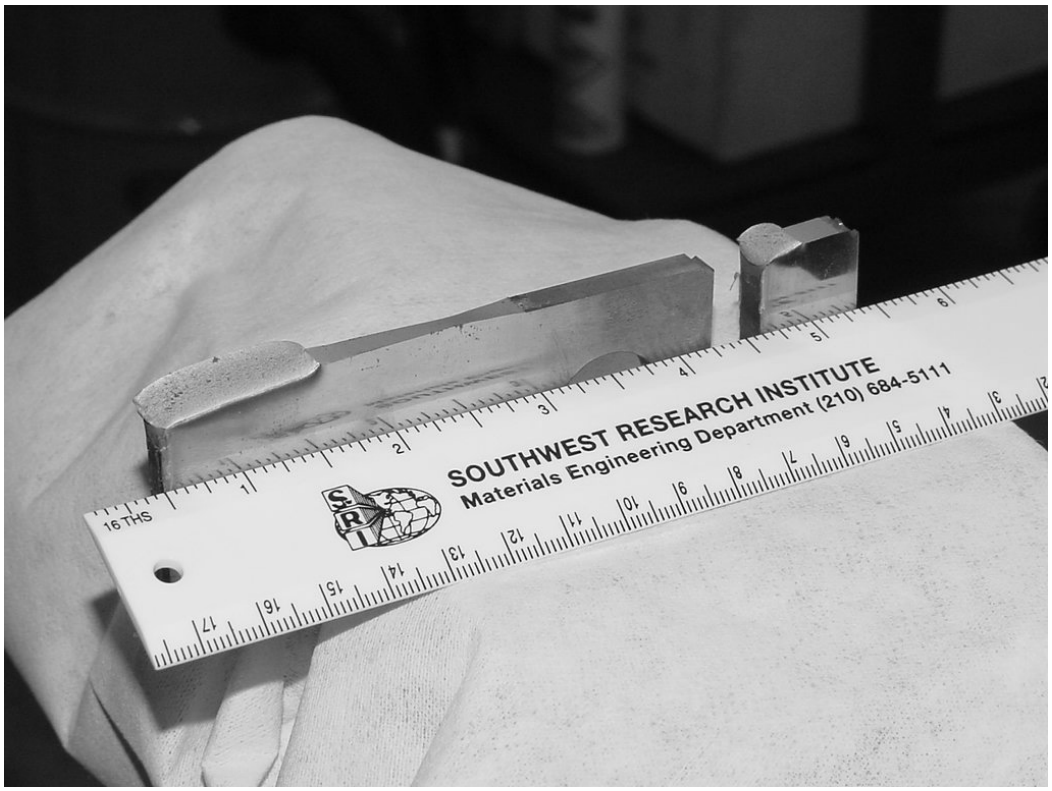

Figure 34. Typical Flat Fracture Surfaces Observed in Bend and C(T) Specimens

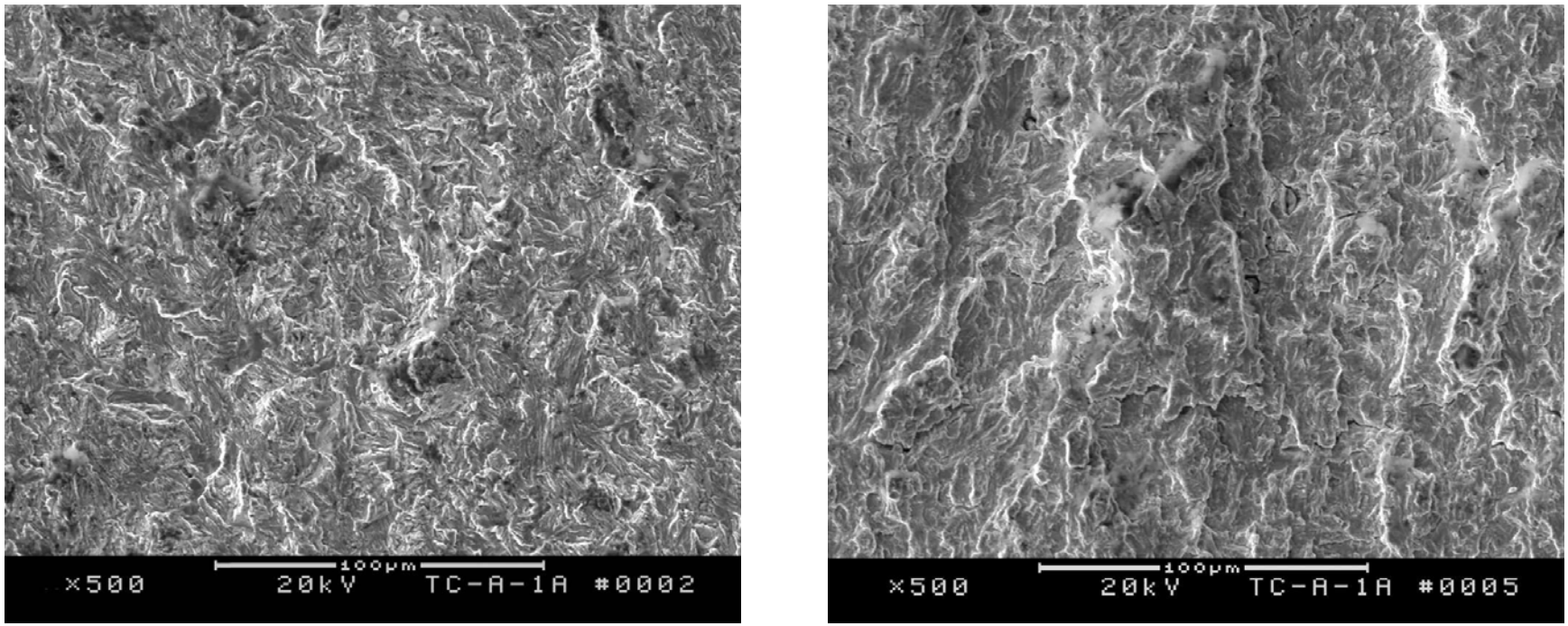

(a) (b)

Figure 35. SEM Micrograph of the Fracture Surface of an R = 0.1 Specimen at (a) 8 ksi√in and (b) 20 ksi√in (Crack Growth Direction Is from Bottom to Top)

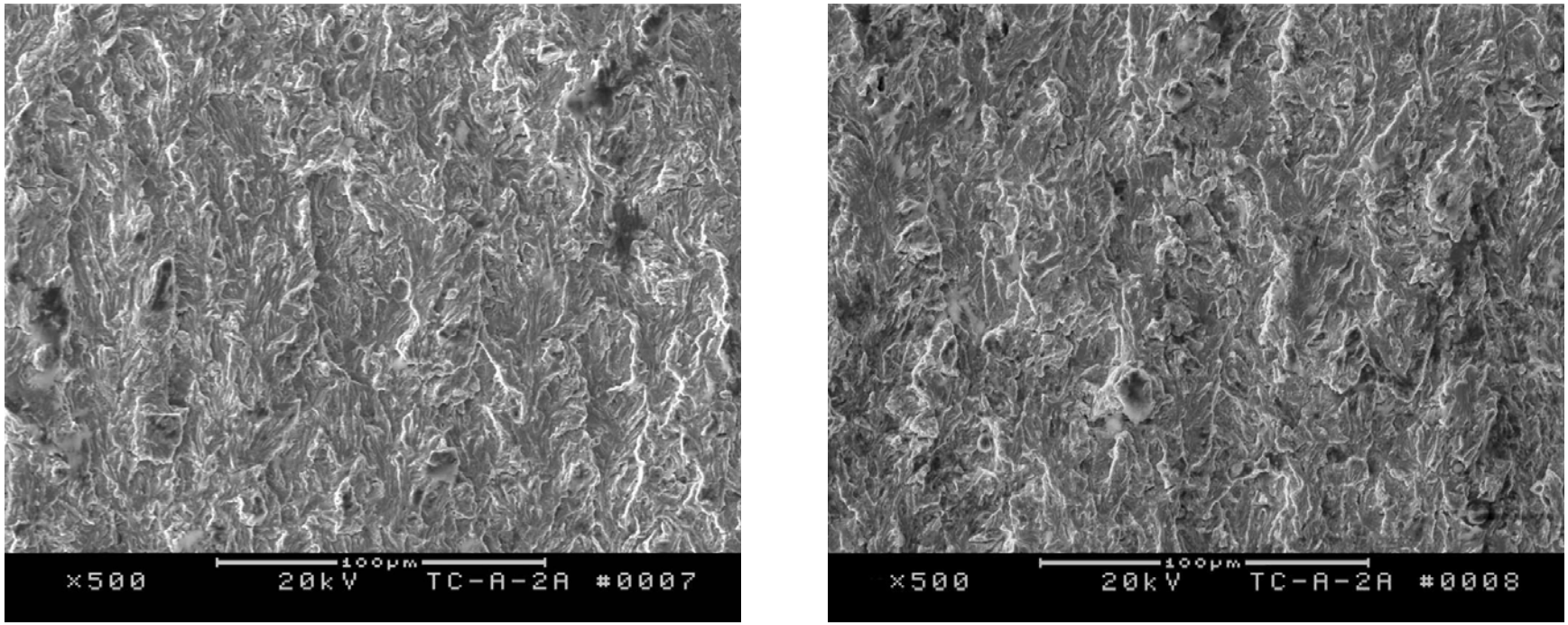

(a) (b)

Figure 36. SEM Micrograph of the Fracture Surface of an R = 0.6 Specimen at (a) 8 ksi√in and (b) 20 ksi√in (Crack Growth Direction Is from Bottom to Top)

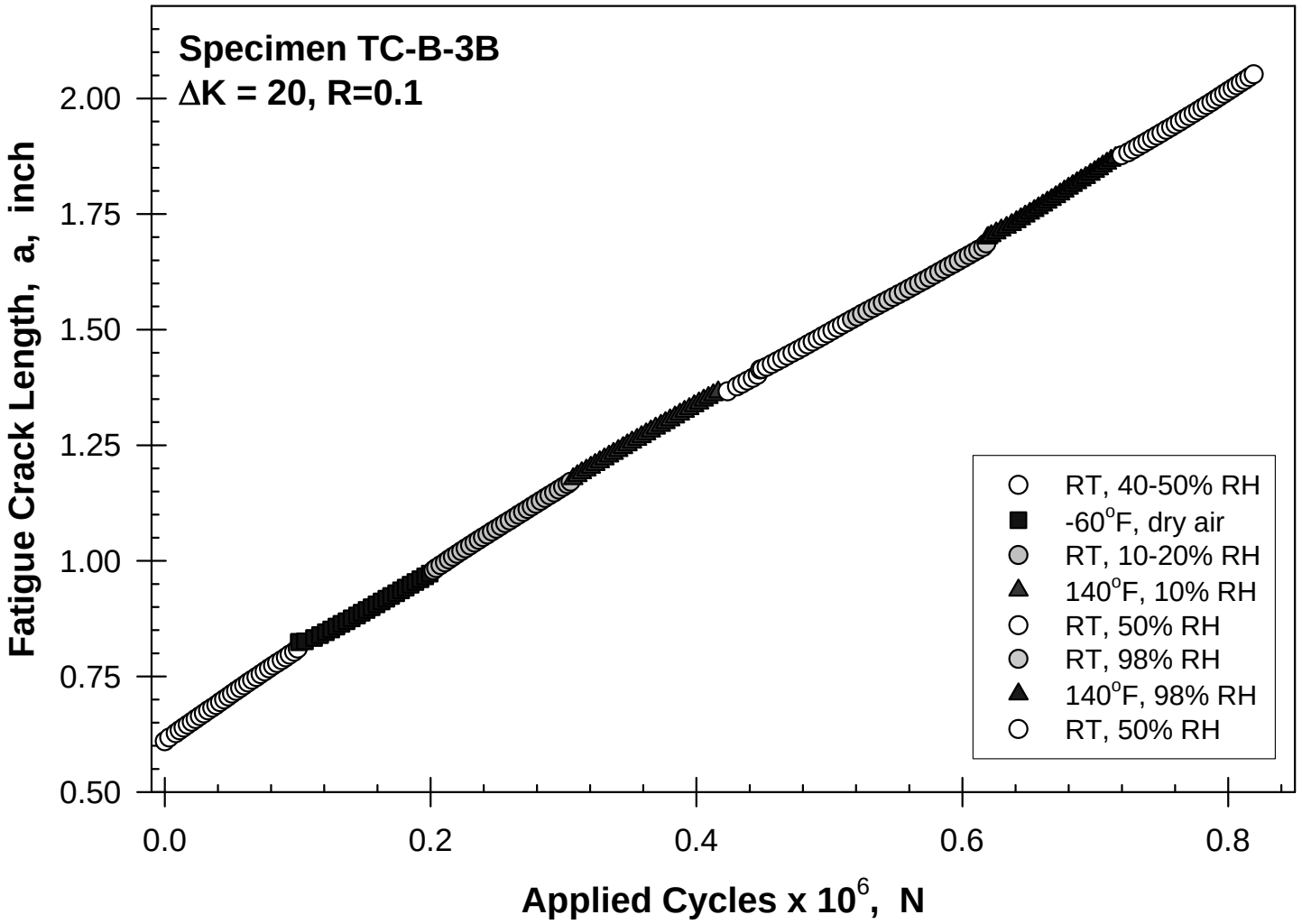

Figure 37. Phase B Environmental Crack Growth for High Constant ΔK, Low R-Ratio Conditions

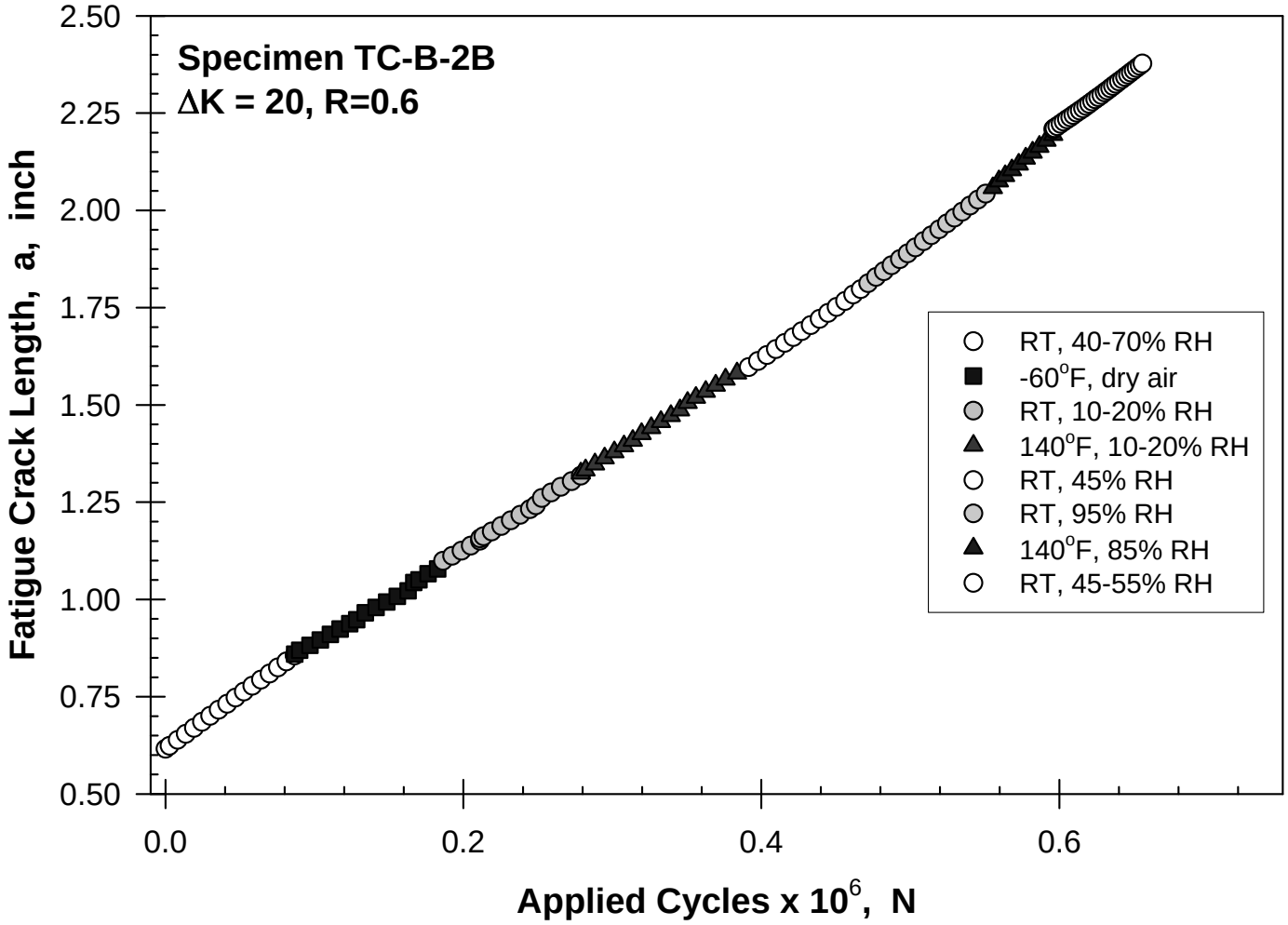

Figure 38. Phase B Environmental Crack Growth for High Constant ΔK, High R-Ratio Conditions

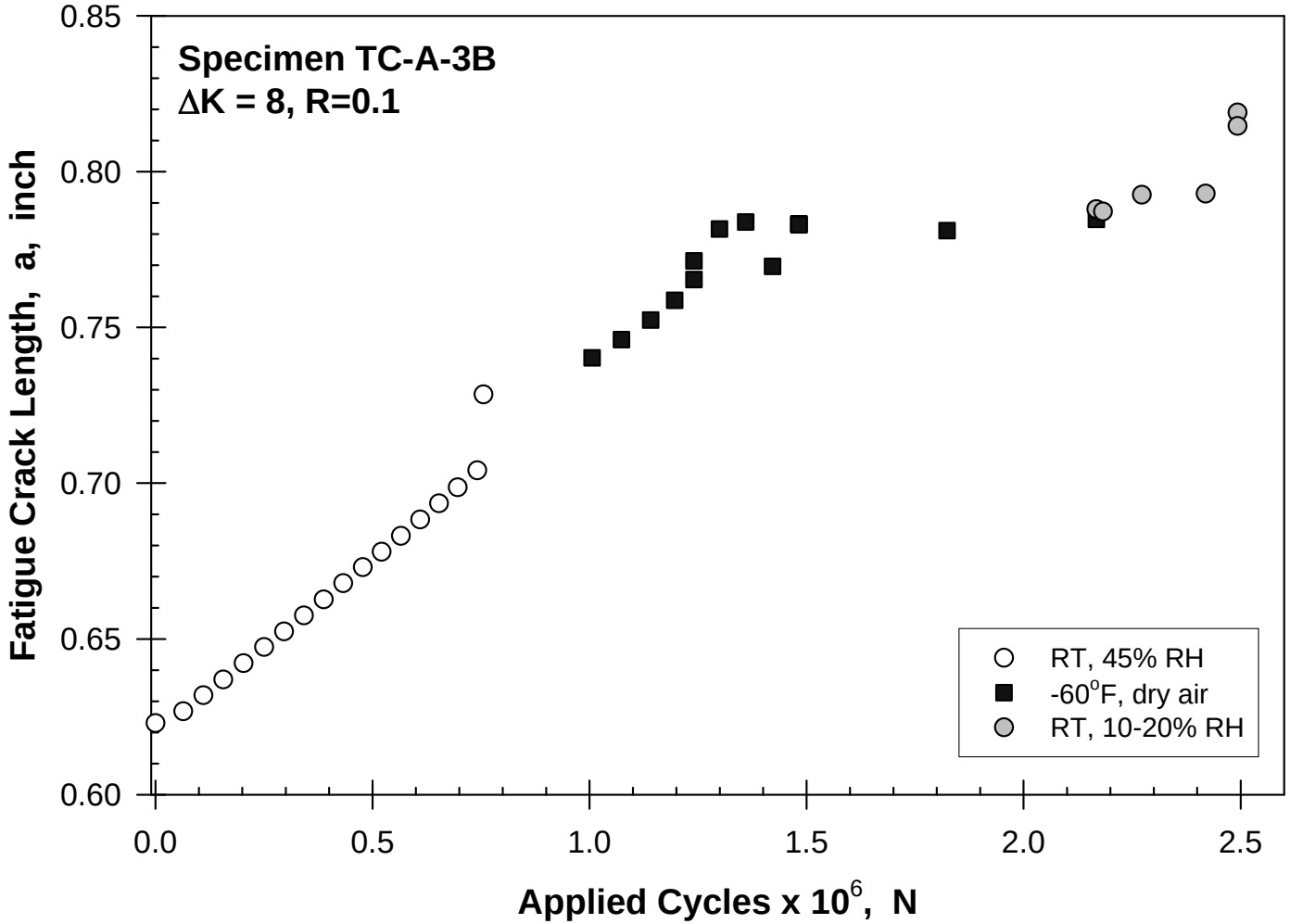

Figure 39. Phase B Environmental Crack Growth for Low Constant ΔK, Low R-Ratio Conditions

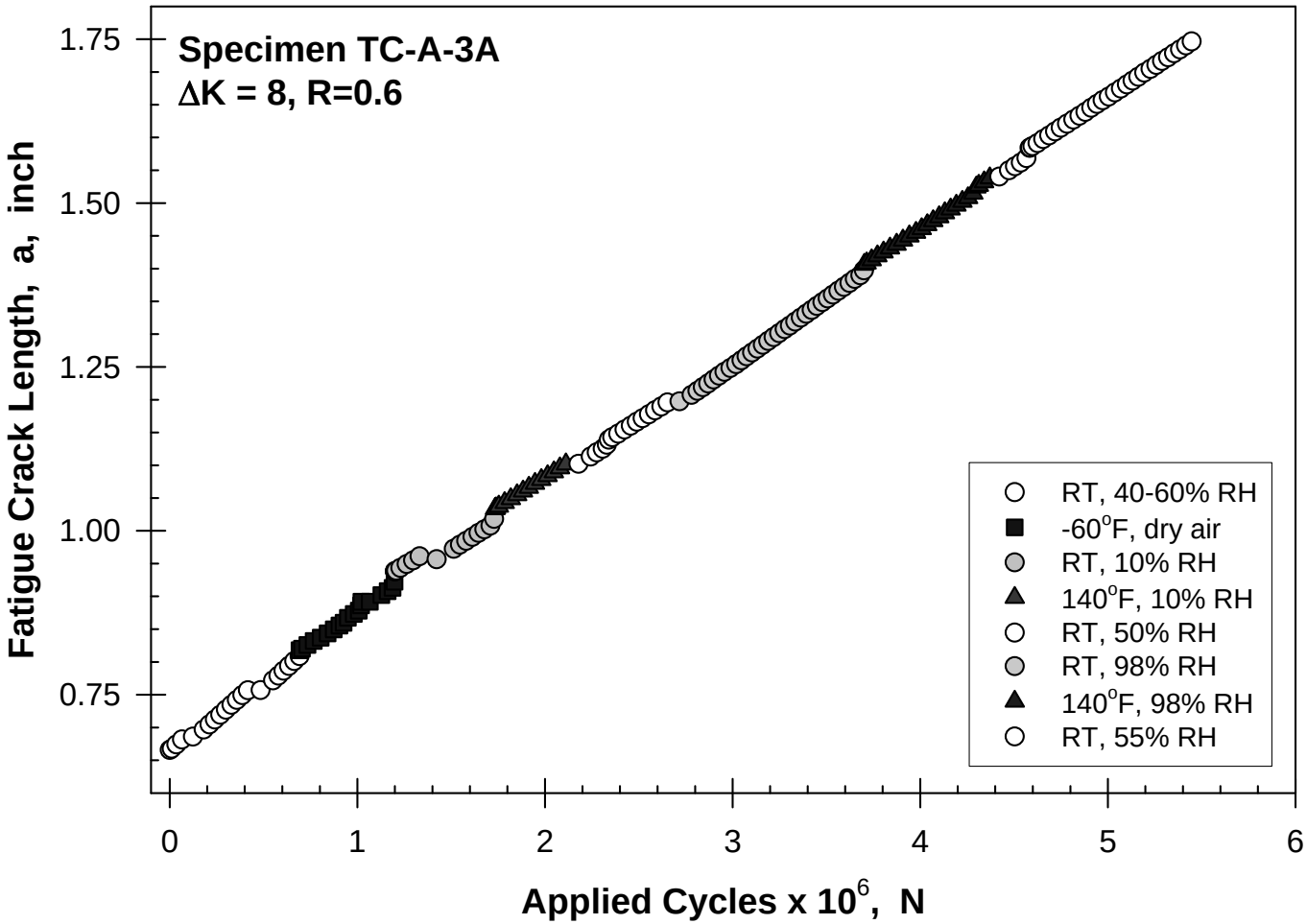

Figure 40. Phase B Environmental Crack Growth for Low Constant ΔK, High R-Ratio Conditions

5 Discussion

Prior to more fully examining the results and the observed trends, it is important to briefly review typical guidelines regarding repeatability in FCG rate tests. A careful study of the ASTM standard[1] suggests that typical FCG rate variability is approximately a factor of two times for a given ΔK level. However, the round-robin during which this factor was developed occurred over 25 years ago, and it is believed that repeatability has improved since that time. Nevertheless, scatter in steel materials can be as great as indicated in Figure 41[3]. In this case, the data shown in Figure 41 include the influence of such variables as welds, seawater, temperature, r-ratio, and orientation.

5.1 Phase A FCG Characterization

5.1.1 K-Gradient and Material Lot Effects

The pre-test expectation was that the effects of K-gradient and material lot variables would be slight. Nevertheless, it is important to assess this supposition experimentally. Figure 42 shows some representative test data for a two-segment (K-decreasing and -increasing) high r-ratio specimen in the L-T orientation. When performing K-gradient testing, it is important to ensure that the load history defined by the value of C, where C = dK/Kda, does not influence the test results appreciably. It is clear from Figure 42 that the K-decreasing ($C < 0$) segment agrees remarkably well with the K-increasing segment. This data also indicates how well the material replicates FCG behavior in the Paris region and the excellent level of control achieved during the test. The obvious conclusion is that the C values chosen for the decreasing and increasing segments are suitable and do not bias the FCG results.

Scatter in FCG rates, such as that shown for A36 steel in Figure 41, is often attributed to material lot variability. Admittedly, A36 steel is not a tightly controlled grade, and the data in Figure 41 samples a wide range of variables, including load ratio, orientation, temperature, corrosive environments, and welds (note that all of these variables are commonly encountered in tank car structure). Nevertheless, the small influence of material lot (Type A or B) on FCG properties for TC-128B is apparent from the low and high r-ratio data shown in Figure 43. The data for each material at each stress ratio consists of results from both increasing and decreasing ΔK tests. The similarity between the FCG responses for Types A and B material is striking. At the lower r-ratio, greater variability within and between the datasets is apparent. At the higher r-ratio, when one expects less effects of crack closure (a contributor to variability), the agreement between the material response is excellent.

5.1.2 Orientation and R-Ratio Effects

Conventional fatigue wisdom suggests that the influence of orientation and r-ratio should be greater than observed for the variables examined so far. Figure 44 shows data from the in-plane L-T and through-thickness L-S orientation for R = 0.1. Although a greater level of variability is noted for the L-S orientation (which is more in accordance with ASTM guidelines at the higher growth rates), a clear difference between the two orientations is evident, especially in the Paris

regime at higher ΔK levels. The FCG rates are slower in the L-S orientation i.e., as the fatigue crack grows through the thickness of the material. This is significant since a high percentage of cracks in tank cars are typically surface initiated (due to bending or residual stress effects) and grow through the thickness of the tank.

Constant r-ratio test results are contrasted in Figure 45 with the constant K_{max} test data where the r-ratio is increased from 0.1 to 0.9 as ΔK is decreased. In the Paris regime of the data, the difference between low and high fixed r-ratio data is slight, typically on the order of two times or less. This difference increases as the FCG rate decreases to less than 10^{-7} in/cycle, regardless of orientation. The constant-K_{max} FCG data in the L-T orientation follows expectation by mirroring the low R data at the start of the test (at high ΔK) and then following the high R data until close to threshold. The high r-ratio threshold for the L-T orientation is in the range of 2-3 ksi√in whereas at low r-ratio it appears more on the order of 5-6 ksi√in. This trend is consistent with typical material behavior where ΔK_{th} decreases as r-ratio increases. This behavior for the L-T orientation is in contrast to the L-S case in Figure 45, where the constant-K_{max} data suggests a high r-ratio threshold of 3-4 ksi√in.

Figure 46 shows negative r-ratio data with the previous L-T data from Figure 45. Although the data appear somewhat obscured from the other datasets on the plots, careful observation of Figure 46 will show that the R = -1 data typically exhibit the lowest growth rates for all conditions at a given ΔK. The overall difference between positive and negative r-ratio, however, is slight. Nevertheless, the observed trend for tension-compression loading conditions is consistent with that observed in other materials, including light alloys and steels, although the effect in most materials tends to be greater than the data shown in this report.

5.1.3 Comparison of FCG Data with Other Sources

The FCG data shown so far exhibit excellent repeatability, and all general trends are in accordance with expectation. It is rare that the FCG behavior of a candidate material is as well characterized as the TC-128B studied in this report. In this case, someone performing a damage tolerance analysis (DTA) must use one of the empirical relationships derived for steel. Three relationships [4-6] apply to different strength levels and classifications of steel. Nevertheless, an examination of each clearly indicates that all are fairly similar. The most conservative of these relations (in terms of predicting a slightly higher FCG rate at a given ΔK level) is that derived by Hudak, Burnside, and Chan (HBC)[4] for structural and low-alloy steels. This empirical relationship, nominally called the HBC relation, is divided into low and high r-ratio behavior (R > 0.5) and is shown with the constant-K_{max} FCG data for the L-T and L-S orientations in Figure 47.

The L-T data in Figure 47 follows this expectation: at the start of the constant-K_{max} test (i.e., at high ΔK), the data are on the low r-ratio HBC line; as the test progresses, the data clearly move toward the high r-ratio line, diverging only as ΔK decreases toward threshold. The data for the L-S orientation are clearly different. Even though R varied from 0.1 to 0.9 during the test, the data remain underneath the low R HBC line. This suggests that (a) the L-S orientation exhibits very slight r-ratio effects (since the data are parallel to the HBC relation) and (b) the observed growth rate in the L-S orientation is slower than predicted by the HBC relationship.

Prior to the earlier described damage tolerance effort, the tank car industry did not require FCG data for TC-128B material. Therefore, to the team's knowledge, no FCG data other than that shown in this report are believed to exist for TC-128B. A612 material is fairly similar in composition and overall mechanical properties, although it is believed that the microstructure and toughness are not as well controlled as in TC-128B. A survey of the literature identified A612 FCG data is found in Poon and Hoeppner[7]. These data are plotted in Figure 48 with the TC-128B data band from the R = 0.1 and 0.6 data in Figure 46. Although the scatter in the literature data appears greater than in the current data, the overall trend agrees reasonably well. It is difficult to tell definitively, but the difference between FCG rates at an R of 0.1 and 0.6 in the Poon data may actually be less than observed herein.

The observation of comparable FCG properties when contrasting 2000 vintage TC-128B and 1977 vintage A612 method is interesting from the viewpoint of the aging tank car fleet. A recent source[8] indicates that the average age of privately operated tank cars is 16.6 years, with 42 percent of the fleet built more than 20 years ago. If the A612 surveyed by Poon is consistent with the same vintage TC-128B, the FCG properties measured for this study might be applicable to older TC-128B tanks in the fleet, not just the newer generation. The hypothesized link between fatigue properties of a 25-year-old A612 and those of similar vintage TC-128B is as yet unsubstantiated. This is, however, a reasonable possibility and worthy of further attention.

The data included in this report provide a baseline assessment of the FCG behavior of TC-128B. Using relations derived from these data in a DTA analysis is clearly more optimal than using a standard relationship, such as the HBC model, since it will yield more accurate life prediction. Nevertheless, it is worth noting that the data agree generally with the HBC model and with the A612 data from the literature. One clear feature of this work is that the data extend all the way down to near threshold, a regime not included in any of the models in References 4-6 and critically important for accurate life prediction. Another significant aspect of this data is FCG behavior in the L-S orientation, which is the critical orientation of primary concern if the objective is to prevent lading leakage.

5.2 Phase B Environmental FCG Data

5.2.1 Role of Environmental Variables

It is useful to briefly review the varied environmental conditions encountered during this work. In the context of this discussion, the general term environment is used to refer to thermal and moisture perturbations. The range of temperature was – 60 ^{o}F to 140 ^{o}F, and moisture ranged from dry air to 100 percent relative humidity.

The raw crack length versus cycle count data shown in Figures 37 to 40 were processed to yield incremental FCG rates in Figures 49 to 52. The first two high ΔK conditions (low and high r-ratio) are shown, followed by the two lower ΔK conditions. Some consistency exists in the behavior observed regarding the role of environmental variables. Nevertheless, in general, the environment had a fairly small impact on overall crack growth rates. If the range of the data in

Figures 49 to 52 is examined closely, it can be fairly stated that, in general, environment impacted FCG rate by an approximate factor of 1.5x (increase or decrease).

Given this general observation, it is useful to examine the trend of the individual environmental segments. In the case of all the loading conditions, when the transition is made from room temperature to dry conditions at low temperature, the FCG rate always decreases. As temperature is increased to 140 ^{o}F and humidity is kept low, however, the FCG rate tends not to vary much. In fact, other than the initial FCG rate decrease with dry and low temperature conditions, no consistent trend is evident with any of the FCG rate data.

5.2.2 Comparison to Literature Data

The approximate rule of thumb is that aqueous FCG rates are approximately two times greater than nominal room temperature levels. In view of the data shown in Figures 49 to 52, the observed impact of both dry to high-humidity air (HHA) and cold to hot was slightly less than this factor of two.

These results are directly contradictory to the limited environmental results presented by Poon and Hoeppner [7]. These investigators found, however, the temperature was lower than that observed on a material whose temperature/ductility curve might have been vastly different. Moreover, they quote some enormously high threshold values, even for room temperature testing (8 and 19 ksi$\sqrt{}$in). This observation is also directly contradictory to the observation made in this report of higher levels. Nevertheless, as the one constant ΔK test (TC-A-3B at low r-ratio and ΔK) indicated, it is likely that the threshold level is greater than 8 ksi$\sqrt{}$in.

5.2.3 FCG Rate Transients with Environmental Variation

One interesting trend, albeit a bit academic in view of the slight steady-state growth rate differences observed in the environmental testing, is what happens to instantaneous FCG rate when the thermal condition is changed. Between segments in the tests depicted in Figures 49, 51, and 52 (but not in the data shown in Figure 50 since the test was restarted for each segment and transient growth information was lost), if the transition is from warmer to cooler, the FCG rate initially plummets before increasing later to reach a steady-state level. Similarly, if the transition is from cooler to warmer conditions, the growth rate will increase dramatically for a short period of time.

This trend is theorized to be a consequence of slight plastic zone size changes due not to the traditional mechanical loading changes but rather to slight differences in mechanical property variation as a function of temperature. The plastic zone is proportional to the ratio of $(K_{max}/\sigma_{YS})^2$. Since K_{max} is fixed, the yield strength variation results in changes to the plastic zone size. Furthermore, Reference 9 indicates that the yield strength of TC-128B actually increases with decreasing temperature (64 versus 57 ksi at room temperature). This implies that the plastic zone size actually decreases with decreasing temperature. This would be equivalent to a load shed in terms of the mechanical loading, given constant ΔK conditions. As load sheds during FCG testing, it is not uncommon to observe arrest or slow transients as the instantaneous FCG rate decreases dramatically. Conversely, with increasing temperature, the plastic zone is

getting larger since, presumably in the absence of any data, the trend of yield is the reverse. This would explain why an accelerated FCG rate is observed when moving from a cooler to a hotter environment.

5.3 Fatigue Crack Closure

With the exception of the first three tests performed in Phase A, automatic crack closure measurements were made during all of these tests. The closure-corrected ΔK levels, summarized in the Appendix, generally did not differ much from the applied ΔK except in the near-threshold regime, where differences between the applied and effective ΔK are typically magnified in terms of their impact on FCG rate. The absence of large differences in the data shown in Figures 42 to 47 as a function of the perturbed variable, especially in the Paris regime of the data, is also consistent with a minor role of crack closure under these loading conditions.

Figure 53 shows some crack closure results for the Phase B constant ΔK tests. In this plot, however, the identification of the different environmental segments for each test has been omitted. Furthermore, the solid colored points are ΔK_{eff} whereas the open points are the applied (mechanical) ΔK for the four tests. Several observations are apparent from Figure 53. First, for all tests, the applied (mechanical) ΔK control was excellent. Moreover, for several tests, ΔK_{eff} did not change with crack length: most notably TC-B-2B, TC-A-3A, and the early portion of TC-A-3B. Furthermore, the stability of ΔK_{eff} for several of the tests is remarkable. Although some perturbations were noted with TC-B-3B, they tended to vary within approximately 2 ksi$\sqrt{}$in. Finally, the crack arrest difficulties that occurred in the low ΔK, low r-ratio test (TC-A-3B) can be clearly understood from the data given in Figure 53. Based upon the arrest, the threshold for growth must be approximately 4-5 ksi$\sqrt{}$in. This is a reasonable observation considering the lab air threshold of approximately 2-3 ksi$\sqrt{}$in.

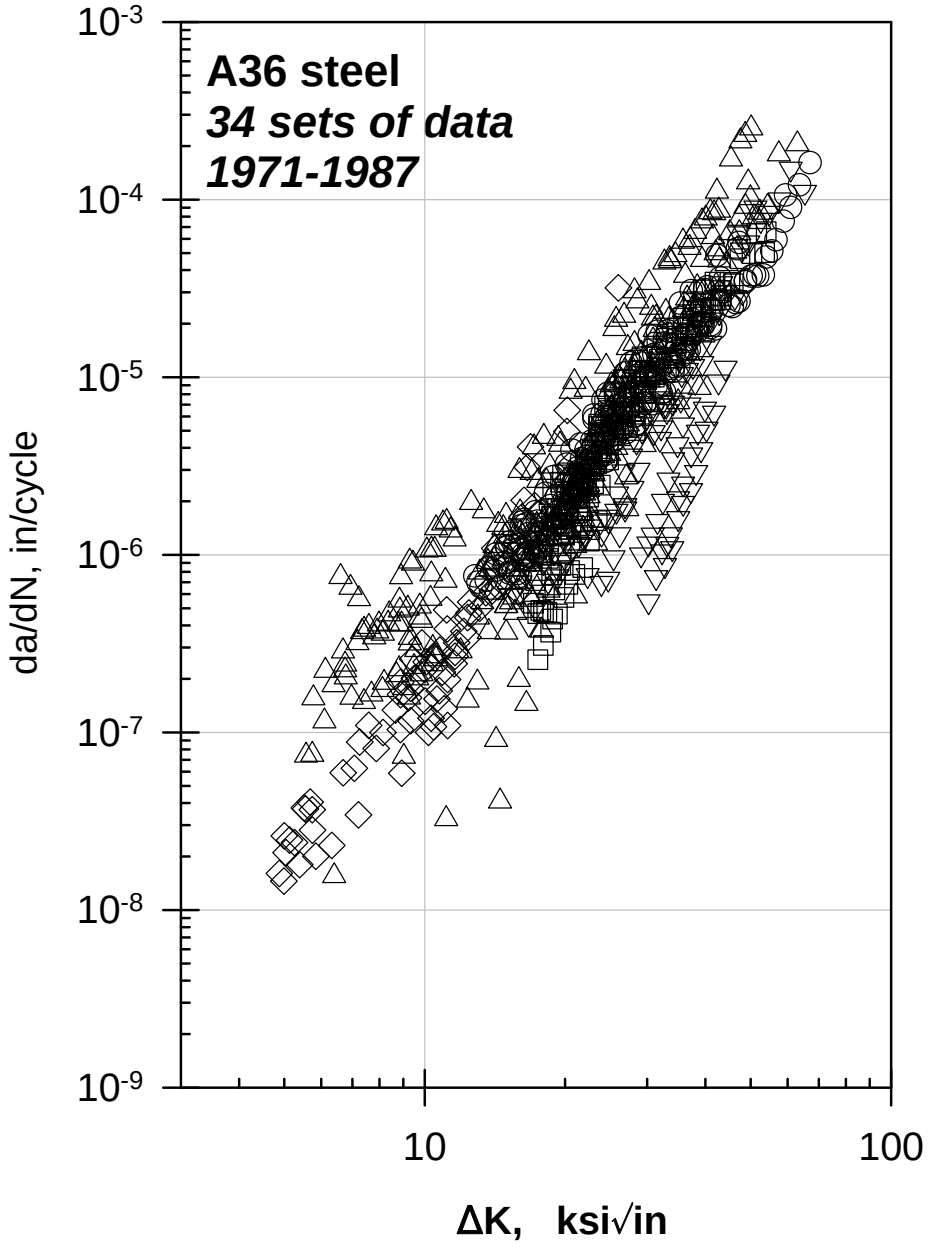

Figure 41. FCG Data Scatter for A36 Steel[3]

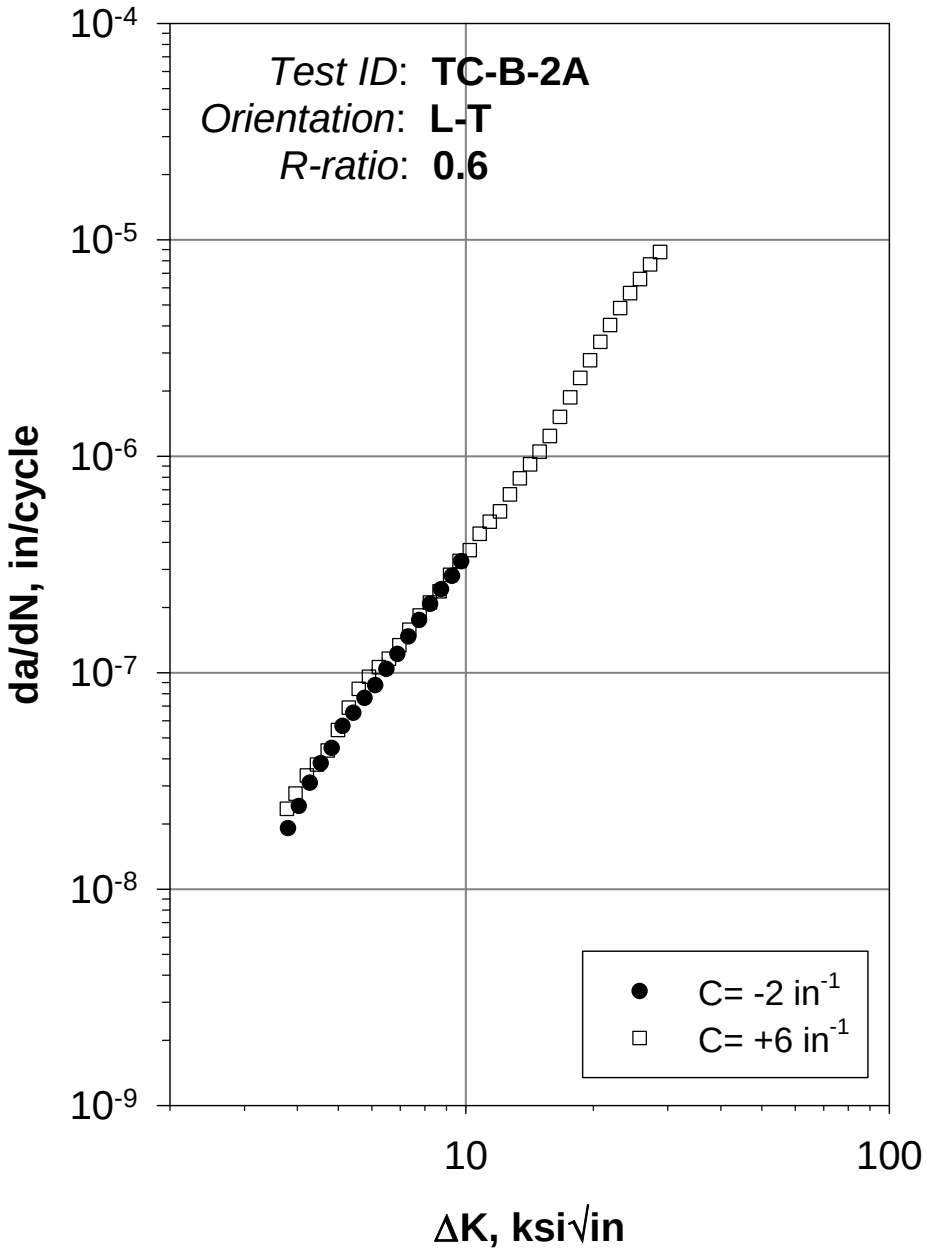

Figure 42. Effect of K-Gradient on FCG Behavior

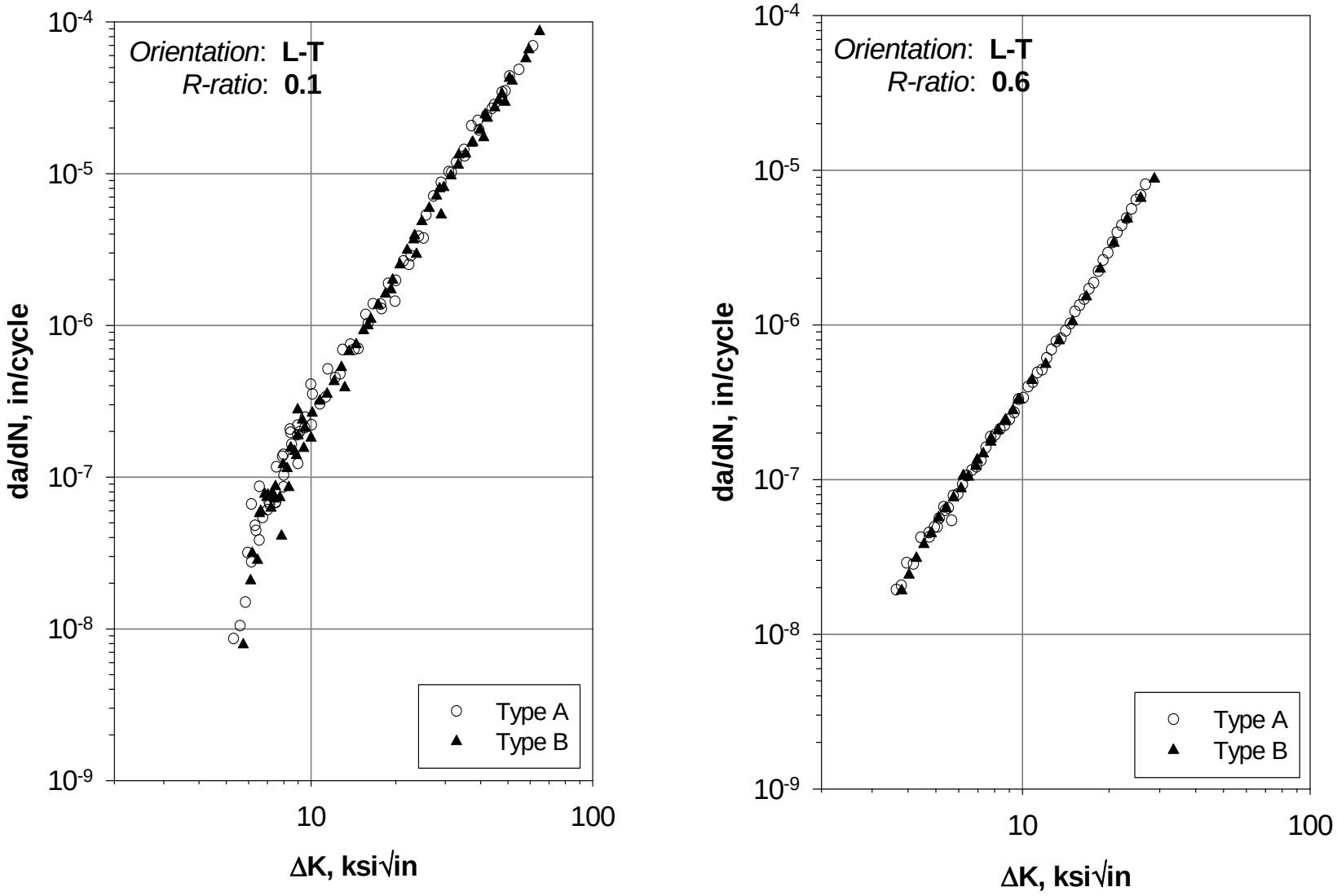

Figure 43. Effect of Material Lot on FCG Behavior at Low and High R-Ratio

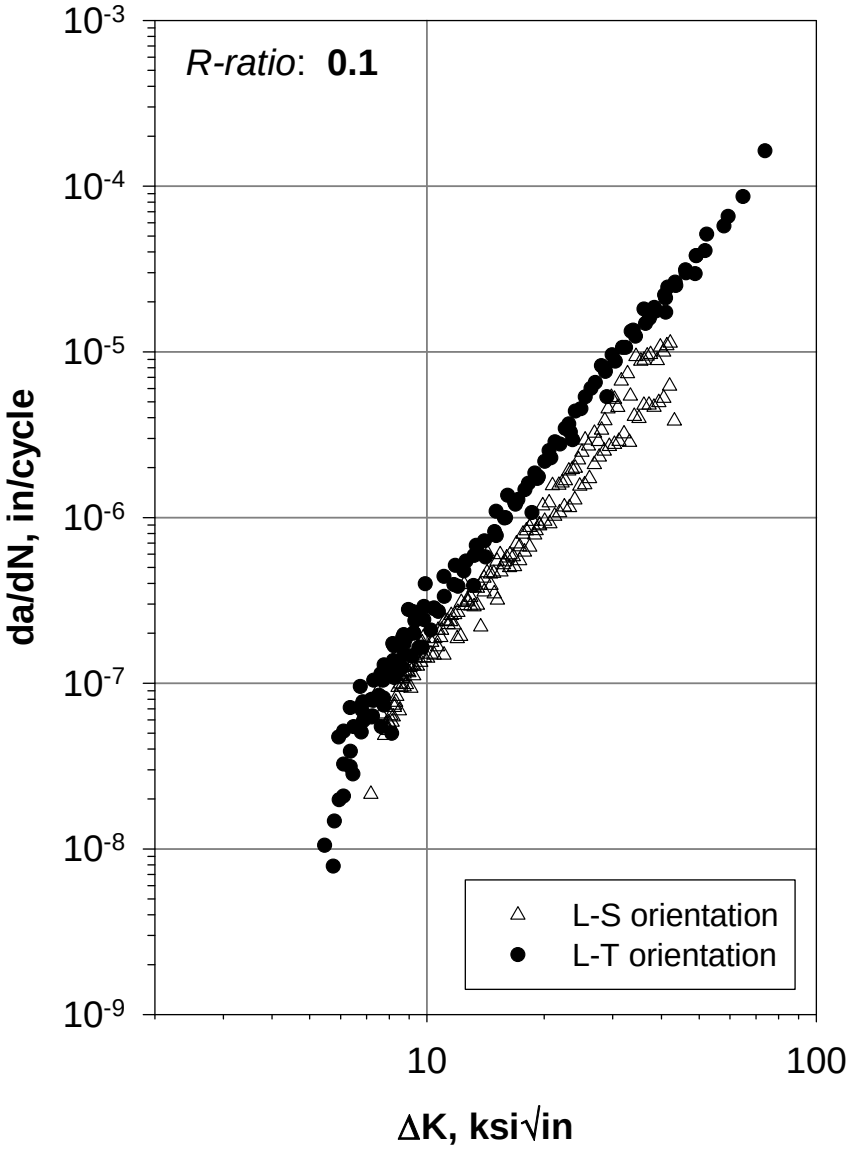

Figure 44. Influence of Orientation on FCG Behavior

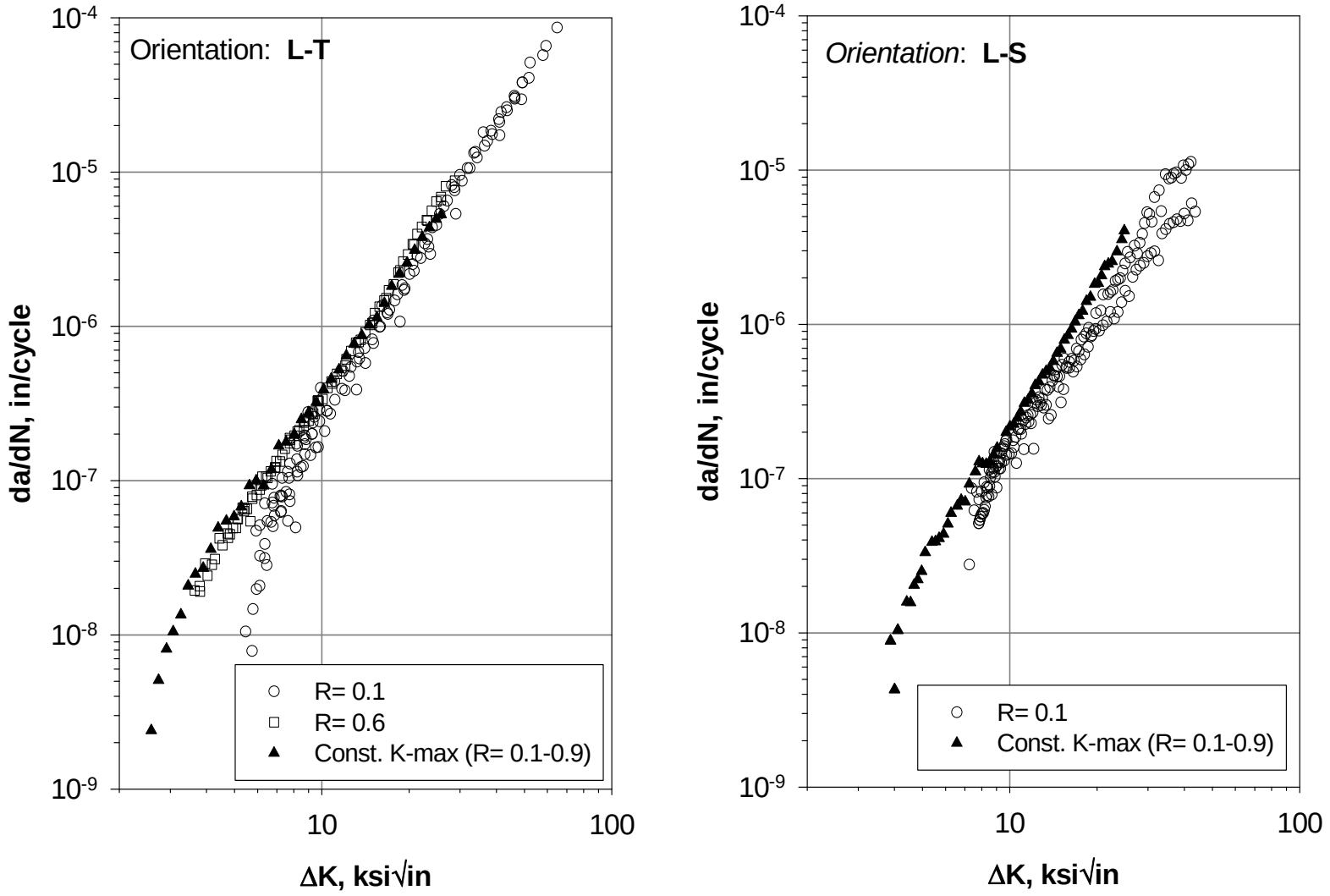

Figure 45. Comparison between Fixed R-Ratio and Constant K_{max} FCG Data for the L-T and L-S Orientations

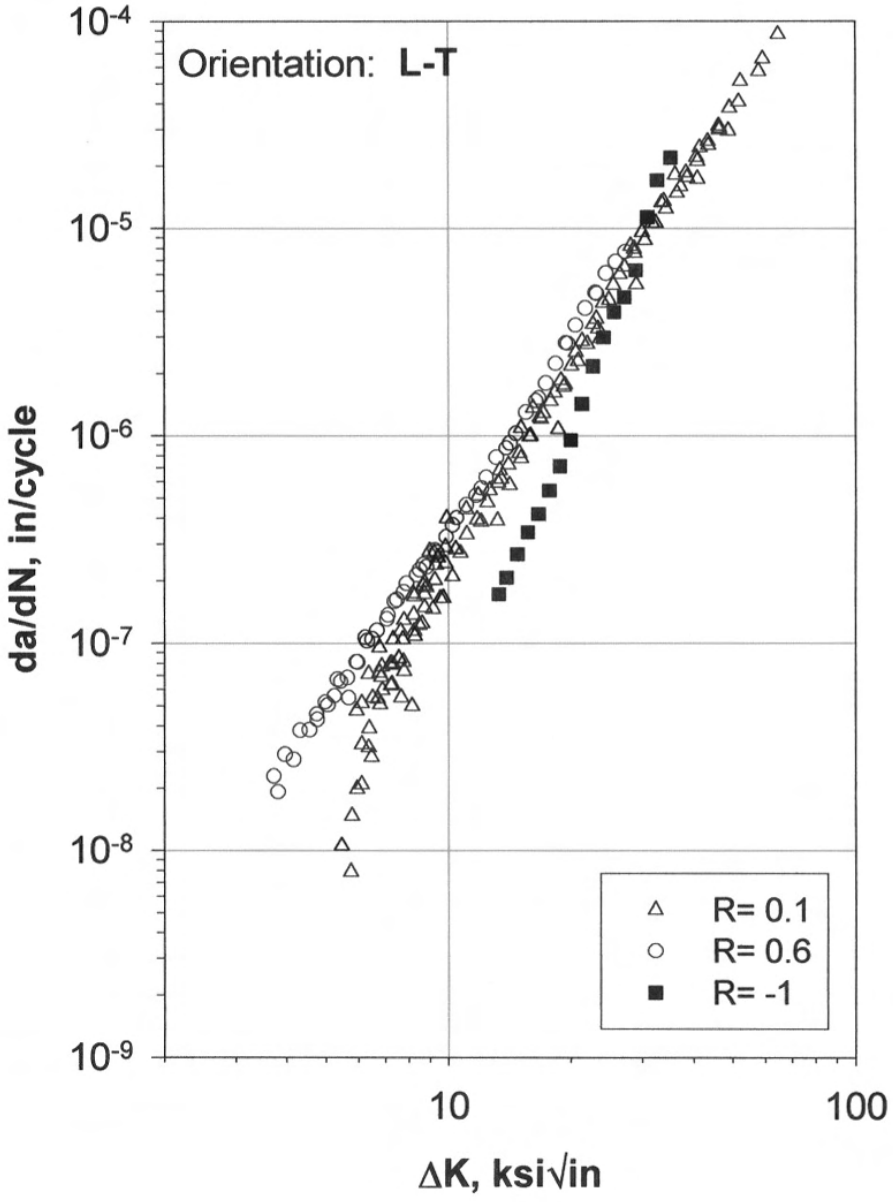

Figure 46. FCG Data for All R-Ratios (L-T)

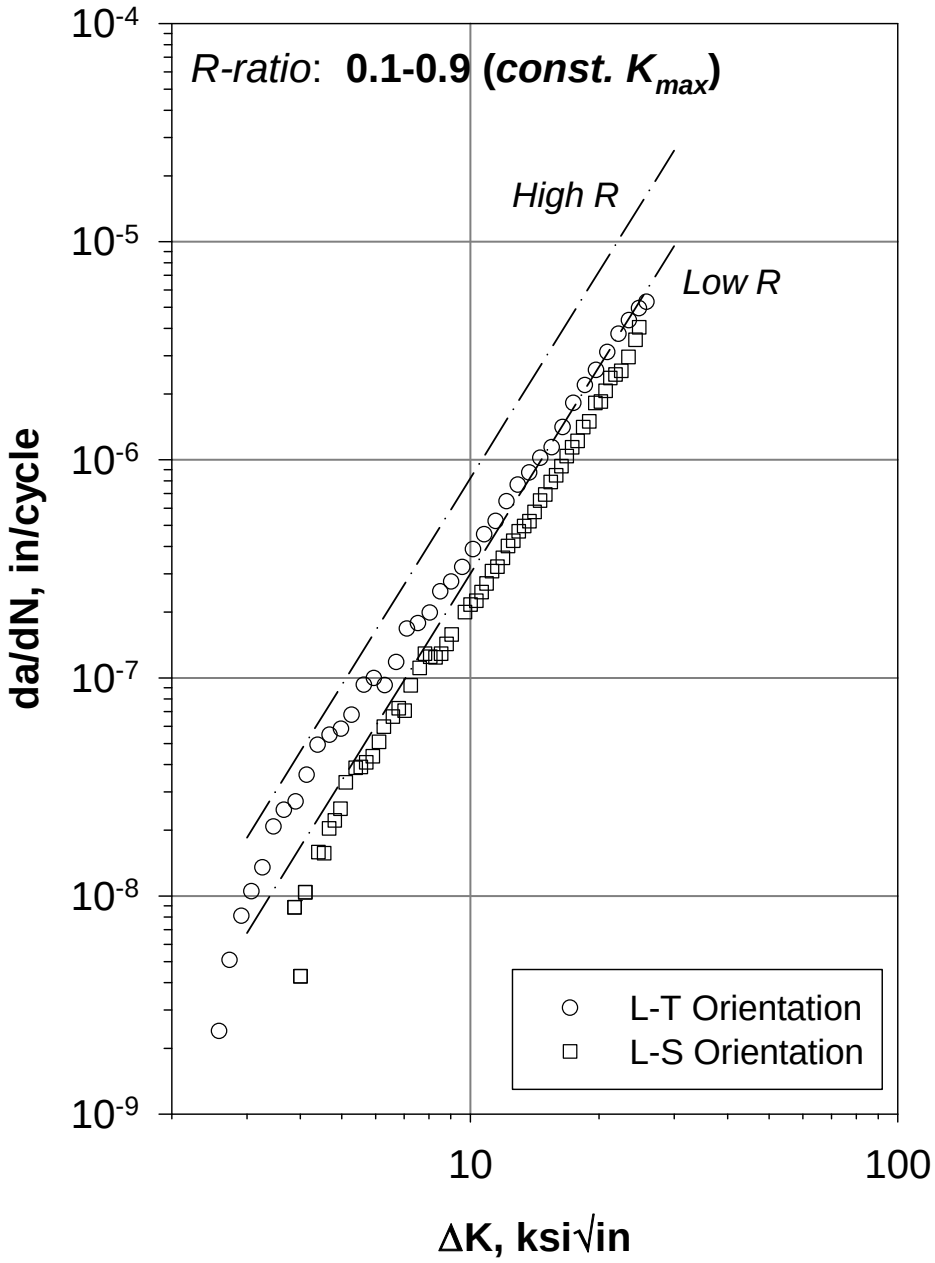

Figure 47. Comparison to HBC Relation[4]

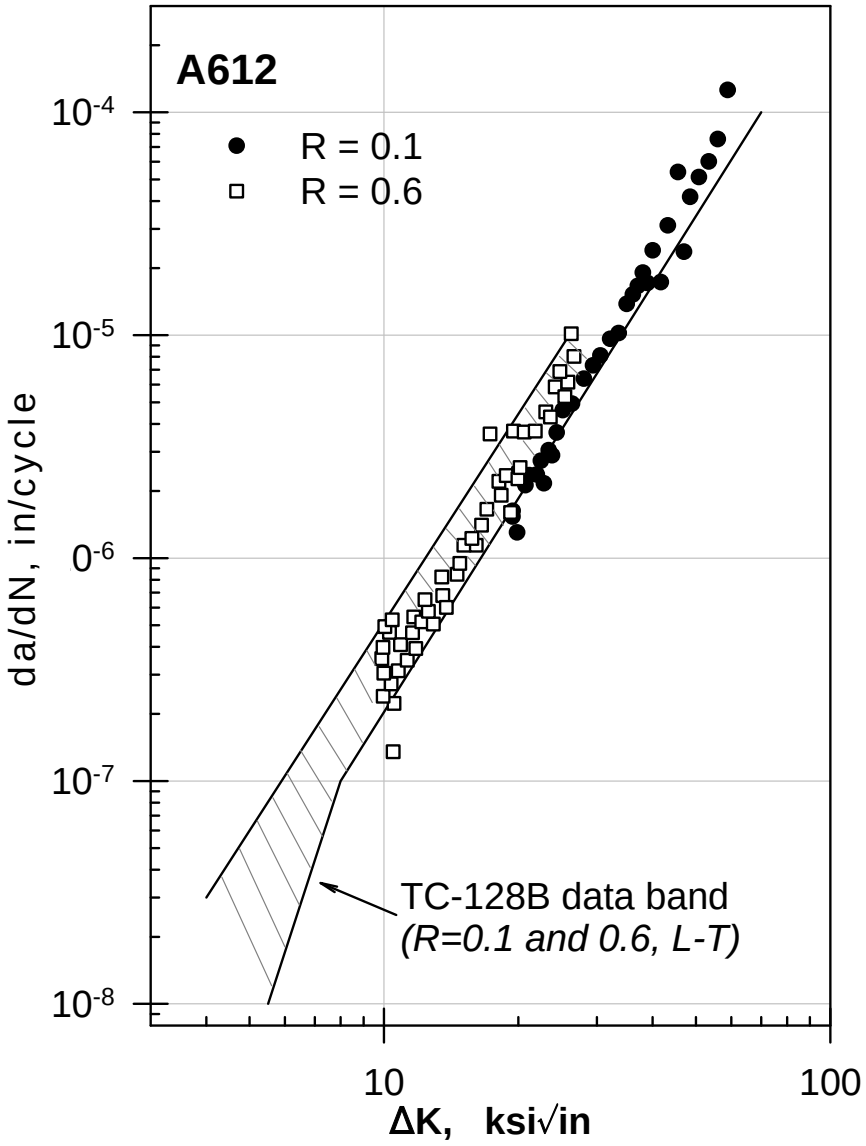

Figure 48. Comparison to Literature Data[7]

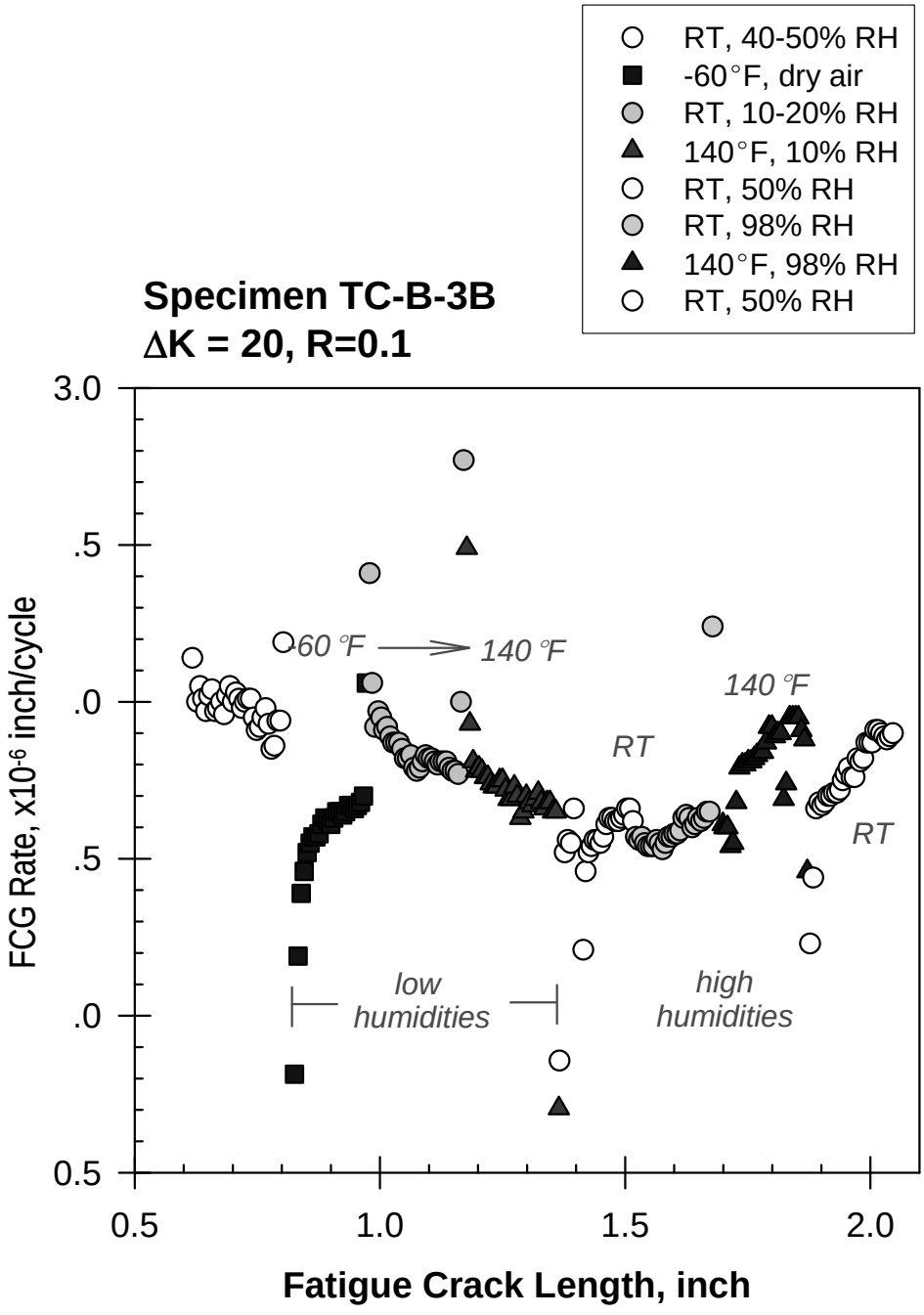

Figure 49. Phase B Environmental FCG Rates for High Constant ΔK, Low R-Ratio Conditions

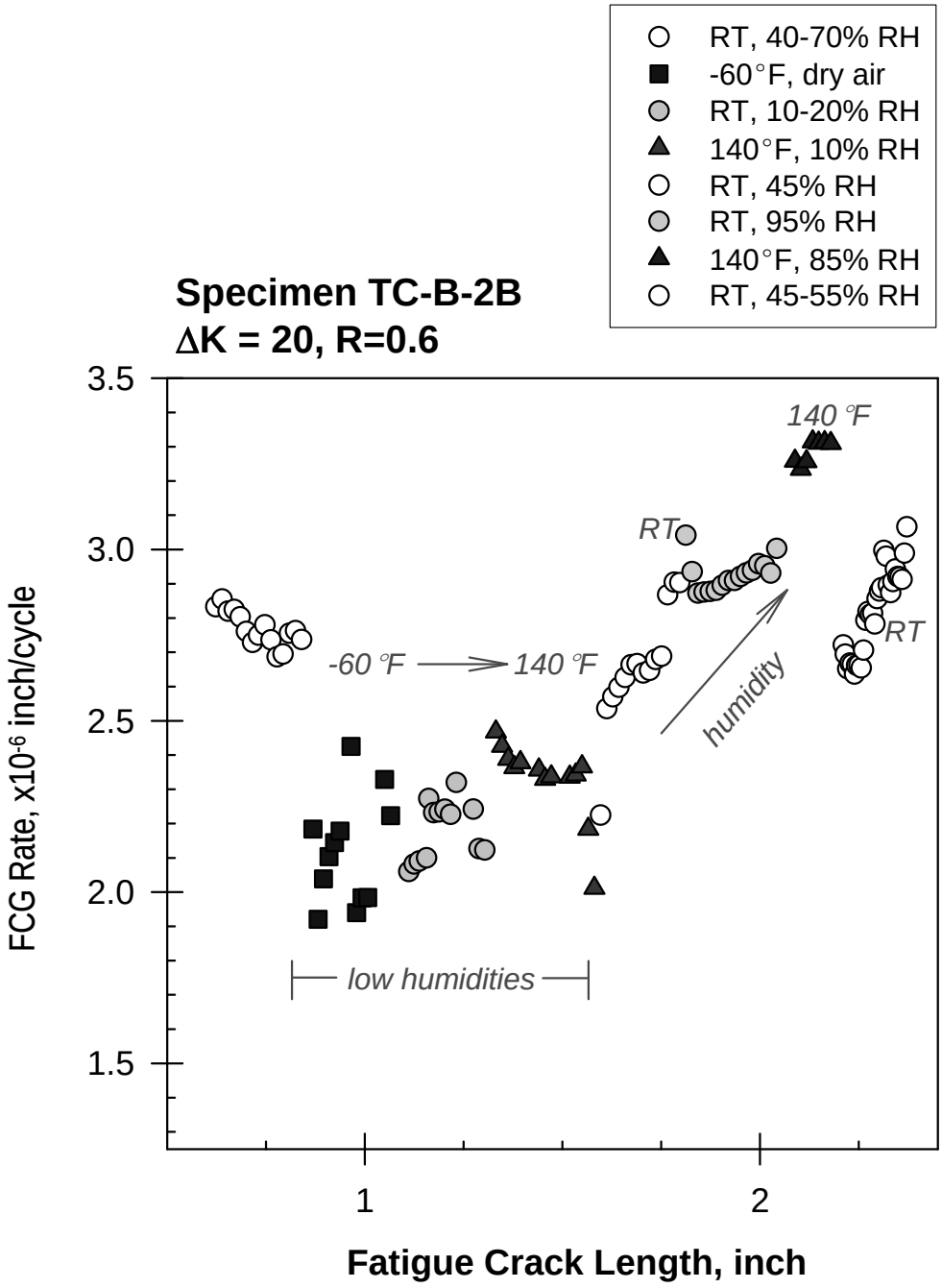

Figure 50. Phase B Environmental FCG Rates for High Constant ΔK, High R-Ratio Conditions

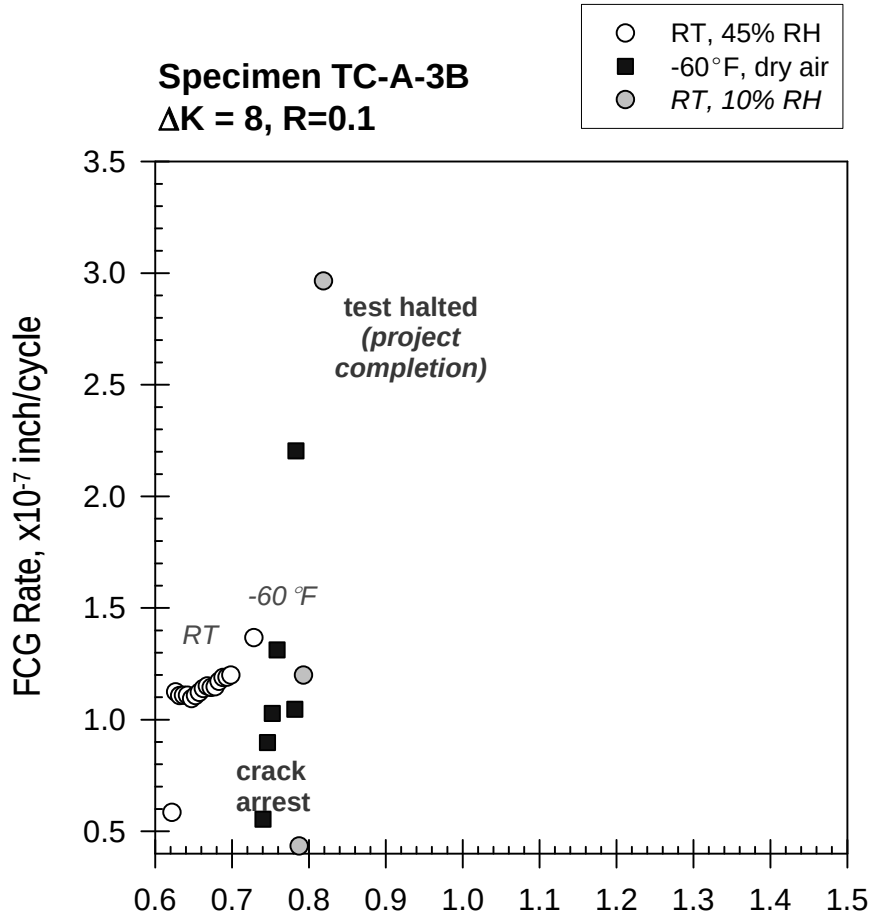

Figure 51. Phase B Environmental FCG Rates for Low Constant ΔK, Low R-Ratio Conditions

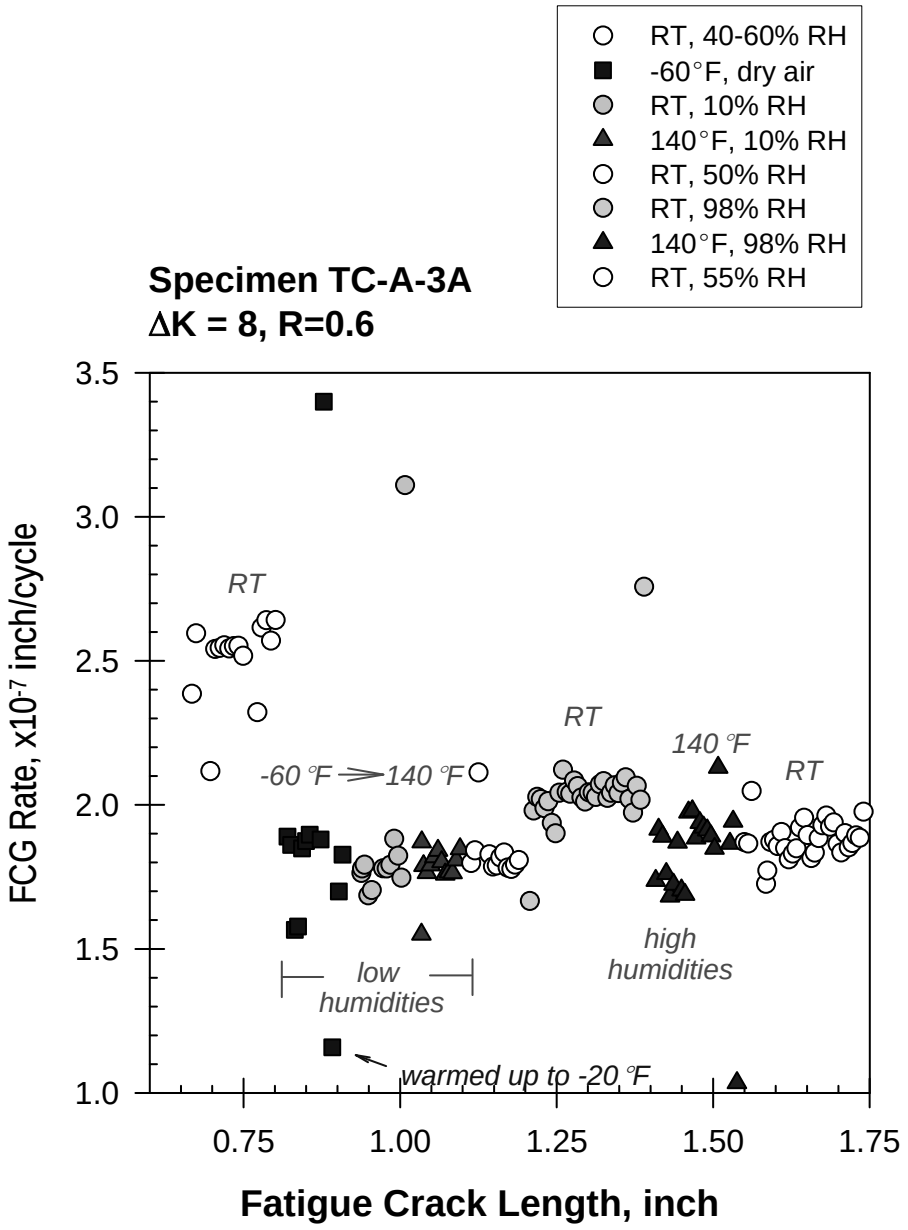

Figure 52. Phase B Environmental FCG Rates for Low Constant ΔK, High R-Ratio Conditions

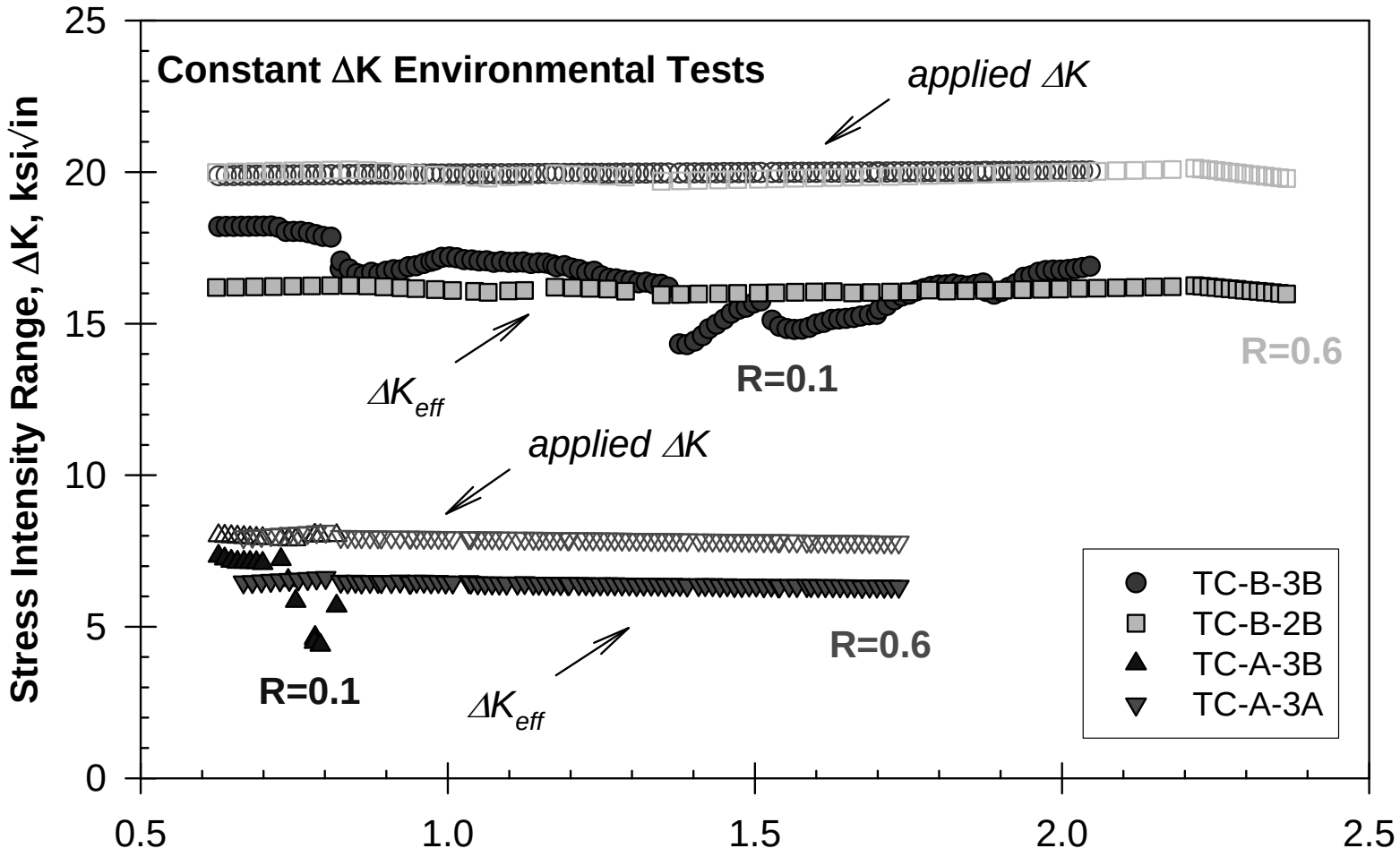

Figure 53. Applied ΔK and Crack Closure Derived ΔK_{eff} for the Constant ΔK Tests with Different Environmental Segments Applied

6 Conclusions

Based upon this two-part test program, several observations can be made regarding the FCG behavior of TC-128B steel in both lab air and at varying thermal and humidity conditions. These include:

- SwRI examined two modern lots of TC-128B steel. Each had been supplied from two different tank car manufacturers who had purchased from two different steel suppliers. The material was either single or double normalized as well as stress relieved. Each had very similar mechanical (e.g., tensile test) and chemical properties, and the grain structures were nearly identical. The measured FCG behavior of each material was extremely consistent.

- The K-gradient techniques used to perform the FCG tests yield similar replicate FCG rates. Hence, the FCG observations made herein are independent of the mechanical loading conditions.

- The effects of r-ratio and specimen orientation both yield an overall two times factor on FCG rate for a ΔK level in the Paris regime. As is consistent with most materials, the higher r-ratio data exhibited faster rates than the low r-ratio data. The in-plane L-T orientation exhibited a faster FCG rate than the through-thickness L-S orientation.

- The high r-ratio threshold behavior for the two orientations was of similar magnitude: 2-3 ksi$\sqrt{}$in and 3-4 ksi$\sqrt{}$in for the L-T and L-S orientations, respectively. As the FCG threshold was approached, the effects of r-ratio and orientation generally increased.

- The measured impact of environment, in this case including the temperature range of–60 ^{o}F to 140 ^{o}F and moisture levels from dry to ≈100 percent humid conditions, was slight and almost immeasurable. The quantified environmental impact is at most approximately a factor of 1.5x, ignoring the transients that can occur when perturbing the environment.

- A favorable comparison was made between TC-128B FCG data measured in this report and several data representations from the literature. The slight environmental effect reported in this study, however, is counter to one of the few FCG datasets (Reference 7) of properties available in the technical literature.

- In general, the effect of crack closure on FCG rate during the lab air Phase A effort was fairly small with the exception of the behavior in the near-threshold regime. In the case of the environmental tests in Phase B, closure conditions were remarkably stable during these assessments.

7 References

1. *Annual Book of ASTM Standards. Section 3: Metals test methods and analytical procedures,* vol. 3.01. West Conshohocken, PA: American Society for Testing and Materials, 2000.

2. Appendix M—Specifications for materials. In *AAR Manual of Standards and Recommended Practices, Section C—Part III, Specifications for Tank Cars, Specifications M1002.* Association of American Railroads, 1992.

3. Cardinal, J.W., McKeighan, P.C., and Hudak, S.J., *Damage* Tol*erance Analysis of Tank Car Stub Sill Cracking. Southwest Research Institute Final Report No. 06-6965.* Prepared for the Tank Car Stub Sill Working Group, November 1998.

4. Hudak, S.J., Jr., Burnside, O.H., and Chan, K.S., "Analysis of corrosion fatigue crack growth in welded tubular joints," *J Energy Resour Technol,* 107:212-219, 1985.

5. Eason, E.D., Gilman, J.D., Jones, D.P., and Andrew, S.I., "Technical basis for a revised crack growth rate reference curve for ferritic steels in air," *J Pressure Vessel Technol,* 114, February 1992.

6. Yazdani, N., and Albrecht, P., "Crack growth rates of structural steel in air and aqueous environments," *Engin Fracture Mechanics,* vol. 32, no. 6, 1989; pp. 997-1007.

7. Poon, C., and Hoeppner, C.W., "The effect of temperature and r-ratio on fatigue crack growth in A612 Grade B steel," *Engin Fracture Mechanics,* vol. 12, 1979; pp. 23-31.

8. *Progressive Railroading,* vol. 44, no. 5. Trade Press Publishing, May 2001.

9. Hicho, G.E., and Smith, J.H., *Mechanical Properties and Fracture Toughness of AAR TC128 Grade B Steel and a Micro-Alloyed Control-Rolled Steel, A8XXX Grade B, from –80 ◦F to +73 ◦F.* NISTIR 90-4289, Report No. 19. U.S. Department of Commerce, National Institute of Standards and Technology, April 1990.

8 Abbreviations and Acronyms

AAR	Association of American Railroads
ASTM	American Society for Testing Materials
BFS	back-face strain
C(T)	compact tension
CMOD	crack mouth opening displacement
DTA	damage tolerance analysis
EDM	Electrical Discharge Machining
FCG	fatigue crack growth
FRA	Federal Railroad Administration
FTA	Fracture Technology Associates
HBC	Hudak, Burnside, and Chan
HHA	high-humidity air
LPG	liquid propane gas
M(T)	middle-crack tension
MCB	Multiple Channel Burst
RH	relative humidity
SE(B)	single-edge bend